ARCHIVES OF ACOUSTICS
17, 3, 343–356 (1992)

IN QUEST FOR CARDINAL VOWELS

W. JASSEM and M. KRZYŚKO

Department of Acoustic Phonetics
Institute of Fundamental Technological Research
Polish Academy of Sciences
Poznań, ul. Noskowskiego 10

Computing Centre, A. Mickiewicz University
Poznań

180 isolate voicings of (near) Cardinal Vowels – 10 of each: [i e ɛ a y ø œ ɶ u o ɔ ɒ ɯ ɤ ʌ ɒ i ʉ] were described using four formant frequencies, which were measured from FFT spectra. In a 4-D space, the tokens could be correctly assigned 95% of the time using Bayes estimators of discriminant scores. The error increases with the reduction of the number of variables to three or two. The mean vectors characterizing the 18 vowel classes were, for the present speaker, somewhat different from those recorded and measured about 20 years ago, which may be due to aging.

1. The background

Until fairly recently, the Cardinal Vowels were used only for the purposes of Linguistic Phonetics. But for over 3 decades now specialists in Speech Acoustics, Speech Pathology and perhaps most of all, Speech Technology have been to a smaller or greater extent forced to use the transcription of the International Phonetic Association at some place or other in their routine work. These specialists often have decidedly insufficient knowledge of the system of IPA (International Phonetic Association) with the result that even if their primary problem is correctly solved, erronious transcription confuses phoneticians who wish to use their data.

In what follows we shall concentrate on those aspects of the Cardinal Vowels that are of interest to the *Speech Technologist*, the *Speech Pathologist* and the *Acoustician* who is dealing with the speaking or singing voice.

The Cardinal Vowels were devised by Daniel Jones some time between 1910 and 1920, and were based on the observation of four extreme vocalic articulations with

respect to the natural, unmodified position of the tonge, its hump taking a maximally (1) high-front, (2) low-front, (3) low-back and (4) high-back position. Of these, (1), (3) and (4) can be indirectly controlled by the speaker's tactile sense, their articulations being minimally different from the palatal [j̟], uvular [ʁ] and velar [ɣ]. The front-low position can only be controlled auditorily and, possibly, kinaesthetically. The four vowels were given the phonetic symbols [i a ɑ u]. The choice of the symbols was a mat-matter of convenience, and the three represented by letters of the roman alphabet are just as normal as the fourth. They were all intended as international reference values independent of any particular language. In 1917 Jones made X-rays of the four extreme vowels and these were published in the later editions of Jones's *The Pronunciation of English* (e.g. JONES 1956 [11] as a frontispiece. They formed the basis of the vowel quadrilateral, which, with minor changes, has been in use by those adhering to the principles of the International Phonetic Association.

Over a period of about 70 to 80 years, the set of Cardinal Vowels was made to include initially (beside the extreme four) an additional set of four, viz. [e ɛ ɔ o]. For some time it was maintained by many phoneticians, including D. Jones himself, that in the front series [i e ɛ a] the *articulatory* distances [i]–[e], [e]–[ɛ] and [ɛ]–[a] were equal, as were the distances in the back series: [u]–[o], [o]–[ɔ], [ɔ]–[ɑ]. The total system was, then:

i	u	close
e	o	half-close
ɛ	ɔ	half-open
a	ɑ	open
front	back	

The trapezoidal form of the arrangement, as seen above, reflects the assumed positions of the tongue hump and has here been slightly simplified (see, e.g. JASSEM (1973), p. 124 [9]).

For several decades the trapezoid was used by phoneticians to describe the vowels of various languages e.g. for English in JONES (1956) [11], ROACH (1983) [23], and GIMSON (1988) [8], for French by ARMSTRONG and JONES (1951) [2], for Russian by JONES and WARD (1969) [12], for Polish by Jassem (1973) [9] etc.

The articulatory basis for the 8-item set of Cardinal Vowels was never confirmed experimentally. What little X-ray work was done on their articulation actually falsified that basis (BUTCHER (1982) [3]). For some forty years now it has been maintained that the trapezoid represents *auditory* (i.e. psychoacoustic) relations. This, too, has been questioned by BUTCHER [3].

The 8 Cardinal Vowels (CVs) were not sufficient for the description of many languages because it was assumed that [i ɛ a ɑ] were unrounded (i.e. spoken with neutral position of the lips) whilst [a ɔ o u] have, in that order, increasing lip-roundig. Although this reflected a strong tendency, many languages have rounded front vowels and some have unrounded back ones. Such symbols as [y] for "close front rounded" or [ø] for "front half-close rounded" were used even towards the end of the 19th century within the International Phonetic Alphabet, but it was not before the end of the II World War that

the complete set of 18 CVs was established. Ignoring the trapezoidal shape of the schematic, the full set of CVs is now arranged as follows:

	central close			
	unrounded	rounded		
	ɨ	ʉ		
	front		back	
	unrounded	rounded	unrounded	rounded
close	i	y	ɯ	u
half-close	e	ø	ɤ	o
half-open	ɛ	œ	ʌ	ɔ
open	a	ɶ	ɒ	ɑ

The front unrounded and back rounded vowels are often referred to as "primary" and the "newer" 8 as "secondary". In the above arrangement of the CVs, the secondaries lie *within*, the primaries if looked upon as placed in a plane.

For several decades the set of 8 primaries or the set of all the 18 CVs has been used in texts on the phonetics of many languages (see a comparative sample in JASSEM (1973) [9] 130 and 134). But X-ray studies of the CVs as well as those of real linguistically used vowels tended to show that the assumed articulatory basis was incorrect (BUTCHER (1985) [3]). It was also shown *loc.cit.* that the *perception* of the CVs was strongly affected by the first language of the hearer. It would seem that the only hopeful level at which the identity of the CVs could be sought was the *acoustic* level.

2. Earlier acoustical data

The earliest data on the acoustic properties of the Cardinal Vowels come from a paper by DELATTRE, LIBERMAN and COOPER (1951) [6] who produced them synthetically. Figures 1 and 2 in that paper show the synthesized 16 vowels, 15 of which were intended to represent the IPA (International Phonetic Association) CVs, in an (F_1F_2) *acoustical plane*. On a straight low–F_1 (first formant) line (250 Hz) lie [i y ɯ u] – the close vowels. Along three other straight lines (1) at F_1 = 440 Hz (2) F_1 = 550 Hz and (3) F_1 = 750 Hz lie [e ø ɤ ɔ], [ɛ œ ʌ ɔ] and [æ a ɒ ɑ], in that order. These relations should be compared with the 8-vowel and 18-vowel arrangements above. Within each of the four subsets, F_2 decreases in the order indicated within brackets. Only the last subset of four requires comment. Cardinal [ɶ] had not yet been approved by the International Phonetic Association at the time of the Delattre–Liberman–Cooper experiment. In the two quadrangles – one for the unrounded and the other for the rounded, published in *Fundamentos* (1944) [7] and *Principles* (1949) [20], the lower-left corner in the "rounded" quadrilateral was left unmarked. Apart from [æ], the arrangement in the acoustical (F_1, F_2) plane in DELATTRE–LIBERMAN–COOPER (1951) [6] can be seen to correspond very well with the arrangement of the sixteen non-central vowels shown above, with one exception: the positions of [ɑ] and [ɒ] were reversed. A very important feature of the Delattre–Cooper–Liberman quadrangle was that the Primaries lie on the circumference while the

Secondaries lie within the quadrangle. The figure is a trapeze, with the bottom side considerably shorter that the top side, so that the [i]–[u] distance is over 3 times that between [æ]–[ɑ]. This should be confronted with the trapezoid on p. 2 above. In the Delattre–Liberman–Cooper trapeze, the distance D(y – ɯ) is only half that of D(i, u), D(ø – ɤ) is about half that of D(e – o) and D(œ – ʌ) is distinctly less than half of D(ɛ – ɔ). This reflects the fact usually tacitly admitted by phoneticians that the "secondary" CVs are *perceptually* less distinct – or less distant – than the Primaries of the same degree of openness (approx. the same value of F_1).

LEE (1968) [18] published an (F_1, F_2) chart of the Primaries pronounced by D. Jones. The geometry of the vowel "loop" turned out quite similar to the Delattre–Liberman–Cooper trapeze, though some of the absolute frequencies were different: [e – o] and [a-ɑ] do not lie on a const F_1 line, F_1[a] > F_1[ɑ] and F_1[e] > F_1[o]. Lee was trying to prove a point which is outside the scope of the present paper. But in order to proceed with his argumentation Lee took into account an important consideration, viz. that the frequencies of F_1 and F_2 vary not only with the phonetic quality of the vowel, but also with its *personal* quality (personal timbre).

It has been realized for some 30 years now that in speech perception a process of normalization takes place which permits phones that are acoustically different to be perceived as linguistically identical. Viewed differently, the hearer extracts from the acoustical speech signal simultaneously two kinds of information: linguistic and personal. Several attempts have been made to describe, sometimes in mathematical terms, the interaction between these two essential and intertwined sources of variation (see, e.g. LADEFOGED and BROADBENT (1957) [17], AINSWORTH (1975) [1] and, especially, NEAREY (1978) [19].

CATFORD (1981 [4], 1988 [5]) has devised two acoustic grids with F_1 and F_2 as non-orthogonal co-ordinates: one for the rounded vowels and the other for the unrounded, and used them to describe the vowels of several languages. But he does not say how he deals with inter-speaker differences. Further data have been published by JASSEM (1973) [9], 1984 [10] including those on all the lower four formant frequencies. An acoustical map of all the 18 CVs, now including also [i] and [ʉ], in an (F_1, F_2) plane was demonstrated. The topography is here very similar to that in the earlier studies, but the absolute values tend to be higher, possibly pointing to a smaller vocal tract. As the earlier investigations are limited to F_1 and F_2, Table 1 below includes only such data, for comparison. Values that had to be read off the (F_1, F_2) plots (the source giving no numbers) appear here in cursive. The values which appeared in JASSEM (1973) [9] and (1984) [10] are here given under WJ1. For comparison, the mean values obtained in the present experiment for F_1 and F_2 also appear in Table 1 as WJ2.

Although in terms of absolute values the data differ between the individual sources, the following regularities may be observed.

(1) F_1 increases with the degree of openness:

[i] > [e] > [ɛ] > [a] (front unrounded)
[y] > [ø] > [œ] > [ɶ] (front rounded)
[ɯ] > [ɤ] > [ʌ] > [ɒ] (back unrounded)
[u] > [o] > [ɔ] > [ɑ] (back rounded)

(2) For each degree of openness, F_2 is higher in the unrounded than for the corresponding rounded vowel:

[i] > [y], [e] > [ø], [ɛ] > [œ], [a] > [ɶ] (front series)

[ɯ] > [u], [ɤ] > [o], [ʌ] > [ɔ], [ɑ] > [ɒ] (back series) (cf. above about the relations between the open vowels in DLC)

(3) For the front series,

[i] > [e] > [ɛ] > [a] (unrounded)

[y] > [ø] > [œ] > [ɶ] (rounded)

Table 1. F_1 and F_2 frequencies of Cardinal Vowels from five sources

vowel		i	y	e	ø	ɛ	œ	a	ɶ
source									
DLC	F_1	*240*	*240*	*360*	*360*	*520*	*520*	*730*	——
	F_2	*2900*	*1900*	*2500*	*1700*	*1650*	*1450*	*1320*	——
Lee	F_1	250	——	375	——	525	——	775	——
	F_2	2500	——	2250	——	1800	——	1100	——
Cat	F_1	240	235	390	370	610	585	850	820
	F_2	2400	2100	2300	1900	1900	1710	1610	1530
WJ_1	F_1	210	220	380	350	590	520	870	790
	F_2	2750	2550	2630	2320	2280	1950	1750	1650
WJ_2	F_1	217	249	417	422	559	511	921	511
	F_2	2775	2255	2538	1968	2151	1769	1560	1769
		ɯ	u	ɤ	o	ʌ	ɔ	ɑ	ɒ
DLC	F_1	*250*	*250*	*360*	*360*	*520*	*520*	*730*	*730*
	F_2	*1050*	*700*	*1100*	*800*	*1180*	*950*	*1050*	*1250*
Lee	F_1	——	250	——	350	——	525	775	——
	F_2	——	625	——	775	——	900	1450	——
Cat	F_1	300	250	460	360	600	500	750	700
	F_2	1390	595	1310	640	1170	700	940	760
WJ_1	F_1	280	270	450	400	570	550	800	710
	F_2	850	615	850	730	940	820	1050	900
WJ_2	F_1	369	308	475	427	591	535	740	680
	F_2	808	577	846	686	911	805	995	931

For comparison, we would cite some data contained in PAPCUN (1980) [2]. Figure 6.3 in this paper contains, in the form of a graph, measured F_1 and $F_{2'}$, of the English vowels as produced by two male speakers. Except, possibly, for [ɑ]/[ɒ] the vowels represent the same linguistic-phonetic entities. In keeping with the position taken by the Phonetics Laboratory at the Department of Linguistics, University of California Los Angeles, where the data was obtained, instead of the straight F_2 frequency, the other variable, beside F_1, is $F_{2'} = F_2 - F_1$.

The F_1 and $F_{2'}$ values, reads as closely as possible from the chart are presented below in Table 2.

Table 2. Frequencies of F_1 and $F_{2'}$ of English monophthongs

	vowel	[i]	[ɪ]	[E]	[æ]	[ɑ] [ɒ]	[ɔ]	[ω]	[u]
speaker 1	F_1	270	400	550	700	710	360	450	310
	F_2	1950	1550	1250	990	390	290	590	560
speaker 2	F_1	250	270	380	470	370	580	300	220
	F_2	1620	1500	1280	950	460	290	430	460

Both voices were male.

As can be seen from Table 2, the differences in the values for F_1 and $F_{2'}$ of linguistically equivalent vowels may be striking. They are due to the effect of *personal* timbre. If spoken by *the same* voice, the corresponding values in each of the columns would easily represent different, even very different linguistic-phonetic entities.

3. The present materials and their acoustic analysis

The purpose of the present experiment is fivefold:

(i) to establish reasonably narrow Cardinal Vowel subspaces in a four-dimensional vowel space.

(ii) to find for each CV a 4-element mean vector for each CV in the vowel space,

(iii) to perform a statistical discriminant analysis of the vectors representing the complete set of 18 Cardinal Vowels,

(iv) to see whether the CVs might be affected by the speaker's aging.

(v) to find, using statistical discriminant analysis, whether the frequencies of the higher formants, i.e. F_3 and F_4 contribute to the discriminability of CVs.

The materials for the present experiment consist of sets of two or three voicings intended to represent the Cardinal Vowels [i ɛ a] (front unrounded) [ɯ ʌ ɑ] (back unrounded), [y ø œ ɶ] (front rounded), [u o ɔ ɒ] (back rounded) and the high central unrounded [ɨ] and rounded [ʉ], and vowels near enough to each Cardinal for the tokens to be transcribed by the respective Cardinal, possibly with such IPA-approved diacritics as [˕, ˔, +].

No set of two or three contained more than just one representation of any Cardinal. For convenience of analysis the experimenter (WJ) avoided combining into one set such vowels as differ strongly in intrinsic intensity level (e.g. close and open or even half-open). The total material included 10 tokens of each of the 18 CVs (or near-CVs). They were spoken in a silent (but not sound-treated) room and the S/N ratio was controlled to enable the extraction of even the weakest formants (F_3 and F_4 of [u]). The analysis was performed using the KAY Elemetric DSP 5500 Workstation. A 512-point FFT analysis was performed of all the 180 voicings (10 replications of 18 VCs). The measurements were made at a moment approx. 15% into the vowel from its beginning, in the middle of the vowel, and approx. 15% into the vowel from its end. This demonstrated that what is intended as a steady vowel cannot normally be produced as a perfectly stationary acoustic event (except by synthesis). At each point, the frequency of each of the four formants was estimated from the 512-point FFT spectrum with an accuracy of 10 Hz. The frequency of a given formant was the arithmetic mean of the three measurements, and this mean was assumed to represent the entire vowel-token. Averaged formant frequencies for each token could of course have been obtained more directly by taking an average cumulative spectrum of the entire voicing, but we were interested in how the formant frequencies are permitted actually to vary in what is intended (and perceived) as an isolate stationary vowel sound. This temporal variation is of little consequence for the issue at hand, but will be taken into account in further experiments which we propose to make with synthetic stationary vowels. We may, however, just mention in passing that these variations were mostly of the order of 2...7%, though occasional higher values of the calculated coefficient of variation were not uncommon in the case of F_1 of close vowels in which there is the well-known interaction between F_1 and F_0. Approx. 2% of the time the temporal variation in the course of one formant was zero within the measurement accuracy. The fundamental frequency, held steady for each voicing, varied among the individual voicings within the range 97...105 Hz (a somewhat low male voice). The duration of the individual vowel tokens varied between approx. 200...300 ms. Altogether, then, 18 (CVs) × 10 Replications × 3 moments in time × 4 Formants = 2160 measurements were made.

The results of the measurements are summed up in Table 3. The coefficient of variation in Table 3 pertains to within-class variability, not to the temporal variability within individual tokens.

Table 3. Mean formant frequencies and their dispersions

vowel category forman front unrounded		mean *F f*-quency	st.dev.	var.coeff.
[i]				
	F_1	217	28.8	0.1326
	F_2	2775	115.3	0.0416
	F_3	3645	108.7	0.0298
	F_4	4107	80.1	0.0195
[e]				
	F_1	417	33.8	0.0811
	F_2	2538	135.4	0.0534

[cont. Tabl. 3]

1	2	3	4	5
	F_3	2944	94.0	0.0319
	F_4	3805	45.5	0.0119
[ɛ]				
	F_1	559	31.8	0.0569
	F_2	2151	123.7	0.0575
	F_3	2743	83.9	0.0306
	F_4	3689	160.5	0.0435
[a]				
	F_1	921	40.3	0.0438
	F_2	1560	83.4	0.0534
	F_3	2741	45.2	0.0165
	F_4	3571	41.2	0.0364
front rounded				
[y]				
	F_1	249	38.3	0.1528
	F_2	2255	152.0	0.0674
	F_3	2663	200.5	0.0753
	F_4	3494	118.2	0.0338
[ø]				
	F_1	422	18.2	0.0431
	F_2	1968	66.1	0.0336
	F_3	2479	79.3	0.0320
	F_4	3647	53.5	0.0147
[œ]				
	F_1	511	32.2	0.0630
	F_2	1769	93.3	0.0527
	F_3	2466	75.8	0.0308
	F_4	3586	51.8	0.0457
[œ]				
	F_1	676	78.3	0.1164
	F_2	1375	105.1	0.0765
	F_3	2616	186.8	0.0714
	F_4	3501	179.8	0.0514
back unrounded				
[ɯ]				
	F_1	369	72.5	0.1965
	F_2	808	113.8	0.1408
	F_3	2525	131.7	0.0522
	F_4	3240	217.9	0.0673
[ɤ]				
	F_1	475	30.7	0.0647
	F_2	846	38.5	0.0455
	F_3	2497	68.3	0.0273
	F_4	3193	125.3	0.0393

[cont. Tabl. 3]

1	2	3	4	5
[ʌ]				
	F_1	591	48.7	0.0824
	F_2	911	74.5	0.0818
	F_3	2794	160.5	0.0575
	F_4	3313	79.3	0.0239
[ɑ]				
	F_1	740	23.0	0.0312
	F_2	995	58.8	0.0591
	F_3	2982	66.3	0.0222
	F_4	3538	214.2	0.0605
back rounded				
[u]				
	F_1	308	30.2	0.0982
	F_2	577	39.7	0.0688
	F_3	2467	121.0	0.0490
	F_4	3133	265.4	0.0847
[o]				
	F_1	427	19.0	0.0445
	F_2	686	78.0	0.1165
	F_3	2583	48.4	0.0593
	F_4	3166	126.9	0.0401
[ɔ]				
	F_1	535	27.2	0.0508
	F_2	805	28.8	0.0375
	F_3	2660	174.2	0.0655
	F_4	3253	54.3	0.0167
[ɒ]				
	F_1	680	46.9	0.0691
	F_2	931	50.6	0.0544
	F_3	3007	107.4	0.0357
	F_4	3516	111.5	0.0317
central unrounded				
[i]				
	F_1	309	26.3	0.0851
	F_2	1936	198.5	0.1025
	F_3	2594	123.7	0.0477
	F_4	3603	104.7	0.0291
central rounded				
[ʉ]				
	F_1	306	43.2	0.1413
	F_2	1004	95.7	0.0953
	F_3	2399	173.8	0.0725
	F_4	3400	164.7	0.0484

Figure 1 represents the (F_1, F_2) means of the 18 CVs as pronounced by WJ for the purposes of the experiment, each point being a two-element vector representing the grand means of F_1 and F_2 of the 18 CVs.

4. Statistical discriminant analysis

The four discriminant linear combinations $w_1 \ldots w_4$ have been calculated. Their values expressed in terms of $F_1 \ldots F_4$ are as follows:

$$w_1 = -0.0068672 * F_1 + 0.0094832 * F_2 - 0.00081388 * F_3 + 0.00096338 * F_4 \quad (1)$$

$$w_2 = -0.023943 * F_1 - 0.27703 * F_2 + 0.0011695 * F_3 - 0.00084285 * F_4 \quad (2)$$

$$w_3 = -0.0015498 * F_1 - 0.0015240 * F_2 + 0.0082357 * F_3 - 0.0045712 * F_4 \quad (3)$$

$$w_4 = 0.040886 * F_1 + 0.016195 * F_2 + 0.064314 * F_3 + 0.87861 * F_4. \quad (4)$$

The above exact relations between the values of the discriminant variables and the formant frequencies should be compared with the coefficients of determination between the discriminant variables and the formant frequencies:

Table 4. Coefficients of determination between the formant frequencies and the calculated discriminant variables

	w_1	w_2	w_3	w_4
F_1	7.8	90.9	0.8	0.5
F_2	89.5	7.2	0.9	2.4
F_3	1.8	1.1	97.0	0.1
F_4	4.1	1.6	6.4	87.9

It transpires from equations (1)...(4) and the Table 4 that

The first discriminant variable w_1 *depends chiefly on* F_2, w_2 *on* F_1, w_3 *on* F_3 *and* w_4 *on* F_4.

The dependence of the discriminant variables on the formants may most simply be demonstrated by the following Table:

Table 5.

w_1 ——> $F_2 \rightarrow F_1 \rightarrow F_4 \rightarrow F_3$

w_2 ——> $F_1 \rightarrow F_2 \rightarrow F_4 \rightarrow F_3$

w_3 ——> $F_3 \rightarrow F_4 \rightarrow F_2 \rightarrow F_1$

w_4 ——> $F_4 \rightarrow F_2 \rightarrow F_1 \rightarrow F_3$

In Table 5, the *F*–frequencies are, in each row, arranged in order of decreasing effect.

We shall refrain, in this study, from presenting the mathematical foundations of Discriminant Analysis, as these may be found in various statistical texts such as LACHENBRUCH (1975) [16] KLECKA (1980) [13] or KRZYŚKO (1990) [14].

The discriminant variables are obtained, as can be seen above, as *linear combinations* of the original variables, so that each discriminant variable represents in varying degrees, each of the original variables. The discriminant variables are so calculated that they are uncorrelated and all their covariance matrices are unit matrices. As demonstrated above, it is usually he case that one discriminant variable (w_n) reflects one particular original variable more strongly than others.

Table 5 shows, in general terms, how the discriminant variables depend, in d e c r e a s i n g order, on the individual formant frequencies. The main advantage of the w_n's is that they make it possible to map the mean vectors of the classes under consideration *in a plane* though the original data vectors lie in a multidimensional space (four-dimensional in our case) since each object under observation has here been represented by measurements on four variables: F_1, F_2, F_3, and F_4.

The Mahalanobis distances were transformed into respective values of the T^2 statistic. The significance of the individual values of T^2 was verified using the method of simultaneous test procedure. The common critical value for T^2 in our case was $T^2_{(0.05)} = 112.14$.

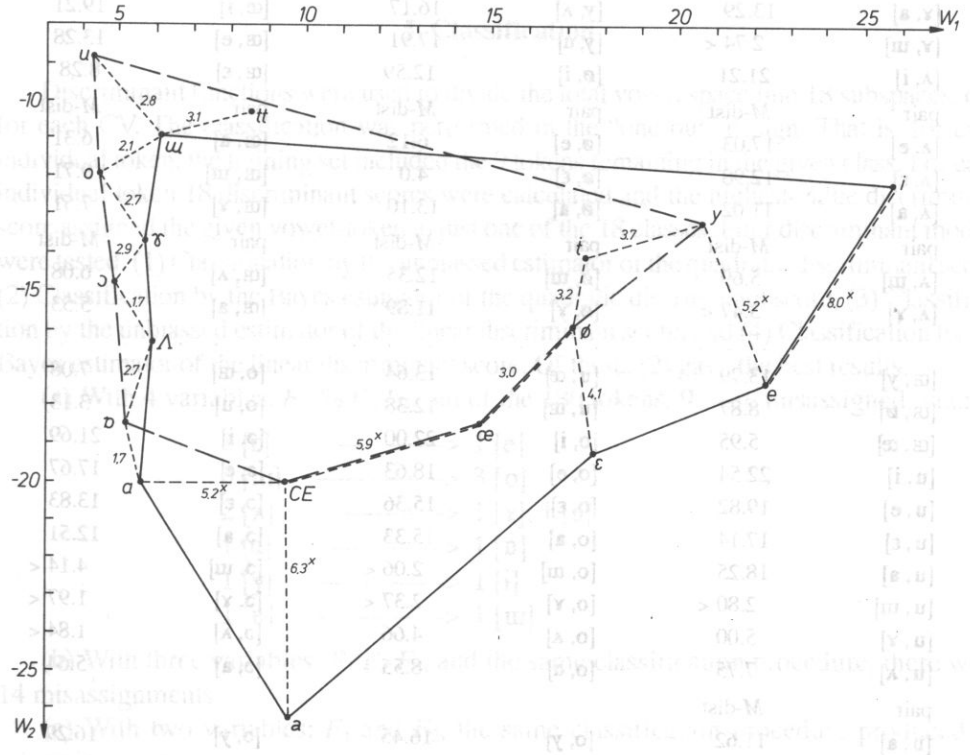

FIG. 1.

Out of the 153 distances between the mean vectors 14 were below the critical T^2 value, i.e., the 14 distances were not significantly different from 0. In Table 6 we give all the Mahanalobis distances ordered in columns rather than in a matrix arrangent in order to facilite the look-up. Those distances that at $\alpha = 0.05$ are not significantly different from 0 are marked <.

Table 6. Mahalanobis distances between the mean vectors

pair	*M*-dist	pair	*M*-dist	pair	*M*-dist
[e, i]	8.05	[ɑ, i]	22.18	[ø, ʌ]	12.52
[ɛ, i]	12.68	[ɑ, e]	17.59	[ø, ɑ]	13.67
[ɛ, e]	5.36	[ɑ, ɛ]	13.05	[ø, y]	5.65
[a, i]	22.38	[ɑ, a]	8.24	[œ, i]	14.86
[a, e]	15.91	[ɑ, ɯ]	9.58	[œ, e]	8.31
[a, ɛ]	10.75	[ɑ, ɤ]	7.30	[œ, ɛ]	4.10 <
[ɯ, i]	20.57	[ɑ, ʌ]	4.01 <	[œ, a]	10.44
[ɯ, e]	17.33	[y, i]	8.75	[œ, ɯ]	10.93
[ɯ, ɛ]	14.41	[y, e]	5.29	[œ, ɤ]	9.91
[ɯ, a]	15.73	[y, ɛ]	7.87	[œ, ʌ]	10.15
[ɤ, i]	21.10	[y, a]	18.07	[œ, ɑ]	10.10
[ɤ, e]	17.02	[y, ɯ]	14.81	[œ, y]	8.37
[ɤ, ɛ]	13.39	[y, ɤ]	15.16	[œ, ø]	2.99 <
[ɤ, a]	13.29	[y, ʌ]	16.17	[œ, i]	19.21
[ɤ, ɯ]	2.74 <	[y, ɑ]	17.91	[ɶ, e]	13.28
[ʌ, i]	21.21	[ø, i]	12.59	[ɶ, ɛ]	8.28
pair	*M*-dist	pair	*M*-dist	pair	*M*-dist
[ʌ, e]	17.03	[ø, e]	6.12	[ɶ, a]	6.31
[ʌ, ɛ]	12.98	[ø, ɛ]	4.0	[ɶ, ɯ]	9.71
[ʌ, a]	11.02	[ø, a]	13.10	[ɶ, ɤ]	7.51
pair	*M*-dist	pair	*M*-dist	pair	*M*-dist
[ʌ, ɯ]	5.69	[ø, ɯ]	12.35	[ɶ, ʌ]	6.08
[ʌ, ɤ]	3.47 <	[ø, ɤ]	11.89	[ɶ, a]	5.53
	. . .	. . .	. . .	. . .	
[ɶ, y]	13.79	[u, œ]	13.64	[o, ɶ]	7.08
[ɶ, ø]	8.87	[u, ɶ]	12.38	[o, u]	3.13
[ɶ, œ]	5.95	[o, i]	22.00	[ɔ, i]	21.69
[u, i]	22.54	[o, e]	18.63	[ɔ, e]	17.67
[u, e]	19.82	[o, ɛ]	15.36	[ɔ, ɛ]	13.83
[u, ɛ]	17.14	[o, a]	15.33	[ɔ, a]	12.51
[u, a]	18.25	[o, ɯ]	2.06 <	[ɔ, ɯ]	4.14 <
[u, ɯ]	2.80 <	[o, ɤ]	2.37 <	[ɔ, ɤ]	1.97 <
[u, ɤ]	5.00	[o, ʌ]	4.66	[ɔ, ʌ]	1.84 <
[u, ʌ]	7.75	[o, ɑ]	8.55	[ɔ, a]	5.64
pair	*M*-dist				
[u, a]	11.62	[o, y]	16.45	[ɔ, y]	16.29
[u, y]	16.90	[o, ø]	13.72	[ɔ, ø]	10.64

[cont. Tabl. 6]

[u, ø]	14.89	[o, œ]	11.98	[ɔ, œ]	7.23
[ɔ, ɶ]	7.23	[a, ɔ]	4.38 <	[ʉ, i]	18.71
[ɔ, u]	6.03	[i, i]	11.01	[ʉ, e]	15.40
[ɔ, o]	2.94 <	[i, e]	6.56	[ʉ, ɛ]	12.94
[ɒ, i]	21.82	[i, ɛ]	6.51	[ʉ, a]	16.13
[ɒ, e]	17.67	[i, a]	15.61	[ʉ, ɯ]	3.13 <
[ɒ, ɛ]	13.42	[i, ɯ]	11.63	[ʉ, ɤ]	4.76
[ɒ, a]	9.81	[i, ɤ]	11.86	[ʉ, ʌ]	7.64
[ɒ, ɯ]	8.19	[i, ʌ]	12.93	[ʉ, a]	11.16
[ɒ, ɤ]	6.13	[i, a]	14.76	[ʉ, y]	12.48
[ɒ, ʌ]	2.75 <	[i, y]	3.67 <	[ʉ, ø]	10.24
[ɒ, ɑ]	1.73 <	[i, ø]	3.22 <	[ʉ, œ]	9.36
[ɒ, y]	17.55	[i, œ]	5.47	[ʉ, ɶ]	9.84
[ɒ, ø]	13.64	[i, ɶ]	10.70	[ʉ, u]	4.94
[ɒ, œ]	11.12	[i, u]	13.90	[ʉ, o]	5.14
[ɒ, ɶ]	6.19	[i, o]	13.26	[ʉ, ɔ]	6.45
[ɒ, u]	10.12	[i, ɔ]	12.99	[ʉ, a]	10.01
[ɒ, o]	7.09	[i, ɒ]	14.36	[ʉ, i]	9.26

5. Classification

Discriminant functions were used to divide the total vowel space into 18 subspaces, one for each CV. The classification was performed in the "one out" design. That is, for each individual token, the training set included the 9 tokens remaining in the given class. For each individual token 18 discriminant scores were calculated and the highest-value discriminant score assigned the given vowel-token to just one of the 18 classes. Four discriminant models were tested: (1) Classification by the unbiassed estimator of the quadratic discriminant score, (2) Classification by the Bayes estimator of the quadratic discriminant score, (3) Classification by the unbiassed estimator of the linear discriminant score, and (4) Classification by the Bayes estimator of the linear discriminant score. Of these, (2) gave the best results:

(a) With 4 variables, $F_1 F_2 F_3 F_4$, out of the 180 tokens, 9 were misassigned, viz.:

1 [ɛ] ——————> 1 [e]
3 [ɯ] ——————> 3 [o]
2 [ʌ] ——————> 1 [ɤ], 1 [ɔ]
1 [ɑ] ——————> 1 [ɒ]
1 [y] ——————> 1 [i]
1 [ʉ] ——————> 1 [ɯ]

(b) With three variables: $F_1 F_2 F_3$, and the same classification procedure, there were 14 misassignments.

(c) With two variables: F_1 and F_2, the same classification procedure produced 19 misassignments.

6. Conclusions

The total 4–D vowel space can be divided into 18 subspaces representing the 18 Cardinal Vowels such that only about 5% of individual isolate voicings are erroneously assigned. In a 3–D space the error is about 8%. With only two variables, F_1 and F_2, the error is increased to almost 10%. So, in order to procure fewer mistakes, especially with fewer variables, such as F_1 and F_2, the statistical dispersions would have to be distinctly smaller than in the present materials.

References

[1] W.A. AINSWORTH, *Intrinsic and extrinsic factors in vowel judgement* in: Auditory analysis and perception of speech, [Eds.] G. Fant, M.A.A. Tatham, Academic Press, London 1975, 103–116.

[2] L. ARMSTRONG, D. JONES, *The phonetics of French*, G. Bell and Sons Ltd., London 1951.

[3] A. BUTCHER, *Cardinal Vowels and other problems*, in: Linguistic controversies, [Ed.] D. Crystal, E. Arnold, London 1982, 50–71.

[4] J.C. CATFORD, *Observations on the recent history on vowel classification*, in: Towards a history of phonetics. [Eds.] R.E. Asher and E.J. Henderson, Edinburgh University Press, Edinburgh 1981, 19–31.

[5] J.C. CATFORD, *A practical introduction to phonetics*, The Clarendon Press, Oxford 1988.

[6] P. DELATTRE, A.M. LIBERMAN, F.S.COOPER, *Voyelles systhétique a deux formantes et voyelles cardinales.* Le Maitre Phonetique, ser. 3, No. 96, 30–35 1951.

[7] *Fundamentos de escritura fonetica*, [Eds.] D. Jones and I. Dahl, Secretaria de la Asociacion Fonetics Internacional, London 1944.

[8] A.C. GIMSON, *The introduction to the pronounciation of English*, 4th ed. rev. S. Ramsaran, E. Arnold, London 1988.

[9] W. JASSEM, *Fundamentals of acoustic phonetics* (in Polish), PWN, Warszawa 1973.

[10] W. JASSEM, *The phonology of modern English*, PWN, Warszawa 1984.

[11] D. JONES, *An outline of English phonetics*, 8th ed. Heffner, Cambridge 1956.

[12] D. JONES, D. WARD, *The phonetics of Russian*, Cambridge University Press, Cambridge 1969.

[13] W. KLECKA, *Discriminant analysis*, Sage Publications, Beverly Hills 1980.

[14] M. KRZYSKO, *Discriminant analysis* (in Polish) 2nd ed. WNT, Warszawa 1990.

[15] W. LABOV, *Sources of inherent variation in the speech process*, in: Invariance and variability in speech processes, [Eds.] J. Perkell and D. Klatt, L. Erblaum, Hillside 1986, 402–423.

[16] P.A. LACHENBRUCH, *Discriminant analysis*, Hafner, New York 1975.

[17] P. LADEFOGED, D.E. BROADENT, *Information conveyed by vowels*, Journ. Acoust. Soc. Am., **9**, 98–104 1957.

[18] H.B. LEE, *A remark on the IPA Cardinal Vowels*. Le Maitre Phonetique III/130, 26–29 (1968).

[19] M. NEAREY, *Phonetic feature systems for vowels*, Indiana Univ. Linguistic Club, Bloomington, Indiana 1978.

[20] *The principles of the International Phonetic Association*, International Phonetic Association, London 1949.

[21] G. PAPCUN, *How do different speakers say the same vowels?* UCLA Working Papers in Phonetics No. 49, Los Angeles 1980.

[22] R. PLOMP, C.W. POLS, VAN DE GEER, *Dimensional analysis of vowel spectra*, Journ. Acoust. Soc. of America **41**, 707–712 (1967).

[23] P. ROACH, *English phonetics and phonology*, Cambridge University Press, Cambridge 1953.

[24] A.Q. SUMMERFIELD, M.P. HAGGARD, *Vocal tract normalization as demonstrated by reaction times*, in: Auditory analysis and perception of speech, [Eds.], G. Fant, M.A.A.A. Tatham, Academic Press, London 1975, 115–141.

Received December 31, 1991

ARCHIVES OF ACOUSTICS
17, 3, 357–374 (1992)

MEASUREMENTS OF DISPERSION OF ULTRASONIC WAVE VELOCITY IN THIN LAYERS BY THE ULTRASONIC SPECTROSCOPY

W. WOJDOWSKI

Institute of Fundamental Technological Research
Polish Academy of Sciences
(00-049 Warszawa, Świętokrzyska 21)

This paper presents the results of measurements of the phase velocity dispersion of ultrasonic waves in thin aluminium sheets. The interaction between ultrasonic waves and a thin solid layer is analysed and the theoretical relations for the transmission and reflection coefficients are presented. Experiments are based on the spectrum analysis of ultrasonic pulses, generated by the broad-band probes in the frequency range of 2–13 MHz. From the maxima of transmission coefficients for different incidence angles the phase velocity of Lamb waves is determined as a function of ultrasonic wave frequency.

Presented method allows to determine the acoustic parameters and the dispersion curves for the velocity of Lamb waves in thin layers.

1. Introduction

The use of new materials in many branches of technology has been an incentive to further the ultrasonic methods of testing materials, especially those nonhomogeneous ones such as composites. Some of their properties, such as strength, resistence to fracture, thermal and electrical parameters largely depend on the current state of their internal structure. Suitable measurement techniques have therefore to be developed to ossess the quality of such materials. It is the ultrasonic methods, based on the interaction of waves and nonhomogeneous media, that have found many applications in the field [1].

Complexity of phenomena that take place during the wave propagation in a multicomponent medium is one of the reasons for the difficulties in proper interpretation of measurement results. The most difficult problem is to separate the geometrical effects that influence the ultrasonic wave parameters from those connected with the material structure and the boundary conditions at the interfaces of various materials. In particular, the response of laminates and adhesive connections is of interest since the relevant properties largely depend on the character of contacting surfaces. The measurement techniques are mainly based on the resonance in layers [2] and on the generation of

a number of Lamb wave modes [3, 4] caused by the incident ultrasonic wave. The Lamb waves are known to disperse considerably, i.e. their velocities are very sensitive to the frequencies. Dispersion curves are functions of material structure as well as boundary conditions on the surfaces. These, in turn, can vary with the changes in properties of glued connections and with the types of connected surfaces. Measurements of ultrasonic wave velocity dispersion are on the means to evaluate the quality of nonhomogeneous materials [4].

However, due to the complexity of involved phenomena and considerable difficulties in the interpretation of test data, some advanced measurement procedure must be employed in which the ultrasonic signals are analysed and digital data processing is used [5].

The present paper is devoted to the application of ultrasonic spectrum analysis in the determination of phase velocity dispersion curves for this layers of materials. The measurement apparatus and broad-band probes were used as described in [6, 7]. Measurement results are compared with theoretical predictions. Accuracy and resolution of the presented results are also assessed.

2. Transmission of ultrasonic waves through a thin material layer. Basic theoretical relationships

The motion equation for the transmission of harmonic acoustic waves in an infinite isotropic medium has the form [8]

$$(\lambda + 2\mu)\Delta v + (\lambda + \mu)\nabla \times (\nabla \times v) = -\omega^2 \rho v \tag{1}$$

where λ, μ – Lamé's constants, v – particle velocity, ω – wave frequency, ρ – density of the medium. As known from the vector analysis, every vector field can be decomposed into two parts solenoidal and irrotational ones

$$v = v_1 + v_2 = \nabla \Phi + \nabla \times \Pi \tag{2}$$

where Φ and Π are the scalar and the vector potentials respectively. For the solenoidal field we have

$$\nabla \times v_1 = \nabla \times (\nabla \Phi) = 0 \tag{3}$$

whereas for the irrotational one the following applies:

$$\nabla v_2 = \nabla (\nabla \times \Pi) = 0 \tag{4}$$

The solenoidal field v_1 corresponds to a longitudinal acoustic wave, associated with volumetric changes of the medium, whereas the irrotational field v_L corresponds to a transverse, or shear, wave for which the volume remains constant. The equation (1) can be replaced by two equations for potentials Φ and Π

$$\begin{aligned} \Delta \Phi + k_L^2 \Phi &= 0 \\ \Delta \Pi + k_T^2 \Pi &= 0 \end{aligned} \tag{5}$$

where k_L – wave number for longitudinal wave, ($k_L = \omega / c_L$), k_T – wave number for shear

wave, ($k_T = \frac{\omega}{c_T}$, c_L and c_T – longitudinal and shear wave velocities in the medium, expressed in terms of Lamé's constants as

$$c_L = \sqrt{\frac{\lambda + 2\mu}{\rho}},$$

$$c_T = \sqrt{\frac{\mu}{\rho}}.$$

Consider a case in which an acoustic wave transmitted in a fluid medium impinges a solid isotropic layer of thickness h at an incidence angle θ. The direction of waves can be defined with the use of the wave vector $\mathbf{k}$, where $|\mathbf{k}| = \omega/c$ and c denotes the velocity of longitudinal waves in the fluid. To determine the transmission coefficient through the layer, the coordinate system and notation will be used as shown in Fig. 1. The longitudinal wave from the medium I impinges at an angle θ and is refracted in the layer (medium II) to be transmitted at an angle θ_L as a longitudinal wave and at an angle θ_T as a transverse wave. These waves are reflected at the lower and upper interfaces. A part of the wave energy is transmitted to the fluid medium III. Ratio of the amplitude in medium III to the amplitude of incident wave is a measure of the transmission coefficient through the layer.

Assume the media I and III to be identical and the longitudinal acoustic wave impinge in the x, z – plane (Fig. 1), i.e. the velocity components v_y vanish. According to the formula (2) the scalar potential Φ cannot depend on the coordinate y and the vector potential has to depend on Π_y only, $\Pi = [0, \Pi_y, 0]$.

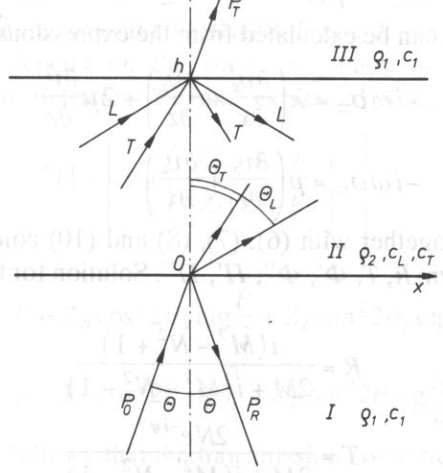

FIG. 1. Coordinate axes and notation for the transmission of ultrasonic waves through a layer.

Acoustic pressures of an incident, reflected and transmitted wave can be shown in the following forms:

$$\begin{aligned} p_0 &= \exp[ik_1(x\sin\theta + z\cos\theta)] \\ p_R &= R\exp[ik_1(x\sin\theta - z\cos\theta)] \\ p_T &= T\exp[ik_1(x\sin\theta + z\cos\theta)] \end{aligned} \tag{6}$$

where p_0, p_R, p_T are the pressure amplitudes of incident reflected and transmitted waves, respectively, R, T denote the reflection and transmission coefficients, $k_1 = \omega/c_1$ is a wave number for the medium I, c, is the wave velocity in the medium I.

The particle velocities in the layer can be derived from the formula (2) and calculated as

$$\begin{aligned} v_x &= \frac{\partial \Phi}{\partial x} - \frac{\partial \Pi_y}{\partial z} \\ v_z &= \frac{\partial \Phi}{\partial z} - \frac{\partial \Pi_y}{\partial x} \end{aligned} \tag{7}$$

The potentials Φ and Π for the transmission of waves in the layer have the form

$$\begin{aligned} \Phi &= \Phi'\exp[ik_L(x\sin\theta_L + z\cos\theta_L] + \Phi''\exp[ik_L(x\sin\theta_L - z\cos\theta_L)] \\ \Pi_y &= \Pi'\exp[ik_T(x\sin\theta_T + z\cos\theta_T] + \Pi''\exp[ik_T(x\sin\theta_T - z\cos\theta_T)] \end{aligned} \tag{8}$$

The angles θ, θ_L, θ_T satisfy the Snell's rule

$$k_L\sin\theta_L = k_T\sin\theta_T = k_1\sin\theta.$$

The following boundary conditions must hold true at the interfaces between the media I, II and II, III: continuity of z–components of velocities and stresses and the absence of shearing stresses at $z = 0$ and $z = h$. This is expressed by

$$\begin{aligned} &v_z^I = v_z^{II}, \quad \sigma_{zz} = -(p_0 + p_R); \quad \sigma_{xz} = 0 \qquad \text{for } z = 0, \\ &v_z^{II} = v_z^{III}; \quad \sigma_{zz} = -p_T; \qquad\quad \sigma_{xz} = 0 \qquad \text{for } z = h. \end{aligned} \tag{9}$$

The stream components can be calculated from the expressions [8]

$$\begin{aligned} -i\omega\sigma_{zz} &= \lambda\left(\frac{\partial v_x}{\partial x} + \frac{\partial v_z}{\partial z}\right) + 2\mu\frac{\partial v_z}{\partial z} \\ -i\omega\sigma_{xz} &= \mu\left(\frac{\partial v_x}{\partial z} + \frac{\partial v_z}{\partial x}\right) \end{aligned} \tag{10}$$

The equations (9) together with (6), (7), (8) and (10) constitute a set of six linear equations in six unknown: R, T, Φ', Φ'', Π', Π''. Solution for the coefficients R and T is the following:

$$\begin{aligned} R &= \frac{i(M^2 - N^2 + 1)}{2M + i(M^2 - N^2 - 1)} \\ T &= \frac{2Ne^{-i\varphi}}{2M + i(M^2 - N^2 - 1)} \end{aligned} \tag{11}$$

where

$$N = \frac{Z_{2l}}{Z_1}\frac{\cos^2 2\theta_T}{\sin P} + \frac{Z_{2T}}{Z_1}\frac{\sin^2 2\theta_T}{\sin Q}$$

$$M = \frac{Z_{2l}}{Z_1}\cos^2 2\theta_T \operatorname{ctg} P + \frac{Z_{2T}}{Z_1}\sin^2 2\theta_T \operatorname{ctg} Q$$

$$\varphi = k_1 h\cos\theta;\quad P = k_L h\cos\theta_L;\quad Q = k_T h\cos\theta_T$$

$$Z_1 = \frac{\rho_1 c_d}{\cos\theta};\quad Z_{2l} = \frac{\rho_2 c_L}{\cos\theta_L};\quad Z_{2T} = \frac{\rho_2 c_T}{\cos\theta_T}$$

$$\cos\theta_L = \sqrt{1 - \frac{c_L^2}{c_1^2}\sin^2\theta};\quad \cos\theta_T = \sqrt{1 - \frac{c_T^2}{c_1^2}\sin^2\theta}$$

When the incident angle θ is greater than the critical angle for either a longitudinal or transverse wave, the magnitudes $\cos\theta_L$ and $\cos\theta_T$ become purely imaginary and the following formulae should be used in the solution (11)

$$\cos\theta_L = i\sqrt{\frac{c_L^2}{c_1^2}\sin^2\theta - 1}$$

$$\cos\theta_T = i\sqrt{\frac{c_T^2}{c_1^2}\sin^2\theta - 1}$$

$$\begin{aligned} \sin P &= i\sinh(\operatorname{Im} P) \\ \sin Q &= i\sinh(\operatorname{Im} Q) \\ \operatorname{ctg} P &= -i\operatorname{ctgh}(\operatorname{Im} P) \\ \operatorname{ctg} Q &= -i\operatorname{ctgh}(\operatorname{Im} Q) \end{aligned} \tag{12}$$

Both reflection and transmission coefficients R and T are complex numbers; their amplitudes and phases depend on the wave frequency $\omega = 2\Pi f$. Using (11), the amplitude of transmission coefficient T can be expressed in the form [9]

$$|T| = \left[1 + \left(\frac{Z_1^2 - E\cdot F}{\frac{1}{2}Z_1(E+F)}\right)^2\right]^{-1} \tag{13}$$

where

$$E = Z_{2l}\cos^2 2\theta_T \operatorname{ctg}\frac{P}{2} + Z_{2T}\sin^2 2\theta_T \operatorname{ctg}\frac{Q}{2}$$

$$F = Z_{2l}\cos^2 2\theta_T \operatorname{tg}\frac{P}{2} + Z_{2T}\sin^2 2\theta_T \operatorname{tg}\frac{Q}{2} \tag{14}$$

From the formula (13) it follows that the transmission coefficient attains its maximum, i.e. equals unity, when

$$E \cdot F = Z_1^2 \tag{15}$$

In the case of acoustic impedance of a medium on both sides of the layer approaching zero ($Z_1 \approx 0$), the formula (15) furnishes $EF = 0$, that is either $E = 0$ or $F = 0$. Remembering (14), we arrive at the equations

$$\frac{\operatorname{ctg}\frac{P}{2}}{\operatorname{ctg}\frac{Q}{2}} = -\frac{Z_{2T}}{Z_{2l}} \operatorname{tg}^2 2Q_T$$

$$\frac{\operatorname{tg}\frac{P}{2}}{\operatorname{tg}\frac{Q}{2}} = -\frac{Z_{2T}}{Z_{2l}} \operatorname{tg}^2 2Q_T \tag{16}$$

After a number of trigonometric rearrangements the equations (16) can be shown to be identical with the dispersion equations for the symmetric and antisymmetric modes of Lamb waves, presented in [10].

Thus, when the wave impedance of the solid layer is much larger than the impedance of the fluid from which the wave travels (i.e. Z, can be neglected in comparison with Z_{2L} and Z_{2T}) the maximum values of the transmission coefficient generate definite modes of Lamb waves in the layer. The above statement amounts to the so-called coincidence rule [9]. The amplitude of vibrations is at its largest for such incidence angles for which a resonance leads to the generation of a Lamb wave mode. The vibration energy is partially transmitted with relatively large amplitude are generated there. The transmission coefficient through the layer assumes its maximum value. The amplitude of reflected wave is also relatively large but, since its phase is opposite to that of the incident wave, the corresponding reflection coefficient attains its maximum.

When the maximum of the transmission coefficient corresponds to the incidence angle θ and the frequency f, a Lamb wave mode is generated in the layer. Projection of the incident wave vector is equal to the wave vector of the mode, Fig. 2. This means that

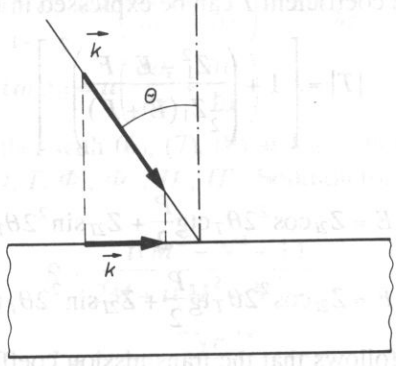

FIG. 2. Wave vector of Lamb wave **k** as a projection of incident wave vector **k**.

$|k_1|\sin\theta = |k|$, where $|k_1| = \frac{2\Pi f}{c_1}$; $|k| = \frac{2\Pi f}{c}$, c – phase velocity of the Lamb wave mode.

Hence

$$c = \frac{c_1}{\sin\theta} \tag{17}$$

Displacements of particles for a given mode of Lamb waves are given by the complicated expressions [10]. Qualitative and quantitative analyses of the motion of the medium transmitting Lamb waves are presented in [8]. Of special interest is the case in which the longitudinal wave impinges from the medium I at such an incidence angle that the resulting wave in the layer is transmitted at 45°, Fig. 3. In this case the mode is termed the Lamé mode [8] and consists of a purely transverse wave that is reflected at 45° from both faces of the layer. Simple geometrical relationships apply in this case:

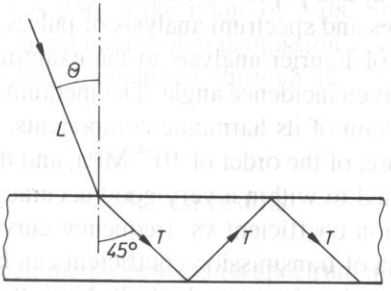

FIG. 3. Lamb mode - transverse wave travels in the layer at 45°.

$$\frac{\sin\theta}{c_1} = \frac{\sqrt{2}}{2c_T} \quad \text{– Snell's law}$$

$$\frac{2\Pi f}{c_T} \cdot \frac{\sqrt{2}}{2} = n \cdot \Pi, \quad n = 1, 2, 3 \quad \text{– boundary conditions on the layer interface [8].}$$

On combining the two above expressions, we get the formula

$$\sin\theta = \frac{n \cdot c_1}{2f \cdot h} \tag{18}$$

This is the condition for the incidence angle of longitudinal wave, expressed in terms of frequency, necessary for the transmission of a purely transverse wave inclined at 45°, i.e. the presence of Lamé's mode. This condition will be used further on to determine the velocities of transverse waves in solid layers.

3. Concept of measurements

The formula (17) determines the phase velocity of Lamb waves generated in a solid layer by a longitudinal ultrasonic wave impinging from a fluid at an angle θ. The wave velocity in the fluid is denoted by c_1.

It follows from previous considerations that a given mode of Lamb waves can only be generated under specific frequency of incident waves and for a specific incidence angle. From the coincidence rule it follows that the maximum of transmission coefficient is associated with those magnitudes. Knowing the suitable incidence angle θ and the frequency f the phase velocity of Lamb mode can be calculated from (17). Lamb waves exhibit dispersion, i.e. their phase velocities depend on frequencies, see expressions (16).

Complete picture is complicated. Nevertheless, experimental determination of dispersion curves is possible with the help of various measuring techniques. In general, the reflection or the transmission coefficients are measured for fixed frequencies and various incidence angles [3, 9]. Relevant curves have a number of maxima or minima that correspond to succesive Lamb modes. To obtain complete characteristics of velocity dispersions many ultrasonic probes must be available to emit waves with various frequencies.

Experiments described in this paper were made for a wide range of frequencies with the use of broad-band probes and spectrum analysis of pulses. The idea of measurements consists in the application of Fourier analysis to the examination of broad-band pulses generated in the layer at a given incidence angle. The medium is assumed to be linear, that is the ultrasonic pulse is a sum of its harmonic components. In the case of small amplitudes of the acoustic pressure, of the order of 10^{-4} MPa, and the wavelength of 1 mm, the linearity condition is satisfied to within a very good accuracy. The measurement results are presented as transmission coefficient vs. frequency curves. By broadly varying the incidence angle the maxima of transmission coefficient can be determined as depending on both the frequency and the incidence angle itself. Next, the formula (17) furnishes the phase velocity of Lamb waves for many modes simultaneously. As a result, the spectrum analysis method supplies a further picture of the velocity dispersion of Lamb waves than any other conventional method. It is also faster and more convenient to apply.

Computer program was prepared, based on the relationships shown in Sec. 2, to compare the test measurements of transmission coefficient with theoretical predictions. The following input data were used: impedance of the layer and the surrounding media, wave velocities in all the media concerned, thickness of the layer and the incidence angle. The transmission coefficient was computed from the formula (13). Three ranges of the incidence angle were distinguished: smaller than the first critical angle, in between the first and the second critical angle and larger than the second critical angle. In the last two cases the relationships (12) were used.

4. Measuring system

The test apparatus consisted of transmitting and receiving broad-band probes [7], ultrasonic defectoscope, sampling converter, micro-computer and printer [6]. The transmitting band was 2–13 MHz (with the drop of 12 dB). The setup is shown in Fig. 4. The incidence angle was changed with the use of micrometer screw to within an accuracy of 0.1° and in the range of 0–34°. The testpieces were made of aluminium sheet metal 0.5 and 1 mm thick, immersed in water.

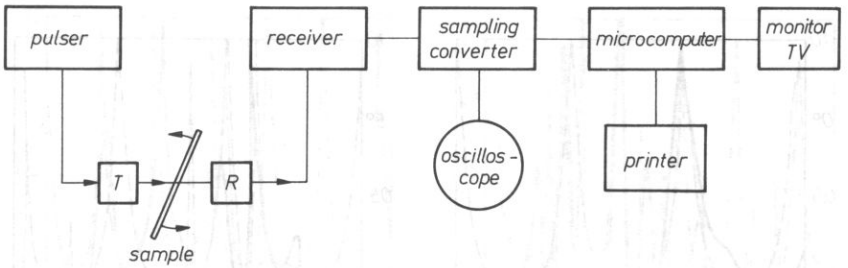

FIG. 4. Measuring set. T, R – broad-band transmitting and receiving probes.

Ultrasonic pulse transmitted through the layer was sampled and fed into the microcomputer. Fast procedure of Fourier transform enabled pulse spectra to be obtained. Sampling density was 256 in the range of 5 μs. Spectral lines were spaced at 0.2 MHz; resolution of measurements of transmission coefficient maxima was about ±0.1 MHz. Spectra of pulses transmitted through the layer were displayed on the monitor and printed.

5. Test results

Ultrasonic pulse between the probes and its spectrum are shown in Fig. 5. From the curves it follows that the useful range of frequencies is from 2 to 13 MHz. Its width is

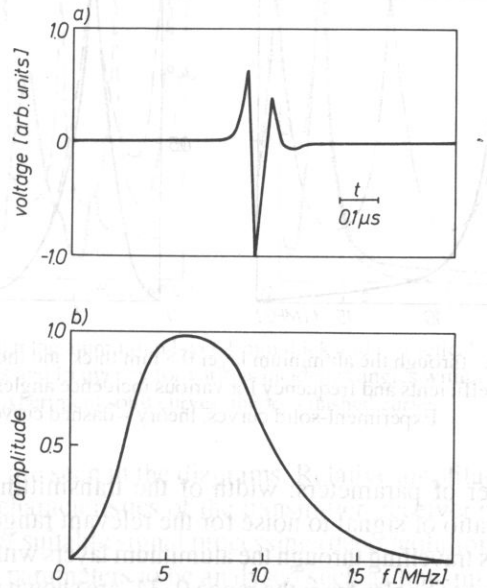

FIG. 5. a – Ultrasonic pulse between the probes at contact,
b – its spectrum.

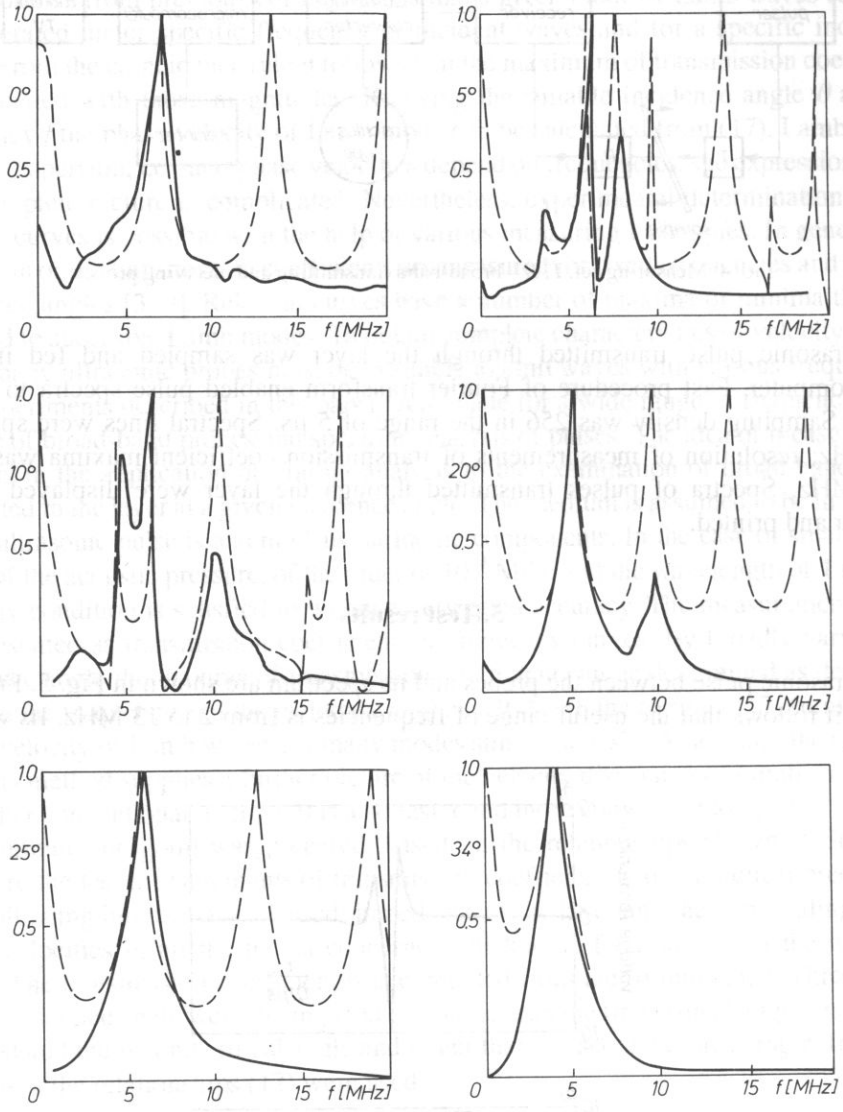

FIG. 6. Spectra of pulses through the aluminium layer 0.5 mm thick and theoretical relationships between the transmission coefficients and frequency for various incidence angles within the range of 0–34°. Experiment-solid curves, theory – dashed curves.

a result of a number of parameters: width of the transmitting band on pulser–probe–medium–receiver, ratio of signal to noise for the relevant range and sampling of signals.

Spectra of pulses travelling through the aluminium layers with thicknesses 0.5 and 1 mm at a number of incidence angles from the range 0–34° are shown in Figs. 6 and 7. Curves are also shown corresponding to the relationships between the transmission coefficients and frequencies, calculated with the use of computer program described in Sec. 4.

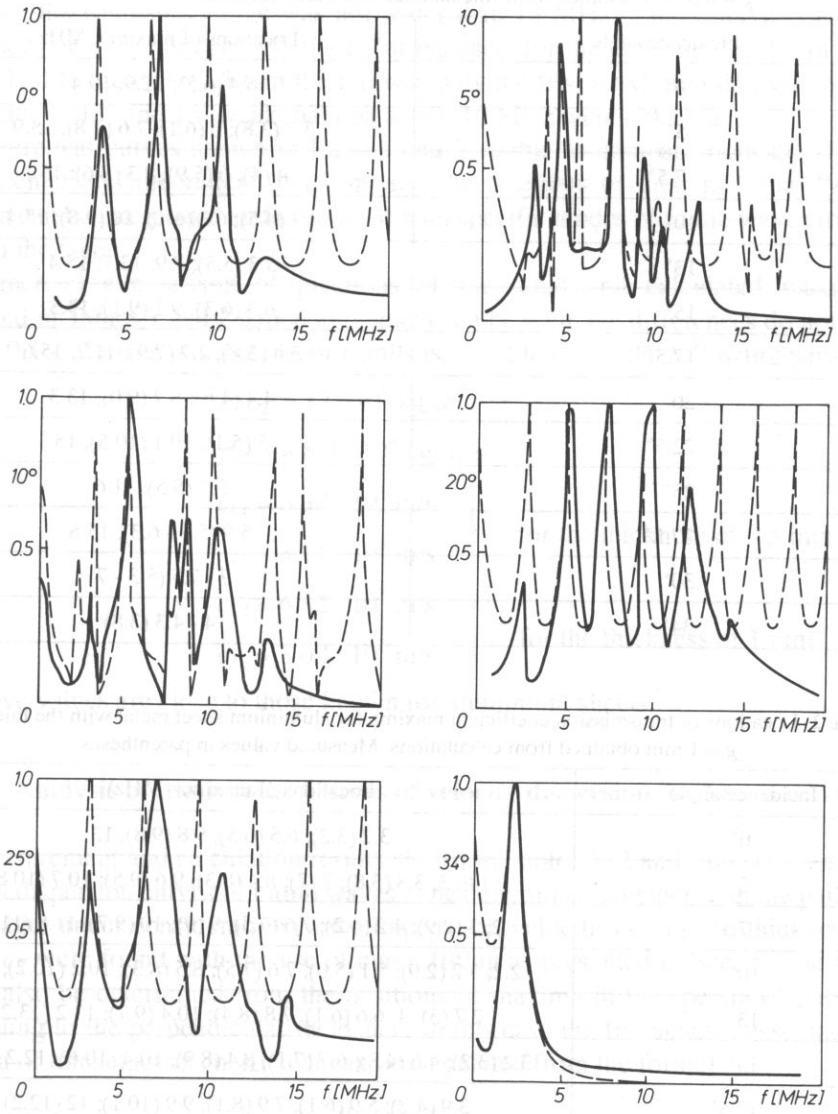

FIG. 7. Spectra of pulses through the aluminium layer 1 mm thick and theoretical relationships between the transmission coefficients and frequency for various incidence angles within the range of 0-34°. Experiment solid curves, theory - dashed curves.

A number of maxima are seen in the diagrams. Relative amplitudes of those maxima depend on the spectrum characteristics of the transmitter–receiver system which can be accounted for by means of suitable signal processing (deconvolution process). However, this would require all the parameters to be analysed such as transmission band, damping in the medium and to on. Presentation of results is here confined to the transmitted pulses since their maxima were of primary interest.

Table 1. Locations of transmission coefficient maxima for aluminium sheet metal with the thickness $g = 0.5$ mm obtained from calculations. Measured values in parantheses

Incidence angle	Locations of maxima (MHz)
0°	6.4 (6.5); 12.9; 19.4
5°	3.7 (3.8); 6 (6.1); 7.6 (7.8); 13.9
7.5°	4 (4); 6 (5.9); 8.3 (8.6); 15
10°	4.4 (4.5); 6.3 (6.1); 10 (9.8); 15.4
13°	5.3 (5.5); 7.9; 13.7; 15.4
15°	6.3 (6.3); 9.1 (9.1); 13.3
17.5°	3.4 (3.8); 7.7 (7.9); 11.7; 15.6
20°	4.4 (4.6); 8.7 (9.0); 13.3
22.5°	5 (5.1); 10.1 (10.5); 15
25°	5.3 (5.5); 11.6
27.5°	5.9 (5.8 - 6.3); 15.8
30°	7 - 7.5 (5.3 - 7)
34°	4 - 4.3 (3.8)

Table 2. Locations of transmission coefficient maxima for aluminium sheet metal with the thickness $g = 1$ mm obtained from calculations. Measured values in parentheses

Incidence angle	Locations of maxima (MHz)
0°	3.2 (3.2); 6.5 (6.5); 9.8 (9.8); 13
5°	1.8; 3; 3.8 (3.8); 7 (7); 8.4 (8.3); 9.6 (9.5); 10.7 (10.8)
7.5°	2; 3 (2.9); 4.2 (4.2); 7.6 (7.5); 9 (9); 10 (9.7); 11.8 (11.7)
10°	2.2; 3.2 (2.9); 5.1 (5.0); 7.6 (7.5); 8.5 (8.3); 10.2 (10.2); 11.3
13°	2.7 (3); 4; 6.6 (6.1); 7.8 (8.4); 10.4 (9.7); 13.2 (13.2)
15°	3.2 (3.2); 4.6 (4.8); 6.7 (7.1); 8.4 (8.9); 10.4 (10.6); 12.2 (12.4)
17.5°	3.9 (4.2); 5.9 (6.1); 7.9 (8.1); 9.9 (10.1); 12 (12.2)
20°	2.2 (2.3); 4.4 (4.4); 6.7 (6.9); 8.9 (9.2); 11.2 (11.4)
22.5°	2.5 (2.6); 5.1 (5.4); 7.6 (7.9); 10.2 (10.5); 12.8 (13.2)
25°	2.7 (2.8); 5.9 (6.7); 9.1 (10.2)
27.5°	3 (3-3.4); 8
30°	3.7 (3.7)
34°	2 - 2.2 (2.1 - 2.3)

Since the frequency range was not wider than 13 MHz, higher maxima had small amplitudes or were not detected at all. For instance, for the incidence angles of 90° and 25° applied to the layer 0.5 mm thick it was only the first maximum that was obtained. For angles of 13° and 15° weak maxima above 10 MHz were detected.

Theoretical curves shown in Figs. 6 and 7 enable to compare both the shapes of experimental and theoretical diagrams and the positions of their maxima. Particular maxima can be interpreted and associated with specific modes of Lamb waves travelling through the layer.

Numerical comparison of positions of measured and calculated maxima are presented in Tables 1 and 2. Good agreement can be seen, the differences do not usually exceed 0.1–0.2 MHz. The best fit of results is found to be for the following parameters:

$$\rho_2 c_L = 17 \cdot 10^6 \text{ kg/m}^2\text{s}$$

$$\rho_2 c_T = 8.3 \cdot 10^6 \text{ kg/m}^2\text{s}$$

$$\left.\begin{aligned} c_{L1} &= 6.37 \cdot 10^3 \text{ m/s} \\ c_{T1} &= 3.11 \cdot 10^3 \text{ m/s} \end{aligned}\right\} \text{ for the thickness of 0.5 mm}$$

$$\left.\begin{aligned} c_{L2} &= 6.32 \cdot 10^3 \text{ m/s} \\ c_{T2} &= 3.08 \cdot 10^3 \text{ m/s} \end{aligned}\right\} \text{ for the thickness of 1 mm}$$

the above values are close to those known for aluminium sheets.

6. Analysis of test results. Curves of velocity dispersion for Lamb waves

Measurement and calculation results shown in Tables 1, 2 and Figs. 6, 7 enable the velocity dispersion curves of Lamb waves to be determined together with the parameters of the layer under consideration (wave impedance, velocities c_L, c_T and thickness. Both c_L and c_T were found with the use of curve-fitting as presented in Sec. 5. The velocity c_L can also be determined from the positions of maxima in the spectra of pulses corresponding to the perpendicular incidence. In this case the frequencies associated with maxima of transmission coefficient can be calculated from the formula

$$f_{\max} = \frac{n \cdot c_L}{2 \cdot h}; \quad n = 0, 1, 2, 3 \tag{19}$$

Given the thickness h, c_L readily follows from the above relationships. The transverse wave velocities can be determined due to the fact that, in the case of Lamb mode, a purely transverse wave propagates at 45° in the layer. Remembering (18) given in Sec. 2, the angle can be obtained as a function of the frequency at which the Lamb mode is generated. This condition, combined with the relationship between the location of transmission maximum and the frequency leads to the velocity c_T. This can be seen in Figs. 8 and 9 where the maxima from Figs. 6 and 7 are shown for various incidence angles and the condition (18) for Lamb modes is indicated. The incidence angles for which Lamb

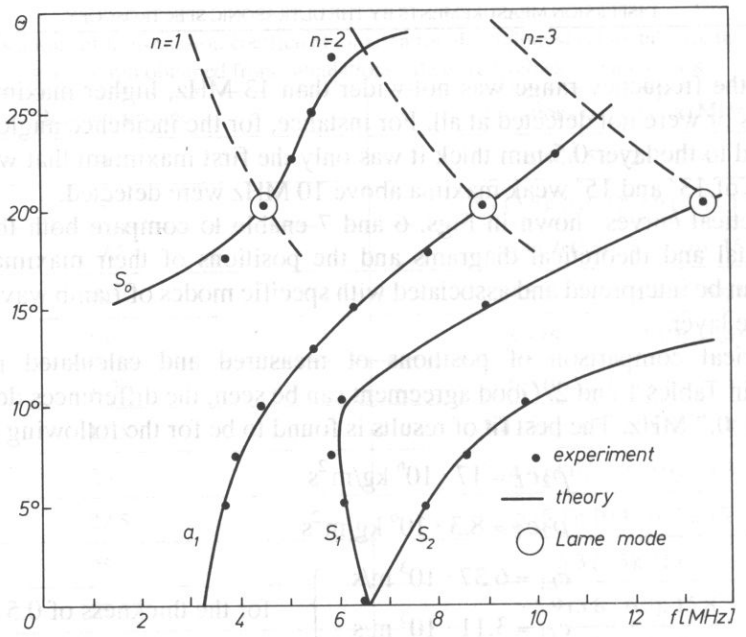

FIG. 8. Maxima of the transmission coefficient as a function of the incidence angle for the layer 0.5 mm thick. Curves applying to Lamb modes, formula (18) are shown dashed.

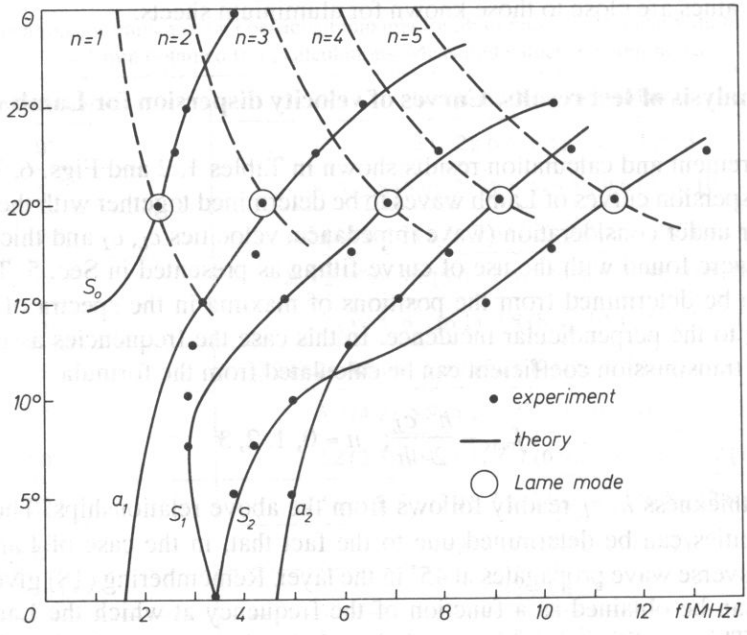

FIG. 9. Maxima of the transmission coefficient as a function of the incidence angle for the layer 1 mm thick. Curves applying to Lamb modes, formula (18), are shown dashed.

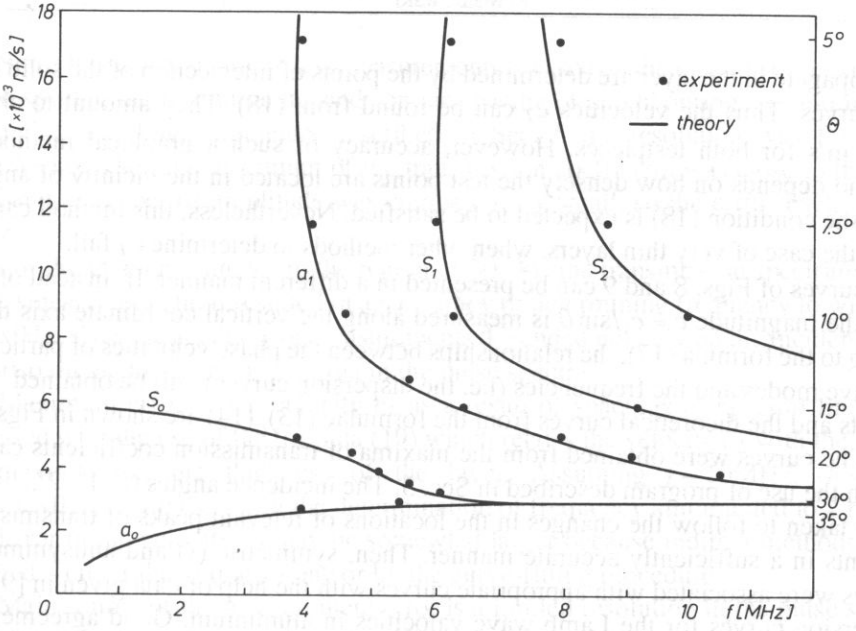

FIG. 10. Phase velocity dispersion curves for Lamb waves in the layer 0.5 mm thick.

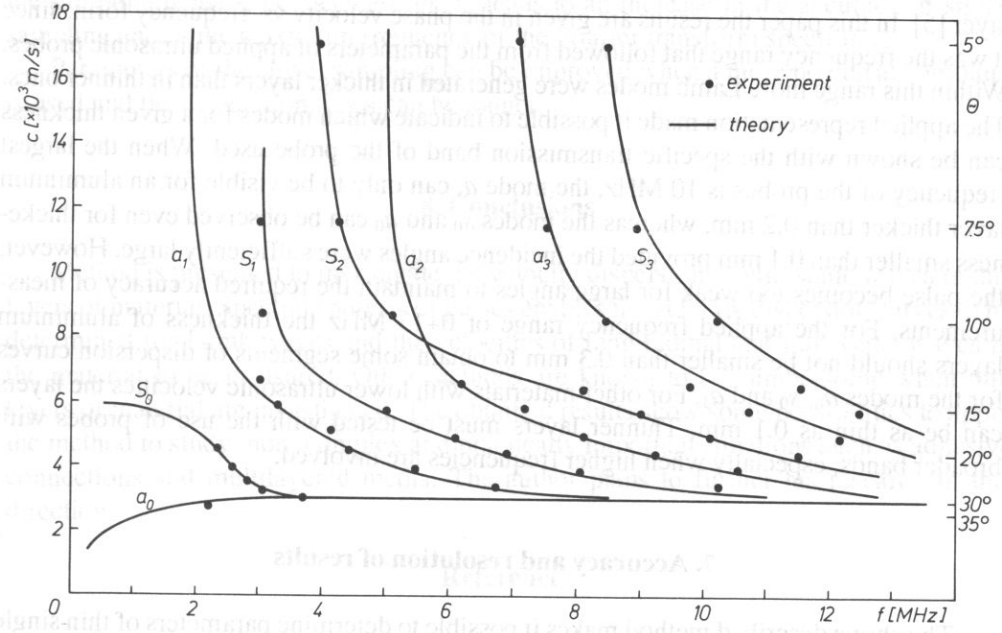

FIG. 11. Phase velocity dispersion curves for Lamb waves in the layer 1 mm thick.

waves propagate in the layer are determined by the points of intersection of the solid and dashed curves. Thus the velocities c_T can be found from (18). They amount to about 3.1×10^3 m/s for both testpieces. However, accuracy of such a graphical method is limited and depends on how densely the test points are located in the vicinity of angles at which the condition (18) is expected to be satisfied. Nevertheless, this method can be useful in the case of very thin layers, when other methods to determine c_T fail.

The curves of Figs. 8 and 9 can be presented in a different manner. If, instead of the angle θ, the magnitude $c = c_1/\sin\theta$ is measured along the vertical coordinate axis then, according to the formula (17), the relationships between the phase velocities of particular Lamb wave modes and the frequencies (i.e. the dispersion curves) will be obtained. The test results and the theoretical curves from the formulae (13), (14) are shown in Figs. 10 and 11. The curves were obtained from the maxima of transmission coefficients calculated with the use of program described in Sec. 3. The incidence angles 0°, 1°, 2°... up to 34° were taken to follow the changes in the locations of relevant peaks of transmission coefficients in a sufficiently accurate manner. Then, symmetric (s) and antisymmetric (a) modes were associated with appropriate curves with the help of data given in [9] for the dispersion curves for the Lamb wave valocities in aluminium. Good agreement is found between the measurements and the theoretical results. The differences do not exceed 0.1÷0.2 MHz, i.e., are within the accuracy of measurements.

It is common in the existing literature to represent the dispersion curves for the velocity of Lamb waves as a functions of a product of the frequency and the thickness of layer [5]. In this paper the results are given in the phase velocity vs. frequency form, since it was the frequency range that followed from the parameters of applied ultrasonic probes. Within this range more Lamb modes were generated in thicker layers than in thinner ones. The applied representation made it possible to indicate which modes for a given thickness can be shown with the specific transmission band of the probe used. When the largest frequency of the probes is 10 MHz, the mode a, can only to be visible for an aluminium layer thicker than 0.2 mm, whereas the modes s_0 and a_0 can be observed even for thickeness smaller than 0.1 mm provided the incidence angles were sufficiently large. However, the pulse becomes too weak for large angles to maintain the required accuracy of measurements. For the applied frequency range of 0÷13 MHz the thickness of aluminium layers should not be smaller than 0.3 mm to obtain some segments of dispersion curves for the modes a_0, s_0 and a_1. For other materials with lower ultrasonic velocities the layers can be as thin as 0.1 mm. Thinner layers must be tested with the use of probes with broader bands, especially when higher frequencies are involved.

7. Accuracy and resolution of results

The above described method makes it possible to determine parameters of thin single layers such as velocities of longitudinal and transverse acoustic waves. Phase velocity dispersion curves can also be found for various Lamb modes. It thus becomes necessary to evaluate the resolution and accuracy of the method.

Since the interpretation of test measurements is based on the location of maxima in the pulse spectra, the resolution depends on the spacing of neighbouring spectral lines. For the pulse sampling parameters described in Sec. 5 the resolution was found to be ±0.1 MHz. When the maximum of the transmission coefficient was close to the ends of the band of probe, its amplitude was comparatively small, so the error reached 0.2–0.9 MHz.

For the incidence angles in the region of 30÷34° the transmission spectrum maxima were smeared out and it resulted in an accuracy of determining frequency to within 0.2 - 0.3 MHz. Thus the accuracy of measurements depended not only on the incidence angles but also on the locations of maxima in the pulse spectra.

Maximum error in the velocity c_L as a result of spacings of spectral lines can be assessed with the use of the formula (19) which relates the velocity c_L with the locations of maxima and the thickness of the layer. Assuming $f \approx 10$MHz, $h \approx 0.5$mm, $f \approx 0.1$ MHz, relative error in the determination of frequency ammounted to 2 per cent.

Error in the velocity c_T may be somewhat larger because indirect methods are here applied – either the graphical one or by the curve-fitting procedure.

Main source of the measurement error is a limited resolution in the pulse sampling. Resolution and accuracy can be enhanced by increase in the length of the sampled signal and the density of sampling. Resolution of the frequency depends on the duration of sampled signal number of samples and is given by $\Delta f = 1/N\Delta t = 1/T$, where T is the signal period, N denotes the number of samples and Δt is their time spacing. Increase in the sampling density, i.e. decrease in Δt, leads to an increase in the accuracy of signal sampling and in the maximum frequency of the Fourier transform spectrum.

Parameters of the signal sampling can be improved when a more powerful computer is used and the calculation times can be longer.

8. Conclusions

Method is presented to investigate the velocity dispersion of ultrasonic waves in this layers of material. Spectral analysis of pulses enables the velocity dispersion curves to be determined for Lamb waves and the velocities of longitudinal and transverse waves in the material to be measured. Other methods are known to be cumbersome when thin layers of material are investigated. The obtained results show some possibilities to apply the method to study more complex and practically important situations such as adhesive connections and multilayered media. The author plans to further his research in this direction.

References

[1] E.G. HENNEKE, J.C. DUKE JR., *Analytical ultrasonics for evaluation of composite material response*, Mat. Eval., **43**, 740–745 (1985).

[2] I.C. COUCHMAN, F.H. CHANG, B.G. YEE, J.R. BELL, *Resonance splitting in ultrasonic spectroscopy*, IEEE Trans. Son. Ultr. **SU-25**, 293–300 (1978).

[3] B. BRIDGE, R. SUDIN, *A study of high frequency Lamb wave propagation in very thin metal foils and plates*, British J. of NDT, **31**, 425–436 (1989).
[4] A. PILARSKI, *Ultrasonic evaluation of the adhesion degree in layered joints*, Mat. Eval. **43**, 765–770 (1985).
[5] W.R. SCOTT, P.F. GORDON, *Ultrasonic spectrum analysis for nondestructive testing of layered composite materials*, J. Acoust. Soc. Am., **62**, 108–116 (1977).
[6] P. GUTKIEWICZ, Z. MOTTL, *Microcomputer system in frequency analysis of ultrasonic pulses* (in Polish) in Electric and Acoustic Methods of Investigations for Material and Biological Structures, IPPT-PAN, SEP, Warszawa–Jabłonna, 305–319 (1984).
[7] S. MACKIEWICZ, P. GUTKIEWICZ, Z. MOTTL, *Determination of damping coefficient for ultrasonic waves by spectral analysis of broad-band pulses* (in Polish), Materials of National Conf. of NDT, Szczecin 1987.
[8] B.A. AULD, *Acoustic fields and waves in solids*, vol. 2, John Wiley and Sons, New York 1973.
[9] L.M. BREKHOVSKIKH, *Waves in layered media*, Academic Press, New York 1960.
[10] M. REDWOOD, *Mechanical waveguides*, Pergamon Press, Oxford 1960.

Received November 20, 1989; English version February 17, 1992

ARCHIVES OF ACOUSTICS
17, 3, 375–388 (1992)

SHEAR ACOUSTIC WAVES IN PLATES

P. KIEŁCZYŃSKI, W. PAJEWSKI and M. SZALEWSKI

Institute of Fundamental Technological Research
Polish Academy of Sciences
(00-049 Warszawa, ul. Świętokrzyska 21)

In the paper the theoretical analysis and results of experimental investigations of SH waves propagation in plates are presented. The dimensions of different plates and methods of SH wave excitation were applied in order to attain mode separation and identification.

1. Introduction

A shear horizontal wave with polarization parallel to a plate surface can propagate in a plate with a definite thickness and other unlimited dimensions. Waves of this type can be generated by shear vibration transducers bonded to a plate edge. Such a wave is dispersive and multimode. A propagation analysis for this wave permits to obtain an exact analytical solution in the form of a relatively simple expression [1, 2]. However, the limitation of transverse dimension introduces new boundary conditions into the calculations. These conditions do not permit to obtain an exact analytical solution of the problem. This is due to reflections and the wave transformation (shear–longitudinal) on the plate edge. In this case oscillograms of pulses propagating in the plate are complicated. The separation of thickness plate modes from modes rising on plate edges is difficult. For more precise experimental investigations of SH wave propagation in plates it is necessary to choose boundary conditions and the method of wave excitation in such a way that the separation and identification of pulses are possible. It is not simple, as shown in the published photographs, owing to small velocity differences and superposition of pulses.

2. SH waves propagation in plate waveguides

2.1. Plates with limited thickness and infinite width

An elastic plate with infinite width and length can be treated as an approximation of real waveguide structures with limited dimensions. A thorough study of SH wave

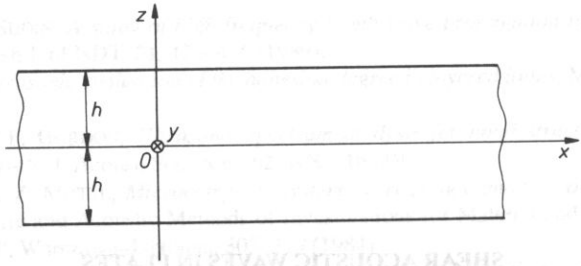

FIG. 1. Elastic plate infinitely extended in directions x and y, thickness 2h.SH wave with displacement in y direction propagates in x direction.

propagation in such a plate is helpful in investigations of two– and three–dimensional waveguides in which the acoustic beam is limited in the cross-section in relation to the propagation direction (x axis). We assume that the SH wave mode propagating in the x direction in the plate shown in Fig. 1 possesses the vibration component u only in the y axis direction. The medium is homogeneous and isotropic, nevertheless the propagating SH wave mode is dispersive as a result of multiple reflections at the boundaries $z = \pm h$ [1]. The problem of SH wave propagation in an infinite plate is described by the following differential problem:

$$\frac{\partial^2 u}{\partial x^2} + \frac{\partial^2 u}{\partial y^2} = \frac{1}{v_0^2} \cdot \frac{\partial^2 u}{\partial t^2} \tag{1}$$

$$\left.\frac{\partial u}{\partial z}\right|_{z=\pm h} = 0 \tag{2}$$

In the general case one can solve the problem of acoustic wave propagation in unlimited plates by applying the potential method, the partial wave method or the transverse resonance method [2]. It appears that the problem (1)–(2) possesses the finite analytical solution [1, 2].

$$u = B_1 \sin\left(\frac{n\pi}{2}\frac{z}{h}\right) \cdot \exp[i(kx - \omega t)] \tag{3}$$

$$n = 1, 3, 5, \ldots$$

for asymmetric modes, and

$$u = B_2 \cos\left(\frac{n\pi}{2}\frac{z}{h}\right) \cdot \exp[i(kx - \omega t)] \tag{4}$$

$$n = 0, 2, 4, \ldots$$

for symmetric modes, where B_1, B_2 – optimal constants, k – propagation constant of the SH plate wave.

The dispersive equation for both SH wave mode types is

$$\frac{\omega^2}{v_0^2} - k^2 = \frac{n^2\pi^2}{4h^2} \tag{5}$$

From the relation (5) the phase velocity results

$$v_p = v_0 \frac{1}{\sqrt{1 - \left(\frac{n\pi}{2hq}\right)^2}} \tag{6}$$

and the group velocity

$$v_g = v_0 \sqrt{1 - \left(\frac{n\pi}{2hq}\right)^2} \tag{7}$$

where $q = \frac{\omega}{v_0}$ – propagation constant of the volume SH wave.

Except for the mode $n = 0$, all other modes are dispersive – Fig. 2.

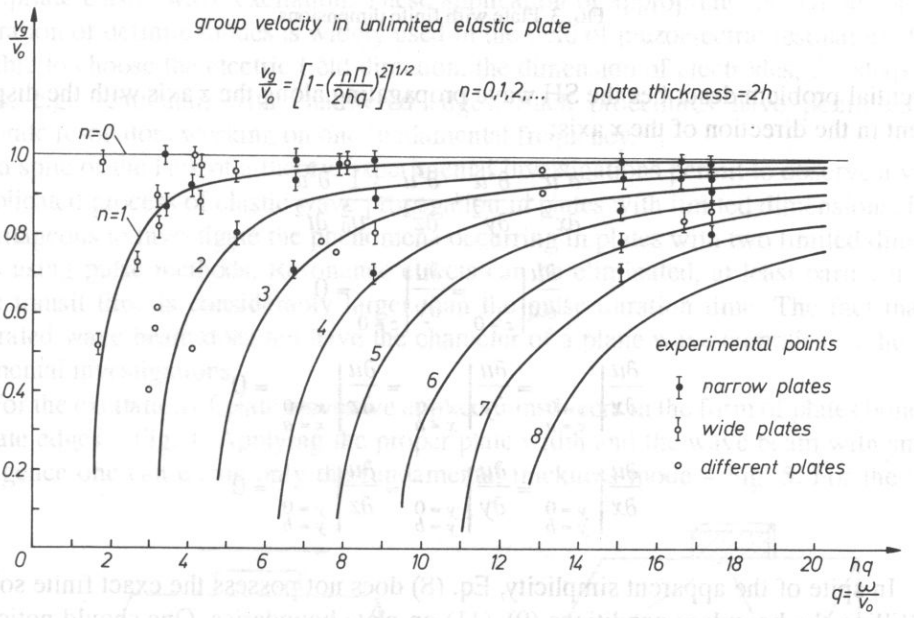

FIG. 2. Dispersion curves of SH modes group velocity in infinite elastic plate with thickness $2h$.

The structure considered hirtherto is infinite in the direction perpendicular to the wave propagation direction. In real waveguide structures one uses acoustic beams with limited width. This implies the application of waveguide structures with limited dimensions. Among these structures one can distinguish strip waveguides, topographic waveguides, ridge waveguides etc.

2.2. Plates with limited thickness and width

The general problem of acoustic SH wave propagation in plates with limited dimensions (Fig. 3), does not have, up till now, an analytical solution [2]. The following dif-

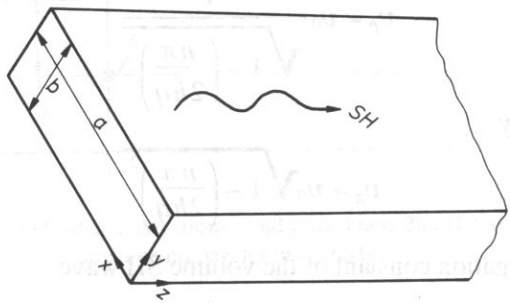

FIG. 3. Plate with finite dimensions.

ferential problem describes the SH wave propagating along the z axis with the displacement in the direction of the x axis:

$$\frac{\partial^2 u}{\partial x^2} + \frac{\partial^2 u}{\partial y^2} + \frac{\partial^2 u}{\partial z^2} = \frac{1}{v_0^2}\frac{\partial^2 u}{\partial t^2} \tag{8}$$

$$\left.\frac{\partial u}{\partial x}\right|_{z=0} = \left.\frac{\partial u}{\partial y}\right|_{z=0} = 0 \tag{9}$$

$$\left.\frac{\partial u}{\partial x}\right|_{\substack{x=0\\x=a}} = \left.\frac{\partial u}{\partial y}\right|_{\substack{x=0\\x=a}} = \left.\frac{\partial u}{\partial z}\right|_{\substack{x=0\\x=a}} = 0 \tag{10}$$

$$\left.\frac{\partial u}{\partial x}\right|_{\substack{y=0\\y=b}} = \left.\frac{\partial u}{\partial y}\right|_{\substack{y=0\\y=b}} = \left.\frac{\partial u}{\partial z}\right|_{\substack{y=0\\y=b}} = 0 \tag{11}$$

In spite of the apparent simplicity, Eq. (8) does not possess the exact finite solution fulfilling the boundary conditions (9)–(11) on plate boundaries. One should notice that the analogical problem of electromagnetic wave propagation in rectangular waveguides possesses an exact analytical solution.

The motion equation for the plate with limited dimensions can be solved only in the approximate way. To this end we can distinguish two procedures:

1) solving numerically the system of exact equations in the approximate way,

2) simplification of motion equations and exact solution of the obtained equations.

Mindlin's theory of vibrations of plates with finite dimensions [3–5] can be included in the second way of proceeding. We encounter similar problems in the case of strip waveguides [6] and topographic waveguides [7]. In both of these cases one can obtain field distributions and dispersive curves only numerically. A considerable limitation of the guided acoustic beam width has been achieved in these waveguides. It leads to the increase of acoustic wave power density, what can be employed in acoustoelectric

devices utilizing nonlinear effects [8]. The complicated character of phenomena appears particularly strikingly in plates with three limited dimensions. Eventually one obtains standing waves using suitable excitation. This case occurs in resonators applied as ultrasonic transducers, constant frequency sources or electromechanical filter elements.

3. Experimental investigations of special cases of plate waves

3.1. Methods of plate wave excitation

Experimental investigations of plate waves aim at separating definite modes using appropriate elastic wave excitation. These application of appropriate excitation for the generation of definite modes is widely used in the field of piezoelectric resonators. It is possible to choose the electric field direction, the dimension of electrodes, the shape of plates, e.g., lenticular, with chamfered edges. Such procedures have permitted to elaborate resonators working on one fundamental frequency.

In spite of the lack of a theory, experimental investigations permit to observe a very complicated process of elastic wave propagation in plates with limited dimensions. It is advantageous to investigate the phenomena occurring in plates with two limited dimensions using pulse methods. Resonance effects can be eliminated, at least partly, if the pulse transit time is considerably larger than the pulse duration time. The fact that a generated wave beam does not have the character of a plane wave complicates the experimental investigations.

For the excitation of plate waves we applied transducers in the form of plates bonded to plate edges – Fig. 4. Applying the proper plate width and the wave beam with small divergence one can excite only the fundamental thickness mode – Fig. 5. For the low

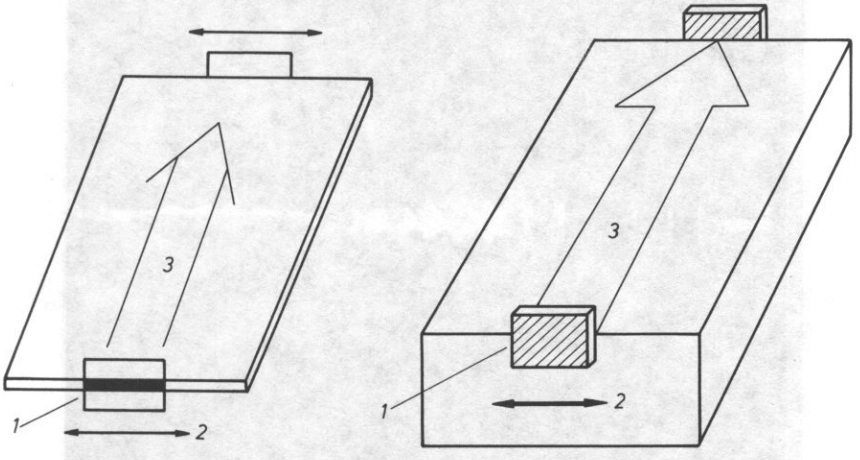

FIG. 4. Methods of plate waves excitation. 1 - piezoelectric transducer, 2 - direction of transducer vibrations, 3 - direction of wave propagation.

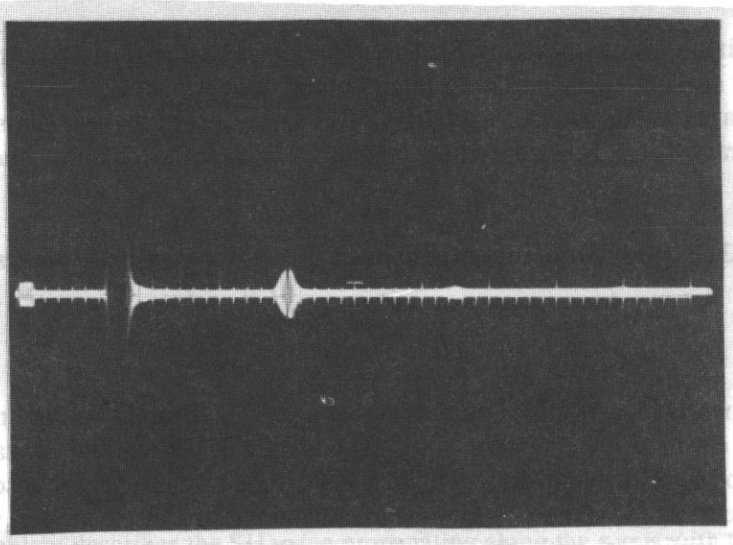

FIG. 5. Plate 15 × 14.9 × 0.5 mm excited as in Fig. 4a, $f = 10$ MHz, 5 μs/div, 100 mV/div.

frequency, when the beam is strongly divergent, transverse (plate thickness) and width SH wave modes are excited. This effect seriously complicates the image of received pulses – Fig. 6. One should also take into consideration shear wave transformations into a longitudinal wave. Mode separation becomes impossible. Narrowing of the plate should eliminate transverse modes but then flexural symmetric and asymmetric modes arise. All these effects can be observed in the photos of pulses.

The edge excitation (Fig. 4b) permits to privilege higher thickness mode but width modes are not eliminated.

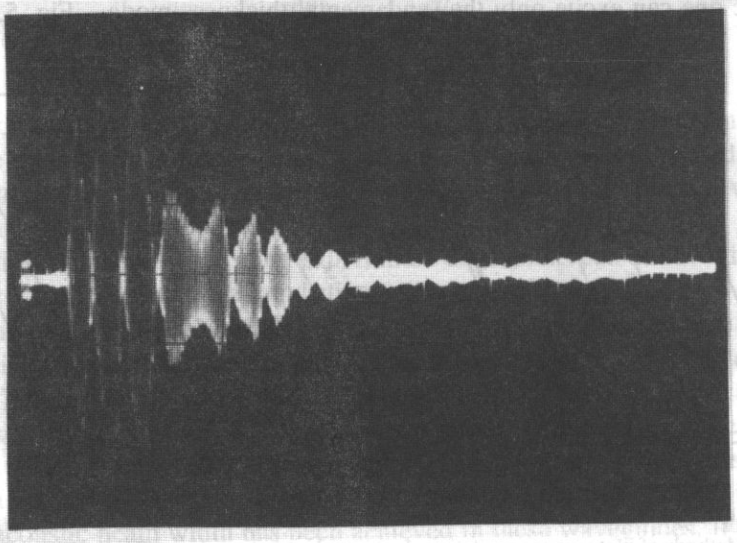

FIG. 6. Plate 15 × 14.9 × 0.5 mm excited as in Fig. 4a, $f = 1$ MHz, 10 μs/div, 0.2 V/div.

3.2. SH waves in plates with large width in relation to length

In order to eliminate SH wave reflections from the plate sides, we applied plates with large dimension in a direction perpendicular to the wave propagation direction. The widths of these plates were greater than their lengths or comparable. In this way we tried to approach unlimited space conditions. The SH wave was excited as in Fig. 4a or Fig.

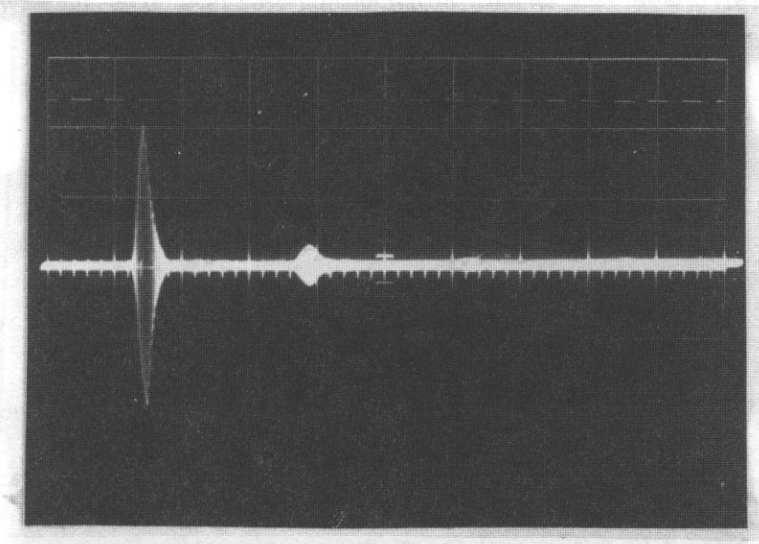

FIG. 7. Plate 16.5 × 15.8 × 1 mm excited as in Fig. 4a, f = 5 MHz, 5 μs/div, 0.5 V/div.

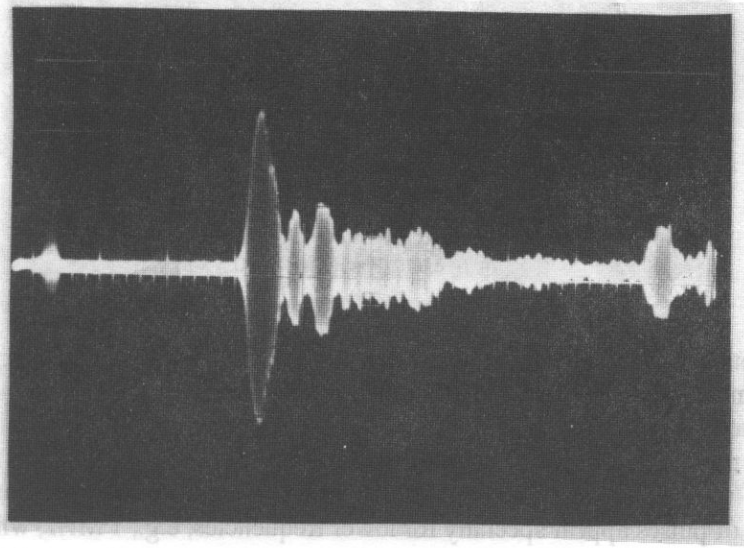

FIG. 8. Plate 16.5 × 15.8 × 1 mm excited as in Fig. 4b, f = 5 MHz, 2 μs/div, 20 mV/div.

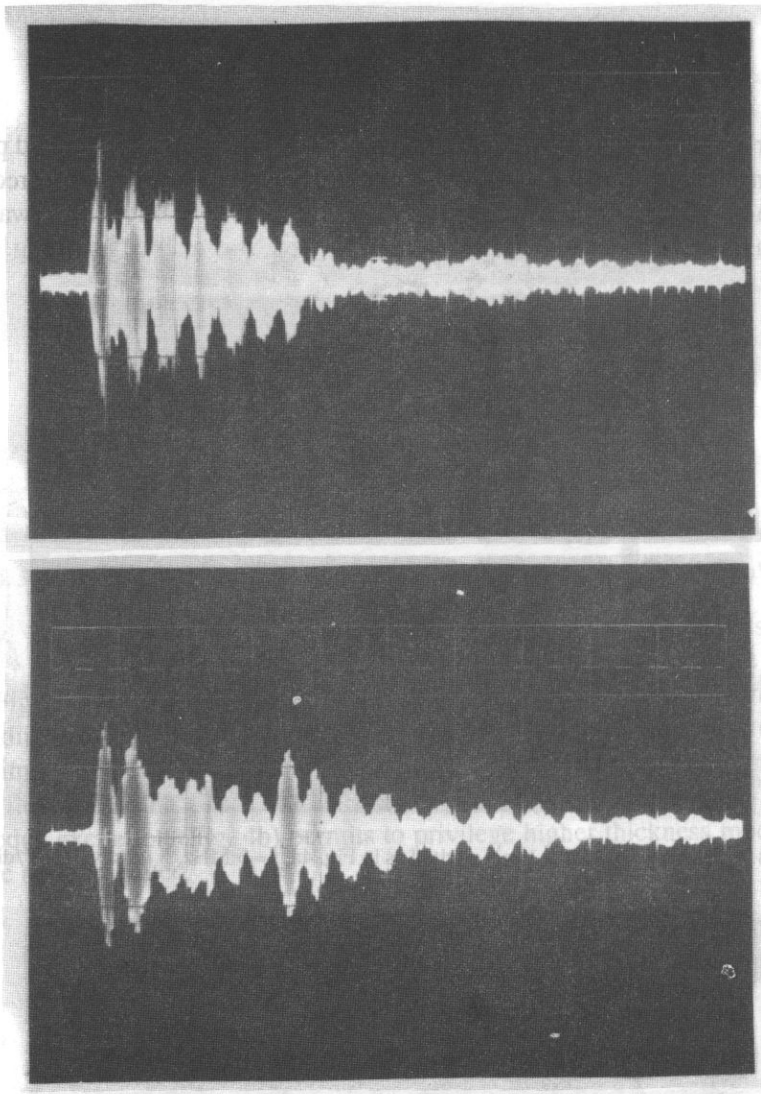

FIG. 9. Plate 16,5 × 15,8 × 1 mm, f = 1 MHz, 10 μs/div
a) excited as in Fig. 4b, 100 mV/div,
b) excited as in Fig. 4a, 0.5 V/div.

4b. The obtained oscillograms of pulses are presented in Fig. 7 and 8. In Fig. 7 the fundamental mode pulse is visible, higher modes are almost imperceptible, whereas in Fig. 8 higher modes are clearly noticeable. The superposition of visible modes and the deformation of transmitted pulses come out here, what makes velocity calculations impossible. The third echo observation does not improve the situation. Difficulties of the separation of pulses appear specially for lower frequencies, e.g., 1 MHz, when the wave beam is more divergent – Figs. 9a and 9b. As one can see in the figures, it is not simple

to obtain measurement conditions close to the theoretical conditions because the generated wave is not the plane wave and the generated pulses are expanded in time.

3.3. SH waves in plates with transverse dimension smaller than the dimension in the wave propagation direction

This case of SH wave propagation in a plate is the most complicated and it corresponds with the theoretical case considered in Chapter 2.2. Figure 10 presents the

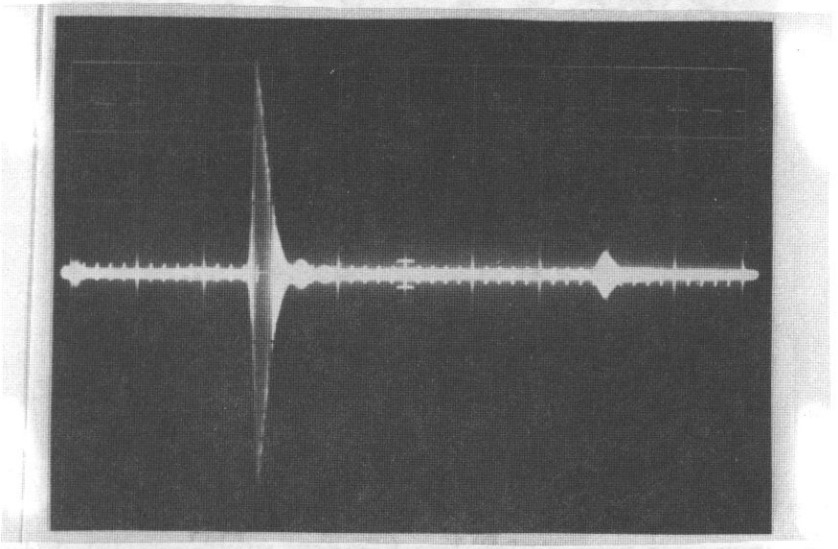

FIG. 10. Plate 26.4 × 17 × 1.1 mm excited as in Fig. 4a, $f = 5$ MHz, 5 μs/div, 100mV/div.

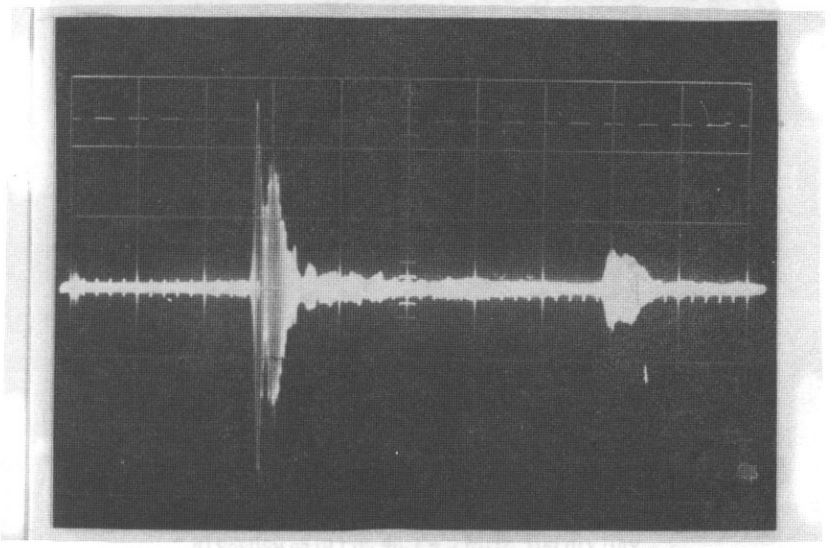

FIG. 11. Plate 26.4 × 17 × 1.1 mm excited as in Fig. 4b, $f = 5$ MHz, 5 μs/div, 20mV/div.

image of pulses rising with the excitation as in Fig. 4a. Besides the main pulse, one can see additional pulses rising as a result of reflections at side edges of the plate. Edge excitation (Fig. 4b) complicates furthermore the image of pulses – Fig. 11. Consequently, the identification of SH wave modes is not possible. The image becomes simplified for higher frequency (10 MHz) when the wave beam is narrow and the side reflections are eliminated. This case does not possess an exact analytical solutions, it is also complicated experimentally.

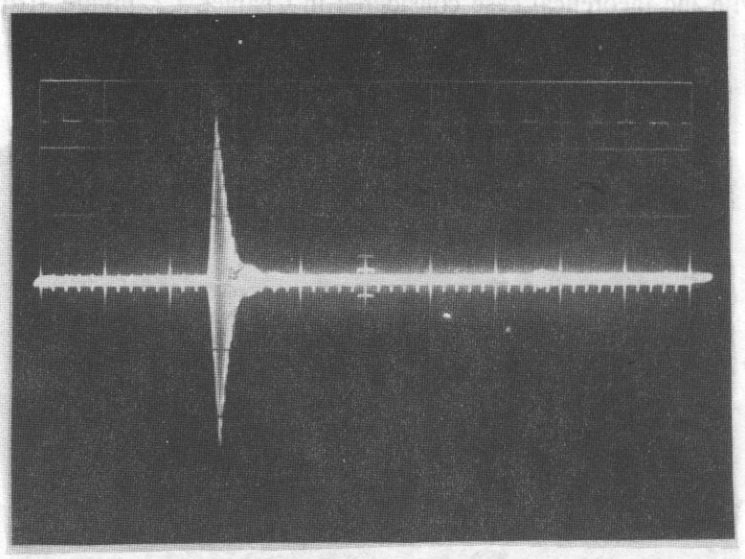

FIG. 12. Plate 25 × 5 × 1.1 mm excited as in Fig. 4a. $f = 5$ MHz. 5 μs/div. 100 mV/div.

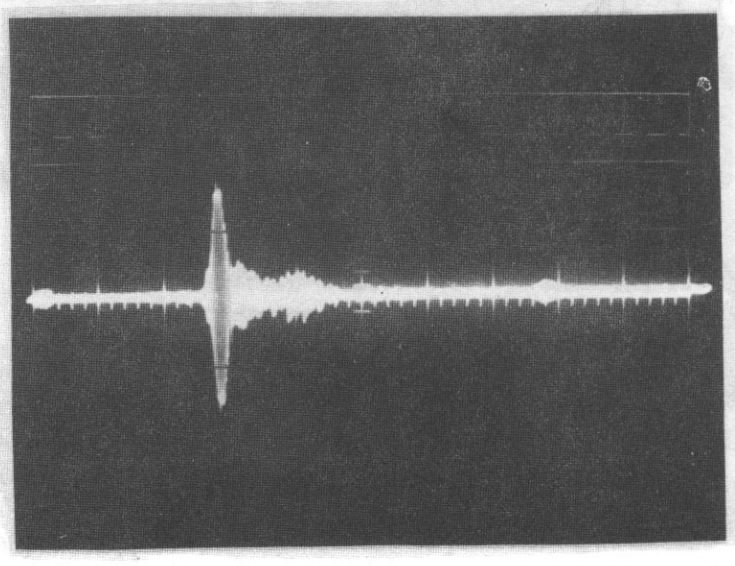

FIG. 13. Plate 25 × 5 × 1.1 mm excited as in Fig. 4b, $f = 5$ MHz, 5 μs/div, 20 mV/div.

3.4. SH wave in narrow plates

The elimination or the reduction of side reflections of SH waves is possible in narrow plates. Figure 12 presents SH wave pulses excited by a plate transducer as in Fig. 4a, while Fig. 13 – as in Fig. 4b.

3.5. SH waves in plates with different thickness

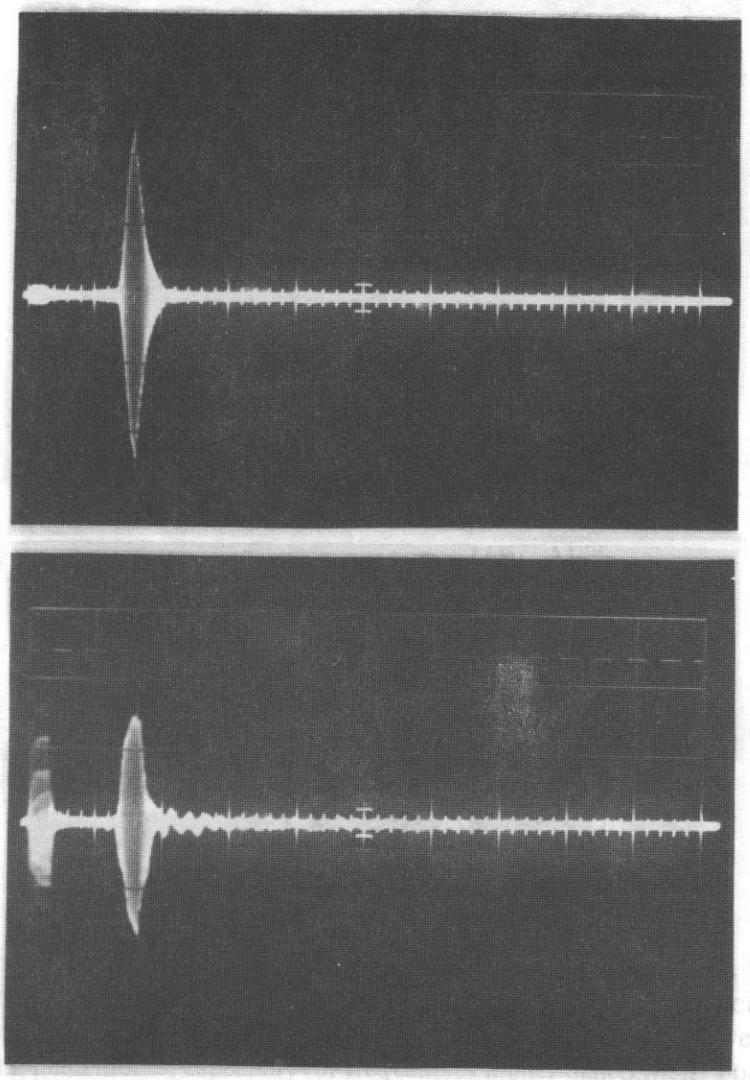

FIG. 14. Plate 25 × 12.1 × 0.5 mm,5 μs/div,
a) excited as in Fig. 4a, f = 5 MHz, 100 mV/div,
b) excited as in Fig. 4b, f = 10 MHz, 10 mV/div.

One can see from the analytical solution for the plate wave that for an unlimited plate the frequency limitation appears in the form of cut-off frequency. Below this frequency plate modes do not exist. The cut-off frequency is defined by the formula

$$f_{\text{cut}} = \frac{v_0}{4h}$$

The experimental investigations of plates with different thickness and also for different frequencies should enable to observe the cut-off frequency. Measurements have

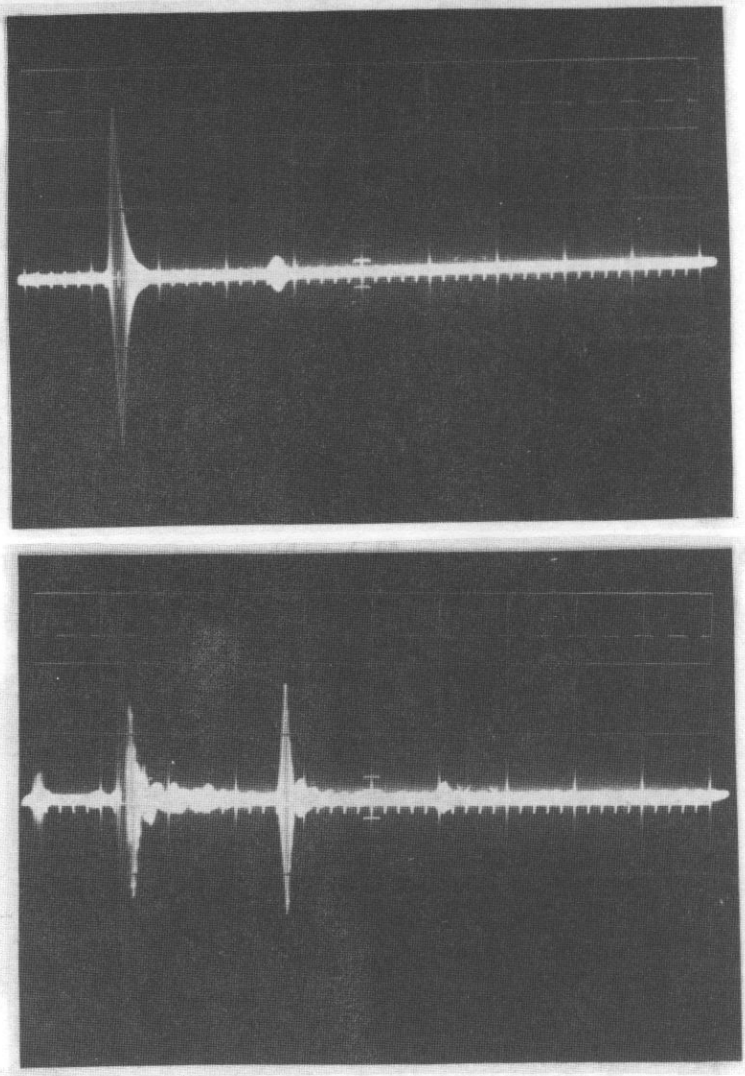

FIG. 15. Plate 16.5 × 15.8 × 1 mm, f = 10 MHz, 5 μs/div,
a) excited as in Fig. 4a, 0.2 V/div,
b) excited as in Fig. 4b, 20 mV/div.

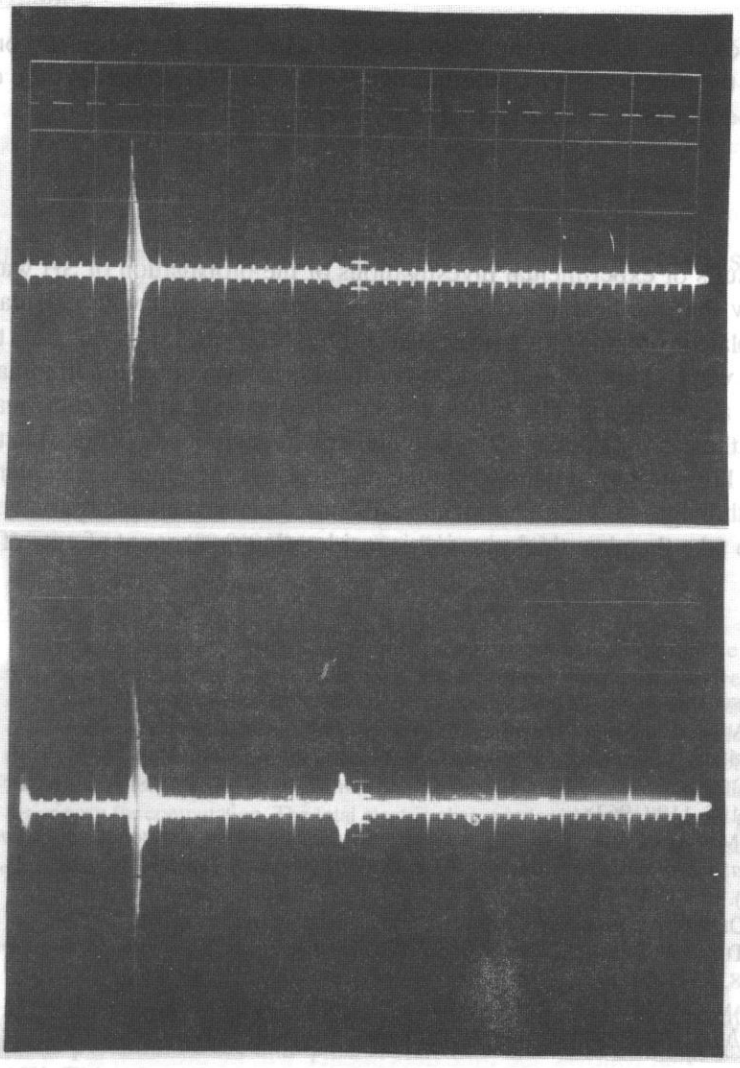

FIG. 16. Plate 33.5 × 18 × 2 mm, $f = 5$ MHz, 10 μs/div,
a) excited as in Fig. 4a, 0.2 V/div,
b) excited as in Fig. 4b, 20 mV/div.

been performed for plates with thicknesses of 0.5 mm, 1 mm, 2 mm. Figures 14a, b, 15a, b and 16a, b present the results of measurements. The results of velocity calculations for SH plate modes are shown in Fig. 2. In spite of the mentioned difficulties, we succeeded in identifying plate modes, especially for frequencies higher than 5 MHz. For this range we succeded in separating the modes particularly for edge excitation. Instead, for the frequencies 1 MHz and 2 MHz, where the considerable differences of mode velocities caused by the cut-off frequency existence should be visible, measurements and observa-

tion of pulses show a very complicated image. In this case we succeeded only partly in identifying the pulses corresponding to SH wave modes. It seems that the existence of flexural modes is possible in this frequency range.

4. Conclusion

The results of experimental investigations of the propagation of SH wave pulses in plates show that the best agreement of measurements results with calculations for an unlimited plate is obtained for narrow plates (ratio 5/20 = 0.25). In this case the SH wave has a plane wave character and shear wave transformation into a longitudinal wave does not appear at the edges. The plates are sufficiently wide and flexural waves are not present. In the case of thicker plates and higher wavenumbers it is possible to excite and to separate higher order modes. From the realized investigations it is evident that plates with a width/length ratio smaller than 0.4–0.5 are the most suitable for waveguides. One should also take the plate thickness into consideration on account of cut-off frequency.

References

[1] Z. WESOŁOWSKI, *Elastic body acoustics* (in Polish), PWN, Warszawa (1989).
[2] B.A. AULD, *Acoustic fields and waves in solids*, John Wiley, New York (1973).
[3] R.D. MINDLIN, *High frequency vibrations of crystal plate*, Quart. Appl. Math., **19**, 1, 51–61 (1961).
[4] H.F. TIERSTEN, R.D. MINDLIN, *Forced vibrations of piezoelectric crystal plates*, Quart. Appl. Math., **20**, 3, 107–119 (1962).
[5] R.D. MINDLIN, W.J. SPENCER, *Anharmonic thickness-twist overtones of thickness-shear and flexural vibrations of rectangular AT-cut quartz plates*, J. Acoust. Soc. Am., **42**, 6, 1268–1277 (1967).
[6] A.A. OLINER, *Acoustic surface waves*, Springer-Verlag, Berlin (1978).
[7] C.C. TU, G.W. FARNELL, *On the flexural mode ridge guides for elastic surface waves*, Electronics Lett., **8**, 3, 68–70 (1972).
[8] J. CHAMBERS, M. MOTZ, P.E. LAGASSE, I.M. MASON, *Acoustic surface waveguides and waveguide convolvers*, Ultrasonic International 1973 Conf. Proc., 333–338.

Received April 17, 1991

ARCHIVES OF ACOUSTICS
17, 3, 389–412 (1992)

SURFACE ACOUSTIC WAVE SCATTERING BY ELLIPTIC METAL DISK ON ANISOTROPIC PIEZOELECTRIC HALFSPACE

E. DANICKI

Institute of Fundamental Technological Research
Polish Academy of Sciences
(00-049 Warszawa, Świętokrzyska 21)

Surface acoustic wave (SAW) propagating in arbitrarily anisotropic piezoelectric halfspace is considered. The wave interacts with a perfectly conducting and weightless metal disk on the substrate surface by means of the electric potential only which is coupled to SAW due to the substrate piezoelectricity. A perturbation theory of scattering plane harmonic SAW by the disk is presented which accounts the dielectric, and elastic anisotropy of the substrate. The solution for electric charge distribution on the disk is given in a form of fast convergent series easy for computation. The total electric charge induced by SAW on the grounded disk is explicitly evaluated. Angular dependences of the scattered SAW in large distance from the disk is also discussed.

1. Introduction

Surface acoustic wave propagating in a piezoelectric halfspace is accompanied with a wave of electric potential on the halfspace surface. Perturbation of the potential allows scattering SAW. This phenomenon is exploited for some technical purposes in SAW devices. The theory presented below concerns SAW scattering by perfectly conducting elliptic disk on anisotropic piezoelectric substrate.

There are similar problems in acoustics and electromagnetics, where a rigorous theory has been developed of wave scattering by ellipsoid and, in limit, by disk [1]. Perturbation theories are also known for small disks [2], [3]. The problem considered in this paper differs from the above ones at least with the substrate anisotropy. The dielectric anisotropy of the substrate directly effects the electric charge distribution on the disk induced by the incident SAW. This, and the angular dependence of SAW velocity and SAW coupling to the electric field resulting from the elastic and piezoelectric anisotropy of the substrate, influence on the angular dependence of the scattered SAW far-field.

The theory presented below is a perturbation one. It relys on neglecting of piezoelectric interaction when the electric charge distribution on the disk is evaluated. This simplification can be applied under the assumption of weak piezoelectricity of the substrate or on the assumption that the disk diameter is not excessively large as compared to the wavelength of SAW.

The formulation of the boundary problem considered is given in Section 2. Appendix B shows how the problem for elliptic disk can be transformed into the problem for circular disk of unit radius. The transformation results however in anisotropic Green's function, which is discussed in Appendix A. Section 3 presents the solution of certain electrostatic problem for anisotropic dielectric halfspace (much more elegant solution was recently presented in [18]). The key features of this solution are discussed in Appendix C. Section 4 is devoted to the evaluation of electric charge distribution induced on the disk by the incident SAW. The scattered SAW is considered in Section 5 where some numerical examples are also presented.

Note. In the paper, several functions are represented in a form of infinite or finite series which components, as well as summation limits are described separately in the main text or in Appendices. To clarify the presentation of the formulas the symbols of summation are usually dropt (there are notes about it however from time to time).

2. Integral formulation of the scattering problem

2.1. Simplified description of the substrate electric property

Consider a traction-free piezoelectric substrate surface with electric charge distribution in a form of the travelling wave on it

$$\Delta D_{\perp} = \rho \exp(j\omega t - j\mathbf{k} \cdot \mathbf{r}) \tag{1}$$

where the denotation $\Delta D_{\perp}$ expresses well known relation between surface electric charge and the discontinuity of electric flux density on both sides of the surface [4], ω – angular frequency (in what follows, the time dependence will be droped), $\mathbf{k}$ – wave-vector, ρ – complex amplitude of the surface electric charge.

Following [5], [6] the wave of electric charge results in the wave of electric potential on the substrate surface. The potential complex amplitude is

$$\Phi = G(\omega, \mathbf{k})\rho \tag{2}$$

where G is the Fourier transform of electric Green's function of the piezoelectric halfspace (the considered Green's function concerns the electric quantities on the halfspace surface only).

Generally, G can be decomposed into three components describing three different physical phenomena, dielectric property of the substrate, generation of surface acoustic wave or bulk acoustic waves coupled to the surface electric potential. A detailed discussion of the function G is given elsewhere [7], [8], let us only note here that both two

former components are singular functions of wave-number k, while the latter component is usually bounded function of k.

In what follows, the latter part of G describing bulk waves is completely neglected, however there are not any substantial difficulties in including it into considerations on a similar way as the surface waves.

Following this simplification we have

$$G(\mathbf{k}) = \frac{1}{k\varepsilon_e}\frac{k^2 - k_0^2}{k^2 - k_v^2} \tag{3}$$

where $k = \|\mathbf{k}\|$, and k_0 – wave-number of SAW for metalized substrate surface, k_v – wave-number of SAW for free substrate surface, ε_e – effective surface permittivity of the substrate, all the above quantities depend on the direction of propagation of the wave $\mathbf{k}/k$, note however that due to point symmetry there is $\varepsilon_e(\vartheta + \pi) = \varepsilon_e(\vartheta)$ and similarly for k_0 and k_v.

It is convenient to write the relation (2) in spatial representation as follows

$$\Phi(\mathbf{r}) = \iint_S g(\mathbf{r}; \mathbf{r}')\rho(\mathbf{r}')dS' \tag{4}$$

where the integral is taken over the whole surface occupied by the electric charge. Explicit form of g is given in Appendix A.

2.2. Simplified formulation of the scattering problem

It is shown in Appendix B how the problem for elliptic disk can be led to the problem for circular one. It is done by suitable scaling and subsequent transformation of the coordinate system. The following considerations concern the transformed spatial coordinates where we have to do with circular disk of unit radius.

Let us consider the grounded disk which electric potential is zero. With help of (4) this can be expressed in a form

$$-\Phi^0(\mathbf{r}) = \iint_S g(\mathbf{r}; \mathbf{r}')\rho(\mathbf{r}')dS' \tag{5}$$

where $\mathbf{r}$ and $\mathbf{r}'$ belong to the disk area S where $\|\mathbf{r}\| \le 1$, and Φ^0 is the incident wave potential on the free substrate surface

$$\Phi^0 = \exp(jk_v z) \tag{6}$$

(for convenience, we apply the unitary potential amplitude and incident SAW propagating in $-z$-axis direction).

In the case of free (floating) disk where the disk potential can have nonzero value (constant over the whole disk), the scattering problem can be divided into three parts which can be solved separately.

i) firstly, the solution for grounded disk should be found and the total electric charge Q induced on the disk evaluated,

ii) secondly, an auxiliary problem should be solved for grounded disk with $-\Phi^0 = V = \text{const}$ applied instead of (6). The total electric charge Q_0 over the disk should be evaluated in this case, too,

iii) the last step is to make a superposition of both solutions with V chosen in such a way that $Q + Q_0 = 0$. The potential V is the floating disk potential induced by the incident SAW.

The problem ii) describes also the generation of SAW by a disk supplied with an external voltage, it can be solved on a similar way as the problem i).

The integral equation (5) is very complicated and, generally, it can not be solved exactly. However, for common piezoelectric substrates we can apply the assumption of weak piezoelectric coupling, that is

$$\Delta v/v = (k_0 - k_v)/k_v << 1 \tag{7}$$

This enable us to apply the iteration procedure in solving (5), speaking in advance we will perform only first step of the iteration.

Applying results given in Appendix A we can write

$$-\Phi^0 = \iint_S g^E \rho \, dS + \iint_S g^R \rho \, dS \tag{8}$$

where g^E is a singular function at $\mathbf{r} = \mathbf{r}'$, while g^R is a regular function proportional to $\Delta v/v$ which value is relatively small. It means that the second component in (8) can be neglected for all $\mathbf{r}$ in vicinity of $\mathbf{r}'$, say for all $\mathbf{r}$ from the disk area S.

Following this simplification the first approximation to (8) is

$$-\sum_m J_m(kr) e^{jm\vartheta} = \iint_S \frac{\rho(r', \vartheta')}{2\pi \bar{r} \varepsilon_e(\bar{\vartheta} - \pi/2)} dx' dy' =$$

$$\frac{1}{2\pi} \int_0^{2\pi} [\, \varepsilon_e(\bar{\vartheta} - \pi/2) \,]^{-1} d\bar{\vartheta} \int_0^{R(\bar{\vartheta})} \rho(r', \vartheta') \, d\bar{r} \tag{9}$$

where $\bar{r} = \|\mathbf{r} - \mathbf{r}'\|$, $\bar{\vartheta} = \arg\{(\mathbf{r} - \mathbf{r}')/\bar{r}\}$ similarly r, ϑ and r', ϑ' represent vectors $\mathbf{r}$ and $\mathbf{r}'$ in polar coordinates on the substrate surface (Fig. 1). The left-hand side of (9) is $-\Phi^0$ in polar coordinates r, ϑ. The equation (9) is the weekly singular Fredholm integral equation of the first kind for charge distribution ρ.

Confining our consideration to the first approximation, the far-field solution for the scattered SAW can be evaluated with help of asymptotic representation for g^R (see Appendix A), that is

$$\Phi(r \to \infty, \vartheta) = \iint_S g^A(\vartheta; r', \vartheta') \rho(r', \vartheta') \, dS' \tag{10}$$

where ρ is the solution of (9).

3. An auxiliary electrostatic problem

3.1. Arbitrary distribution of electric charge over the disk

Charge distribution which is a smooth function over the circular disk can be represented by a series (summation over m, n will not be explicitly marked troughout the paper)

$$\rho(r', \vartheta') = \sigma_{mn} \frac{T_n(r')}{(1 - r'^2)^{1/2}} e^{jm\vartheta'} \tag{11}$$

where T_n is the n–th order Tchebyshev polynomial and σ_{mn} is an arbitrary constant. The applied charge distribution (11) exhibits square-root singularity at $r' \to 1$ which is typical for the problem considered here [2]. The condition that $\rho(r', \vartheta') \equiv \rho(-r', \vartheta' + \pi)$ constrains n in (11) to numbers having the same parity as m.

Substitution of the above representation into (9) gives the potential Φ under the disk (that is for $r \leq 1$) in the form (see Fig. 1 for geometric interpretation of r_1 and r_2)

$$\phi = \frac{1}{4\pi} \int_0^{2\pi} d\bar{\vartheta} \chi(\bar{\vartheta} - \pi/2) \int_{-(1-r_1^2)^{1/2}}^{(1-r_1^2)^{1/2}} \rho(r', \vartheta') dr_2 \tag{12}$$

where $\chi = 1/\varepsilon_e$ and

$$\begin{aligned} r_1 &= r \sin(\bar{\vartheta} - \vartheta) \\ r_2 &= \bar{r} + r \cos(\bar{\vartheta} - \vartheta) \\ r' &= (r_2^2 + r_1^2)^{1/2} \\ \vartheta' &= \bar{\vartheta} - \frac{1}{2} \arg[\,(-r_2 + jr_1)/(-r_2 - jr_1)\,] \end{aligned} \tag{13}$$

where $\arg\{e^{j\alpha}\} = \alpha$.

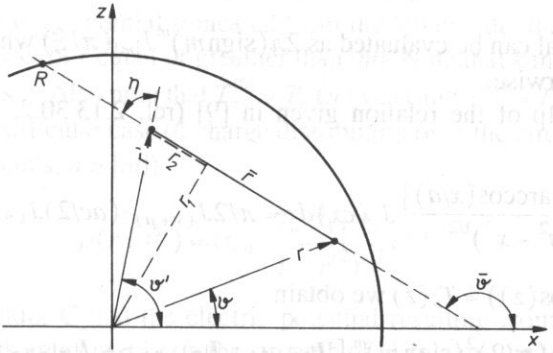

FIG. 1. Geometrical interpretation of integral variables.

It follows from (13) that the substitution can be made

$$r_1 = \xi \sin\eta$$
$$r_2 = \xi \cos\eta \tag{14}$$

resulting in variables

$$\vartheta' = \bar{\vartheta} - \eta$$
$$r' = \xi \tag{15}$$

both dependent on r_2 and $\bar{\vartheta}$, which applied to (12) yield

$$\phi = \frac{\sigma_{mn}}{4\pi} \int_0^{2\pi} \chi(\bar{\vartheta} - \pi/2) e^{jm\bar{\vartheta}} d\bar{\vartheta} \int_{-(1-r_1^2)^{1/2}}^{(1-r_1^2)^{1/2}} \frac{T_n(\xi)}{(1-\xi^2)^{1/2}} e^{-jm\eta} dr_2 \tag{16}$$

Let us introduce an auxiliary function $f(r_1)$ the domain of which is $-1 \le r_1 \le 1$ so that $f(r_1)$ can be further expanded into a Fourier series as follows

$$f(r_1) = \int_{-(1-r_1^2)^{1/2}}^{(1-r_1^2)^{1/2}} \frac{T_n[(r_1^2 + r_2^2)^{1/2}]}{(1 - r_1^2 - r_2^2)^{1/2}} e^{-jm\eta} dr_2 = \sum_{l=-\infty}^{\infty} c_l e^{-j\pi l r_1} \tag{17}$$

where

$$c_l = \frac{1}{2} \int_{-1}^{1} dr_1 e^{j\pi l r_1} \int_{-(1-r_1^2)^{1/2}}^{(1-r_1^2)^{1/2}} \frac{T_n[(r_1^2 + r_2^2)^{1/2}]}{(1 - r_1^2 - r_2^2)^{1/2}} e^{-jm\eta} dr_2 \tag{18}$$

We easily note that the integration area in the double integral (18) appears to be a circle of unitary radius on the plane (r_1, r_2) then applying new polar coordinates (14) the integral (18) can be transformmed into

$$c_l = \frac{1}{2} \int_0^1 \frac{\xi T_n(\xi)}{(1-\xi^2)^{1/2}} d\xi \int_0^{2\pi} e^{j\pi l \xi \sin\eta} e^{-jm\eta} d\eta \tag{19}$$

The second integral can be evaluated as $2\pi(\operatorname{sign} m)^m J_{|m|}(\pi l \xi)$ where $\operatorname{sign}\{m\} = +1$ for $m \ge 0$ and -1 otherwise.

Now, with help of the relation given in [9] (rel. 2.13.30.2, p.209) for $a > 0$ and $\nu > -1$

$$\int_0^a \frac{\cos[\mu \arccos(x/a)]}{(a^2 - x^2)^{1/2}} J_\nu(cx) dx = \pi/2 J_{(\nu+\mu)/2}(ac/2) J_{(\nu-\mu)/2}(ac/2)$$

where $\cos(n \arccos(z)) = T_n(z)$ we obtain

$$c_l^{(m,n)} = (\pi/2)^2 (\operatorname{sign} m)^m \left[J_{\frac{|m|-n+1}{2}} J_{\frac{|m|+n-1}{2}} + J_{\frac{|m|-n-1}{2}} J_{\frac{|m|+n+1}{2}} \right] \tag{20}$$

where the argument of each Bessel function J above is $\pi l/2$. Also note that all these Bessel functions have half-integer indices because m and n have the same parity. Upper indices in the left-hand side of (20) mark the dependence of c_l on m and n.

It is easy to prove that

$$c_0^{(m,n)} = 0, \quad \text{for } m \neq 0 \text{ and arbitrary } n,$$

$$c_0^{(0,n)} = \pi(-1)^{n/2}(1-n^2)^{-1}, \quad \text{for } m = 0 \ (n \text{ even}). \tag{21}$$

Some further properties of the coefficients c are discussed in Appendix C.

Having $f(r_1)$ expanded into the Fourier series (17) the relation (16) gives after simple transformation

$$\phi = \frac{1}{2}\sigma_{kn}\chi_{m-k}c_l^{(k,n)}e^{jm\vartheta}J_m(\pi l r) \tag{22}$$

(note that there are summations over m, k and l in infinite limits and after n from 0 to ∞). Taking into account (C.2) the above relation can be further transformed into

$$\Phi = \frac{1}{2}\sigma_{kn}\chi_{m-k}e^{jm\vartheta}J_m(\pi l r)\begin{cases}\left[\dfrac{a_p^{(k,n)}}{(\pi l)^p}(-1)^l + \dfrac{b_p^{(k,n)}}{(\pi l)^p}\right] & \text{for } l \neq 0 \\ c_0^{(k,n)} & \text{for } l = 0\end{cases} \tag{23}$$

(summation after p – see Appendix C).

3.2. *Particular case of charge distribution*

Let us introduce a polynomial (m and n have the same parity, $n \geq 0$)

$$T_n^{(m)}(r) = \sum_{k=|m|(2)}^{n} w_k r^k, \quad |m| \leq n \tag{24}$$

which is a Tchebyshev polynomial truncated from the lower side, the only components left are these with power of r equal or greather than $|m|$. Note that k in the definition (24) has the same parity as n. Also note that $T_n^{(0)} = T_n$ (n even) and $T_n^{(1)} = T_n$ (n odd).

Consider now a particular case of charge distribution over the circular disk in a form (σ_{mn} – arbitrary constants, $n \geq |m|$)

$$\rho(r', \vartheta') = \sigma_{mn}\frac{T_n^{(m)}(r')}{(1-r'^2)^{1/2}}e^{jm\vartheta'} \tag{25}$$

It is shown in Appendix C that the electric potential resulting from the above charge distribution in the disk area ($r < 1$) on the strength of (12) takes the form similar to (23) but without terms $(+1)^l/l^p$, that is (summation over m, n, l and p as previously)

$$\Phi = \frac{1}{2}\sigma_{kn}\chi_{m-k}e^{jm\vartheta}\cdot \begin{cases} 0; & \text{for } l=0 \text{ and } m\neq 0 \\ (-1)^l \dfrac{\alpha_p^{(k,n)}}{(\pi l)^p} J_m(\pi l r); & \text{for } l\neq 0 \\ c_0^{(0,n)}; & \text{for } l=0 \text{ and } k=0 \end{cases} \tag{26}$$

where $\alpha_p^{(k,n)}$ can be expressed by $a_p^{(k,n)}$ by suitable superposition (C.5) (transforming (23) to (26) we took into account that $J_m(0)=0$ for $m\neq 0$ as well as (21) and Appendix C).

Moreover, some components in (26) can be completely neglected because ([9], rel. 5.7.19.9, p.678)

$$\sum_{k=1}^{\infty}(-1)^k k^{2n-\nu}J_\nu(kx)=0 \;;\; 0<x<\pi \;,\; \nu-2n>1/2$$

It means that all components with $p<|m|$ in (26) can be dropt independently on the values of σ_{kn} and $\alpha_p^{(k,n)}$.

Let us consider net, or total electric charge on the disk resulting from integration of charge distribution (25) over the whole disk. We have (summation after even n)

$$Q=\iint_S \rho dS = 2\pi\sigma_{0n}\int_0^1 \frac{rT_n(r)}{(1-r^2)^{1/2}}dr = 2\pi\sigma_{0n}\frac{(-1)^{n/2}}{1-n^2} = 2c_0^{(0,n)}\sigma_{0n} \tag{27}$$

4. Charge distribution induced by SAW

4.1. Approximation of the incident potential wave

In (9) the wave of electric potential coupled to incident SAW is represented in polar coordinates. This representation can be further expanded with help of the relations given in [9], rel. 5.7.17. (26) and (2) (below taken with $n=1$)

$$\sum_{k=1}^{\infty}(-1)^{k+1}\frac{k^{2n-\nu}}{k^2-a^2}J_\nu(kx)=\frac{\pi}{2}a^{2n-\nu-1}\operatorname{cosec}(a\pi)J_\nu(ax)$$

$$\sum_{k=0}^{\infty}(-1)^k J_0(kx)=\frac{1}{2} \;;\; \nu>2n-5/2\,,\; n=1,2,\ldots\,,\; 0<x<\pi$$

The result is (summation over m dropt)

$$-\Phi^0 = -\frac{\sin k_v}{k_v}e^{jm\vartheta}\sum_{l=-\infty}^{\infty}(-1)^l\cdot \begin{cases} 0; & \text{for } l=0 \text{ and } m\neq 0 \\ \dfrac{(k_v/\pi l^{-|m|-\nu}}{1-(k_v/\pi l)^2}J_m(\pi l r); & l\neq 0 \\ 1; & \text{for } l=0 \text{ and } m=0 \end{cases} \tag{28}$$

where $\nu=2$ for $m=0$ and $\nu=0$ for $m\neq 0$.

As known, $J_m(\pi l r) \sim 1/\sqrt{l}$ for large l and $r \neq 0$. It means that the above series over l is absolutely convergent for all m and $0 < r < 1$ under consideration. Allowing certain error of an order of $O(1/N)$, components with large l, say with $|l| > N$ can be omited when the series is evaluated. Thus we can replace infinite limits of summation over l in (28) with $\pm N$, where $N >> k_v/\pi$.

Now consider Lagrange interpolation allowing representation of $[l^2 - (k_v/\pi)^2]^{-1}$ in a form of finite series of terms like l^{-2p}, $p = 1, 2, ..., N$ with strict equality of both representations for $|l| = 1, 2, ..., N$ (see Appendix D). Applying this representation in (28) we obtain series like

$$\sum_{l=1}^{N} (-1)^l \sum_{p=1}^{N} \frac{\beta'_p}{l^{2p}} \left(\frac{k_v}{\pi l} \right)^{|m|+\nu} J_m(\pi l r)$$

(ν as above in (28)). Once more it is seen that the summation over l can be extended to infinity with error of an order of $O(l/N)$.

Finally, an admissible approximation to (28) is

$$-\Phi^0 = -\frac{\sin k_v}{k_v} e^{jm\vartheta} \sum_{l=-\infty}^{\infty} (-1)^l \begin{cases} 0; & \text{for } l = 0 \text{ and } m = 0 \\ \sum_{p=\nu+|m|(2)}^{N} \frac{\beta_p^{(m)}}{(\pi l)^p} J_m(\pi l r); & l \neq 0 \\ l; & \text{for } l = 0 \text{ and } m = 0 \end{cases} \qquad (29)$$

where summation over m is limited to $|m| < M$ and β_p appearing above are corresponding coefficients of the Lagrange interpolation calculated for N dependent on $|m|$, namely for $N_m = N - |m|$. Note that p varies from $|m| + \nu$ to N by step of 2 so that both p and m have the same parity. To obtain good approximation one has to apply large value of N, at least to fulfil $N - M >> k_v/\pi$.

4.2. Evaluation of charge distribution

A comparison of (29) and (26) makes evident that:

i) electric charge distribution induced by SAW can be expanded into a series like (25), resulting in the similarity of both the above series.

ii) the expansion coefficients σ_{mn} can be evaluated on the strength of equality of similar components appearing in (26) and (29) at the same m and p.

iii) when comparing the above series, components with $p < |m|$ must be neglected what ensures that the number of equations equals the number of unknown (see Section 3.2).

A direct comparison of (29) and (28) takes place for every m and $p \neq 0$, and separately for free term at $l = 0$ (only for $m = 0$). On the strength of (21), (27) the later gives directly the total electric charge induced on the grounded disk by the incident wave of electric potential of unitary amplitude (6)

$$Q = (4/\chi_0) \frac{\sin k_v}{k_v} \qquad (30)$$

It follows from this relation taken for $k_v \to 0$ that the disk capacitance is [10], [15]

$$C = 4/\chi_0 \tag{31}$$

The simultaneous equations obtained as a result of the comparison ii) can be solved numerically on the usual way. However note that for the simplest case of circular disk on isotropic substrate, when only $\chi_0 \neq 0$ and the remaining $\chi_k = 0$ the simultaneous equations are separated for every m. What's more, the matrix of the equations has a triangular form in this case (this follows from the triangular form of truncated matrix $\alpha_p^{(\cdot,n)}$ for $p \geq |m|$, where the dot upper index means any particular value of m, see Appendix C and the discussion at the end of Section 3.2, below (26), concerning zero-valued series of Bessel functions).

It is seen that the above equations allow to evaluate all σ_{mn} except σ_{00} which can be evaluated on the strength of (30) and (27). This concludes the evaluation of charge distribution on a grounded disk. It was discussed in Section 2.2 above how it can be exploited in the case of free (floating) disk. The simple result is that the disk potential induced on the floating disk is $V = Q/C = \sin k_v / k_v$.

5. Angular dependence of the scattered far-field

5.1. Asymptotic analysis of the scattered SAW

Relation (10) describes the scattered electric potential wave on the substrate surface at point (r, ϑ), far from the disk, where the wave can be considered as plane wave which Poynting vector is oriented in direction ϑ. The double integral over the disk area S can be evaluated on the similar way as the integral (19) in Section 3 above. Indeed, we have after simple transformations with taking into account (C.2) (summation after m, n, k, note that g^A is inversely proportional to $\sqrt{r}$, see Appendix A)

$$\Phi = \iint_S g^A \rho \, dS' = \frac{C_\vartheta}{\sqrt{r}} \sigma_{mn} e^{jm(\theta_\vartheta + \pi/2)} \int_0^1 \frac{r'(T_n - t_k^{(m,n)} T_k)}{(1 - r'^2)^{1/2}} J_m(r' k_\vartheta) \, dr' \tag{34}$$

We easily note the similarity of every k-th term of (34) and (19), if only (πl) is replaced by k_ϑ. Thus we can write

$$\Phi = \frac{C_\vartheta}{\sqrt{r}} \sigma_{mn} e^{jm(\theta_\vartheta + \pi/2)} 2 \left(c_l^{(m,n)} - t_k^{(m,n)} c_l^{(m,k)} \right) \Big|_{(\pi l) = k_\vartheta} \tag{35}$$

Taking into account (C.2), (C.4) we see that

$$\Phi = \frac{C_\vartheta}{\sqrt{r}} \sigma_{mn} e^{jm(\theta_\vartheta + \pi/2)} \left[\frac{\alpha_p^{(m,n)}}{(\pi l)^p} \cos(\pi l) + \frac{\gamma_p^{(m,n)}}{(\pi l)^p} \sin(\pi l) \right] \Bigg|_{(\pi l) \to k_\vartheta \neq 0} \tag{36}$$

where α_p – see (C.5), similarly $\gamma_p = (\operatorname{sign} m)^m (d_p^{(m,n)} - \sum_m d_p^{(m,k)} t_k^{(m,n)})$.

Below we show that we need not evaluate all γ_p, but only γ_1 (for m even). Indeed, it is easy to prove that the right-hand side of (35) is a regular function at $k_\vartheta \to 0$, then (36) should be regular as well. It means, that every term like $\alpha\cos(k_\vartheta)/k_\vartheta$ must be accompanied with term like $\gamma\sin(k_\vartheta)/k_\vartheta^2$ just necessary to eliminate singularity from the expression $[\alpha\cos(k_\vartheta) + \gamma\sin(k_\vartheta)/k_\vartheta]/k_\vartheta$ at $k_\vartheta = 0$. This allows to evaluate γ for the given α.

Exactly, the expression in brackets in right-hand side of (36) can be rewritten as follows

$$\gamma_1 \sin k_\vartheta/k_\vartheta + \frac{\alpha_2\cos k_\vartheta + \gamma_3 \sin k_\vartheta/k_\vartheta + \dfrac{\alpha_4\cos k_\vartheta + \gamma_5 \sin k_\vartheta/k_\vartheta}{k_\vartheta^2} + \dots}{k_\vartheta^2}; \quad \text{for } m \text{ even}$$

$$\frac{\alpha_1\cos k_\vartheta + \gamma_2 \sin k_\vartheta/k_\vartheta + \dfrac{\alpha_3\cos k_\vartheta + \gamma_4 \sin k_\vartheta/k_\vartheta}{k_\vartheta^2} + \dots}{k_\vartheta}; \quad \text{for } m \text{ odd} \tag{37}$$

As we see, every γ_p can be evaluated from the given vector of α_p this way, except γ_1 which appears only for m even and which must be evaluated directly from (35), (36). It should be noted however that the above representation is not convenient for computation for small value of k_ϑ, in which case it is better to apply (35) and to evaluate suitable Bessel functions (20) in ordinary way.

5.2. Numerical examples

All results shown below (except Fig. 11) were obtained either for circular disk of unitary radius or for elliptic disk with main axes $1/\alpha$ and α (that is for $R = 1$, see Appendix B).

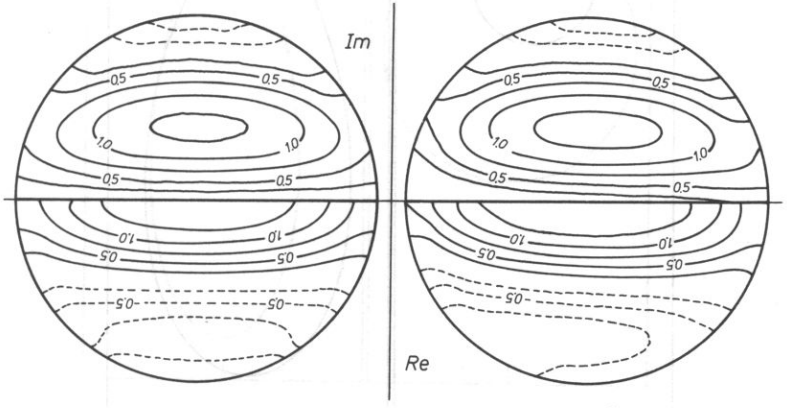

FIG. 2. Diagram of electric charge distribution on a circular disk of unitary radius for $k_v = \pi$. Left figure – isotropic substrate, right figure – dielectrically anisotropic substrate ($\chi_0 = 1$, $\chi_2 = -j.2$), upper part of the figures – imaginary component, and lower part – real component of $\rho(1 - r^2)^{1/2}$ (see relation (11)).

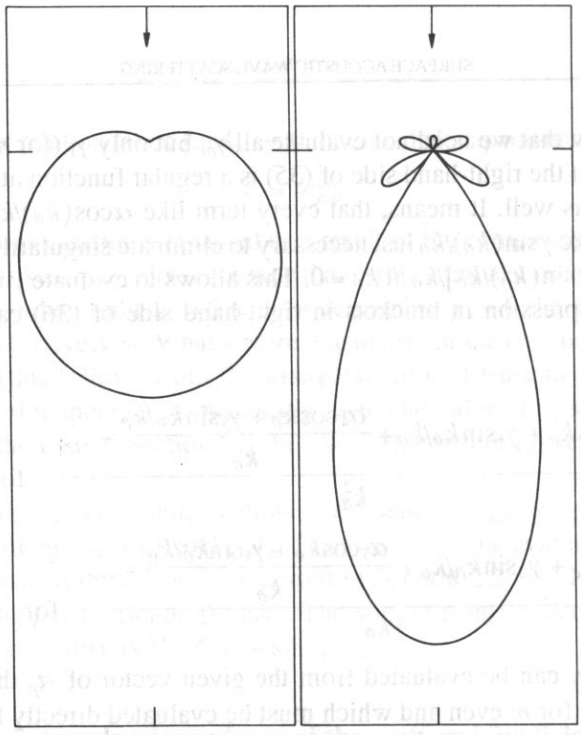

FIG. 3. Angular scattering pattern for grounded circular disk on isotropic substrate, $k_v = \pi/2$ (on left) and $k_v = 3\pi/2$ (right figure).

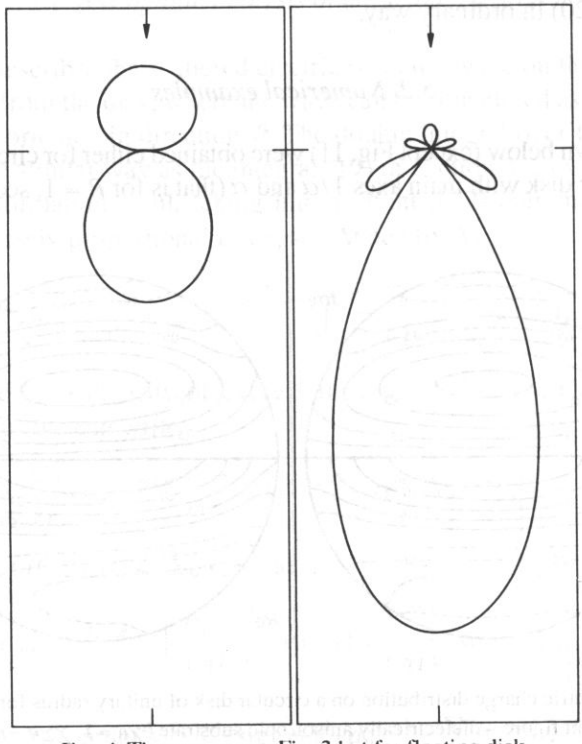

FIG. 4. The same as on Fig. 3 but for floating disk.

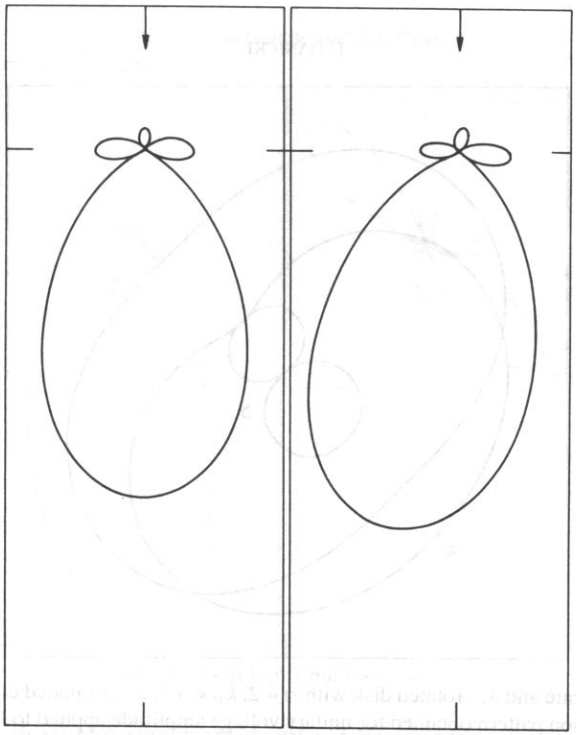

FIG. 5. Circular disk on isotropic (left) or anisotropic substrate (right, the dielectric anisotropy only, the same as in Fig. 2), for $k_v = \pi$.

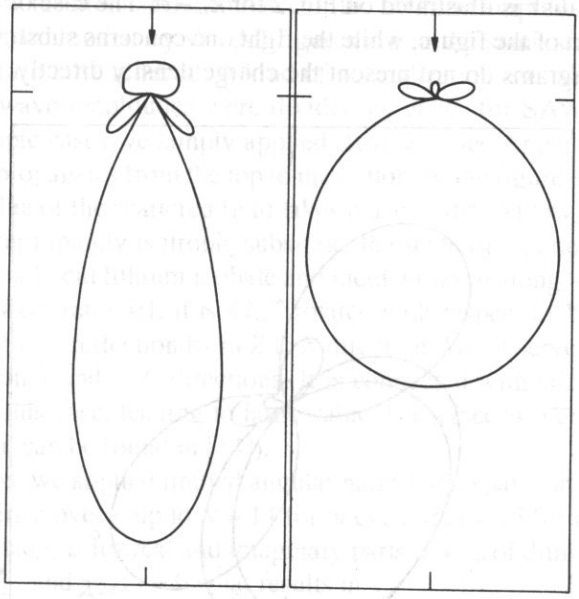

FIG. 6. Isotropic substrate and elliptic disk with $\alpha = \sqrt{2}$, longer axis horizontally oriented and $k_v = \pi\sqrt{2}$ (left figure), and vertically oriented and $k_v = \pi/\sqrt{2}$ (right figure), incident SAW from top of the figures.

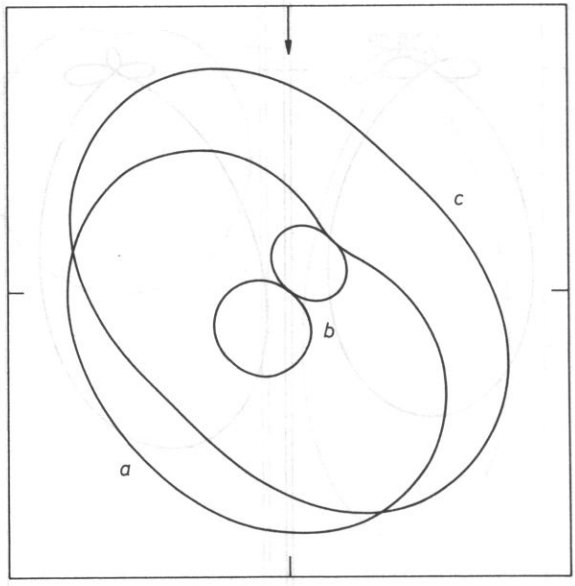

FIG. 7. Isotropic substrate and 45° rotated disk with $\alpha = 2$, $k_v = \pi/4$, a – grounded disk, b – floating disk, c – radiation pattern obtained for unitary voltage amplitude applied to the disk.

The influence of dielectric anisotropy of the substrate on the electric charge distribution on the circular disk is illustrated on Fig. 2 for $k_v = \pi$. The case of isotropic substrate is shown on left part of the figure, while the right one concerns substrate with $\chi_0 = 1$ and $\chi_2 = -j0.2$. The diagrams do not present the charge density directly, it illustrates rather

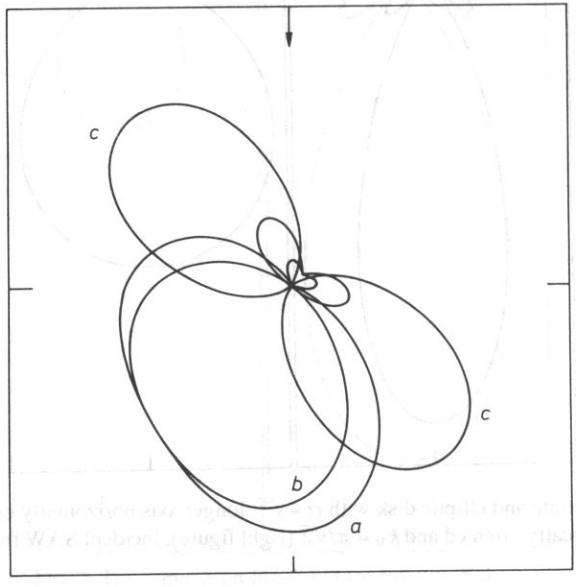

FIG. 8. As in Fig. 7 but for $k_v = \pi/2$.

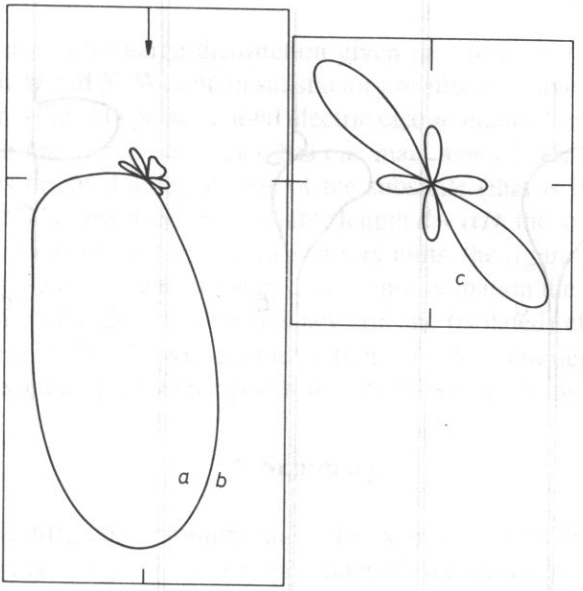

FIG. 9. As in Fig. 7 but for $k_v = \pi$.

the relation (25) with square-root term dropt for better presentation of the charge distribution in vicinity of the disk border. We see that the charge distribution is effected well by the dielectric anisotropy of the substrate.

Figs. 3–10 show the angular dependence of the far-field amplitude S (see (A.12)) of the scattered SAW, multiplied by $\sqrt{r}$. All figures are in the same scale except Fig. 10, which dimensions are 50% reduced. A kind of normalization was also applied, namely the values of the wave amplitudes were divided by $\Delta v/v$ for SAW propagating in z-direction (in isotropic cases we simply applied $\Delta v/v = 1$, see Appendix A). In all cases the incident wave propagates from the top to the bottom of the figures. As we see, in each case the largest value of the scattered field takes place in the shadow area.

Figs. 2–9 concern mainly isotropic substrate, the scattering patterns are rather typical. Fig. 10 concerns Y–cut lithium niobate and incident wave along $-Z$-axis. The disk is elliptic with main axes ratio 4:1, it is 47.2° rotated with respect to X-axis, as it is commonly applied for SAW reflection from Z to X direction. We observe large amplitude of the scattered field in + and − Z directions. It is connected with small curvature of the slowness curve in this case, leading to large value of C_ϑ (see Appendix A) for $\vartheta \approx 90°$ (detailed discussion can be found in [14]).

In computations, we applied limited angular harmonic expansion (25) with $|m|$ up to $M = 9$ and finite series over n up to $N = 14$ for m even or $N = 15$ for m odd. This results in simultaneous equations for real and imaginary parts of σ_{mn} of dimension up to 60*60. Note that $\chi_{-2n} = \chi^*_{2n}$ and $\chi_{2n+1} = 0$ what results in

$$\sigma_{-mn} = (-1)^m \sigma^*_{mn} \tag{38}$$

so that the equations are separated for even and odd m. The calculations can then be arranged in such a way that only components with $m \geq 0$ are to be evaluated. The conver-

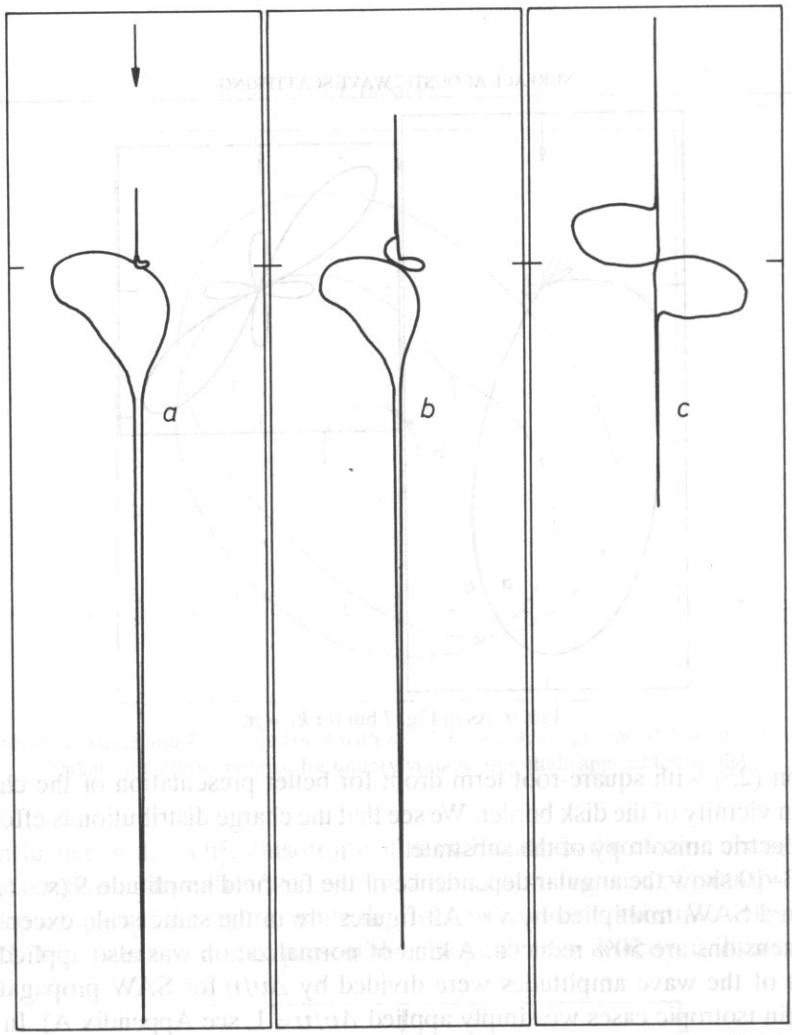

FIG. 10. 4:1 elliptic disk ($\alpha = 2$), 47.2° rotated with respect to X–axis of $LiNbO_3$, Y-cut, incident wave in $-Z$ direction (vertical axis of the figures), $k_v = \pi/2$, a, b, c – as in Fig. 7.

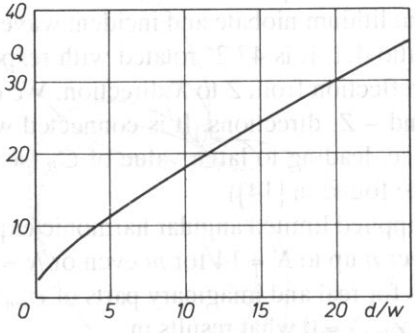

FIG. 11. The dependence of total electric charge amplitude Q induced on elliptic electrode on the electrode length d (that is on the disk main axis which is perpendicular to the direction of SAW propagation). Vertical axis in arbitrary units. The electrode width w is assumed constant, applied as a unit for figure horizontal axis.

gence of the solution for charge distribution given in a form of (25) was checked by applying different M and N. We obtain satisfactory results for wave-numbers up to 6.

The last figure (Fig. 11) presents total electric charge induced on the grounded elliptic disk on YZ lithium niobate. The disk has one main axis of constant (unitary) length $w = D/\alpha$ which is oriented along Z–axis of the substrate (that is in SAW propagation direction), and the other main axis has variable length $d = \alpha D$, the total charge is dependent on (the vertical axis of the figure is in arbitrary units, the figure presents the relation (30) with $k_v w$ assumed constant). In very coarse approximation the figure may be interpreted as concerning the detection "efficiency" of one (isolated) electrode of an interdigital transducer of SAW. As we see, the "efficiency" does not depend linearly on the electrode length what may effect the performance of apodized transducers [8].

6. Summary

An anisotropic diffraction problem cannot be expected to be solved explicitly so that computations are necessary. The theory presented above allows to perform some computations only once ($\alpha_p^{(m,n)}$ can be stored and applied in all cases). It is worth to note that important part of computations are performed with integer numbers (α_p are integer numbers), however the value of these numbers grows very fast with m, n, p, so that applying FORTRAN double precision variables on IBM-PC allows to perform exact computations with $|m| \le 9$ and $n \le 15$ only. This work was supported by grant 312129101.

Appendix A

With help of new spatial and spectral coordinates

$$k_x = k\cos\theta; \quad x = r\cos\vartheta$$
$$k_z = k\sin\theta; \quad z = r\sin\vartheta \tag{A. 1}$$

the inverse Fourier transform of $G(\mathbf{k})$ can be written as

$$g(r, \vartheta) = (2\pi)^{-2}\int_0^\infty dk \int_0^{2\pi} e^{-jrk\cos(\theta-\vartheta)}\chi(\theta)d\theta + \\ -(2\pi)^{-2}\int_0^\infty dk\int_0^{2\pi}\chi(\theta)\frac{k_0^2(\theta)-k_v^2(\theta)}{k^2-k_v^2(\theta)}e^{-jrk\cos(\theta-\vartheta)}d\theta \tag{A. 2}$$

where (n takes even values only because of polar symmetry of ε_e)

$$\chi(\theta) = 1/c_e(\theta) = \varepsilon_e(\theta+\pi) = \sum_{-\infty(2)}^{\infty}\chi_n e^{jn\theta} \tag{A. 3}$$

(2 in brackets means that n varies **step 2**).

First component of g is [11]

$$g^E(r, \vartheta) = \frac{1}{2\pi r}\chi(\vartheta+\pi/2) \tag{A. 4}$$

while the second one can be transformed into

$$g^R(r,\vartheta) = (2\pi)^{-1}\int_{-\infty}^{\infty} dk \int_0^{\pi} \frac{\Delta(\theta+\vartheta+\pi/2)}{k^2 - k_v^2(\theta+\vartheta+\pi/2)} e^{jrk\sin\theta} d\theta \tag{A. 5}$$

allowing to apply Jordan's lemma on the complex k–plane. The result is

$$g^R(r,\vartheta) = j/(4\pi)\int_{\vartheta-\pi/2}^{\vartheta+\pi/2} [\Delta(\theta')/k_v(\theta')] e^{-jrk_v(\theta')\cos(\theta'-\vartheta)} d\theta' \tag{A. 6}$$

where

$$\Delta/k_v = (k_0 + k_v)(k_0 - k_v)/(k_v\varepsilon_e) = 2(k_0 - k_v)/\varepsilon_e = 2\chi\Delta k$$

The function $g = g^E + g^A$ taken with arguments $(\bar{r}, \bar{\vartheta})$ describing vector $(\mathbf{r} - \mathbf{r}')$ in polar coordinates presents the electric Green's function for piezoelectric half-space. This function expresses electric potential at point $\mathbf{r}$ resulting from the point electric charge at point $\mathbf{r}'$, where both $\mathbf{r}$ and $\mathbf{r}'$ are on the substrate surface.

Let us evaluate the relation between $\|g^R\|$ and $\|g^E\|$ for the simplest case of isotropic substrate. We have

$$\|g^R\|/\|g^E\| < \pi r\,\Delta k \approx 20(\Delta v/v) r/\lambda$$

where $\Delta v/v$ is of an order of .001 for week piezoelectrics and .01 for strong ones ($\Delta v/v = .024$ for YZ lithium niobate). The above estimation means that in all cases g^R can be neglected when evaluating potential in the distance of about one wave-length λ from the point electric charge, and up to above 10λ for week piezoelectrics. This justifies the approximation (9) in the main text of the paper.

An asymptotic Green's function g for large value of r (it follows from the above reasoning that g^E can be neglected in this case) can be obtained applying the stationary phase method [12] to (A.6). Taking into account that

$$\bar{\mathbf{r}} = \mathbf{r} - \mathbf{r}' \tag{A. 8}$$

for $r \to \infty$, where r is the distance from the disk center to point (r, ϑ), where electric potential is evaluated, while (r', ϑ') is the point in the disk area, where electric charge is placed, and r is the distance between these two points, we obtain

$$g^A(\vartheta; r', \vartheta') = g^R(r \to \infty, \vartheta; r', \vartheta') \approx$$

$$\approx j/(2\pi)\int_{\vartheta-\pi/2}^{\vartheta+\pi/2} \chi(\theta')\Delta k(\theta') e^{-j(\mathbf{r}-\mathbf{r}')\cdot\mathbf{k}_v(\theta')} d\theta' \tag{A. 9}$$

Let us denote a stationary phase point as θ_ϑ (below we assume that there is only one such a point). This is an angle, for which the Poynting vector of the wave with wave-number $k_v(\theta_\vartheta)$ is directed to the observation point (r, ϑ) (as known, the Poynting vector is perpendicular to the slowness surface $k_v(\vartheta')$, here $\vartheta' = \theta_\vartheta$ [13]). The stationary phase method yields

$$\mathbf{k}'_\vartheta = \mathbf{k}_v(\theta_\vartheta) \tag{A. 10}$$

$$g^A(\vartheta; r', \vartheta') = \frac{C_\vartheta}{2\pi\sqrt{r}} \exp[jr' k_\vartheta \cos(\vartheta' - \theta_\vartheta)] e^{-j\mathbf{r}'\cdot\mathbf{k}_\vartheta} \qquad \text{(A. 10)}$$

[cont.]

$$C_\vartheta = \left[\frac{j2\pi}{\frac{d^2}{d\theta'^2}[k_v(\theta')\cos(\theta' - \vartheta)]\Big|_{\theta' = \theta_\vartheta}} \right]^{1/2} \chi(\theta_\vartheta)\Delta k_v(\theta_\vartheta)$$

on the assumption that the second derivative in the denominator in C_ϑ is different from zero [14]. Further transformations gives (phase term $\exp[-jrk_\vartheta\cos(\vartheta - \theta_\vartheta)]$ dropt)

$$g^A(\vartheta; r', \vartheta') = \frac{C_\vartheta}{2\pi\sqrt{r}} \sum_m J_m(r' k_\vartheta) e^{-jm\vartheta'} e^{jm(\pi/2 + \theta_\vartheta)} \qquad \text{(A. 11)}$$

Let us define the amplitude of plane SAW as S, where Poyinting vector of SAW is $\Pi = SS^*/2$ by the definition of S. Unitary amplitude SAW propagating in z-direction is coupled to electric potential of amplitude Φ_z, while propagating in direction ϑ is coupled to potential Φ_ϑ. Taking this into account one obtains the dependence of scattered SAW far-field on the the angle ϑ as follows

$$S(\vartheta) = \Phi(\vartheta)[\Phi_z/\Phi_{\theta_s}] \qquad \text{(A. 12)}$$

Appendix B

Let us consider an elliptic disk having main axes R/α and αR. The disk orientation in the coordinate system x, z is described by rotation angle θ_0. The disk is transformed into a circle of unitary radius on the (ξ, ζ) plane, where new cartesian coordinate system ξ, ζ is defined by

$$z/R = (\zeta/\alpha)(1 + \alpha^4 \mathrm{tg}^2\theta_0)^{1/2}\cos\theta_0$$
$$x/R = [\alpha\xi - \zeta(1 - \alpha^4)\sin\theta_0]/\cos\theta_0 \qquad \text{(B. 1)}$$

(the new system is chosen in such a way that ζ–axis is directed along z–axis, it means that the incident wave propagates along $-\zeta$–axis in new coordinate system).

Consider a wave propagating in the direction that is ϑ' rotated with respect to ξ in the new coordinate system, and the wave-number of the wave in new coordinate system is k'. In old coordinate system this wave correspond to (that is, it is transformed into) the wave with wave-number k, and its propagation direction is rotated from x–axis with angle ϑ, where

$$\mathrm{tg}\,\vartheta = \frac{(1 - \alpha^4)\mathrm{tg}\theta_0 + (1 + \mathrm{tg}^2\theta_0)\alpha^2 \mathrm{tg}\,\vartheta'}{1 + \alpha^4 \mathrm{tg}^2\theta_0}$$
$$k = sk' \qquad \text{(B. 2)}$$
$$s = \frac{1}{R}\left(\frac{(1 + \alpha^4 \mathrm{tg}^2\theta_0)}{\alpha^2(1 + \mathrm{tg}^2\theta_0)\cos^2\vartheta'}(1 + \mathrm{tg}^2\vartheta) \right)^{1/2}$$

Note also, that the point described in polar coordinates by r' and ϑ' in the new system corresponds to point described in polar coordinates by r and ϑ in old system, where

$$r = r'/s \tag{B. 3}$$

On the strength of the relation (3) the amplitude of electric potential resulting from the wave of surface charge fulfils

$$\frac{\Phi}{\Delta D_\perp} = \frac{1}{\varepsilon_e(\vartheta) s k'} \frac{(sk')^2 - k_0^2}{(sk')^2 - k_v^2} = \frac{1}{k'[s\varepsilon_e(\vartheta)]} \frac{k'^2 - (k_0/s)^2}{k'^2 - (k_v/s)^2} \tag{B. 4}$$

As we see, in the coordinate system (ξ, ζ) we obtain similar relation as in the original system (3), but with $\varepsilon_e'(\vartheta') = s\varepsilon_e(\vartheta)$, $k'(\vartheta') = k_0(\vartheta)/s$, $k_v'(\vartheta') = k_v(\vartheta)/s$ with $\vartheta = \vartheta(\vartheta')$, instead of ε_e, k_0, k_v.

The relation (36) gives the scattered potential amplitude. In the transformed coordinate system where the disk is a circular one with unitary radius. To transform the angular dependent scattered potential $\Phi(\vartheta)$ into the original system of coordinates one should take into account the relations (B.1). To apply it we need to denote polar coordinates of the same point in the old system of coordinates as r and θ, while polar coordinates in the new system (that is in the system applied in (36)) as r' and θ'. With these denotations the far-field potential wave is

$$\Phi(\theta) = \Phi(\theta')(r'/r)^{1/2} \tag{B.5}$$

where $\theta = \theta(\theta')$ and $\sqrt{(r'/r)}$ term appears above as a result of the dependence of g^A on r (θ and ϑ from (B.2) are different angles!).

It is worth to note that the scattered far-field amplitude can be also calculated directly in the original system of coordinates, with applying suitable asymptotic Green's function and charge distribution expressed in the original coordinates. The evaluation of the integral (10) however, needs integral variable transformation leading to integration over a circle. Both approaches give the same results.

Appendix C

As known, it is for integer k

$$J_{k+1/2}(z) = z^{-1/2} \sum_p \left(\frac{a_p^{(1)}}{z^p} \cos(z) + \frac{a_p^{(2)}}{z^p} \sin(z) \right)$$

where $a_p^{(1)}$ and $a_p^{(2)}$ can be found elsewhere [16], and summation after $p \geq 0$ takes place in finite limits. The above allows to rewrite (21) in form (for $l \neq 0$)

$$c_1 = (\pi/2)^2 (\operatorname{sign} m)^m \left(\sum \frac{{}^1a_p^{(m,n)}}{(\pi l/2)^p} \cos^2(\pi l/2) + \sum \frac{{}^2a_p^{(m,n)}}{(\pi l/2)^p} \sin^2(\pi l/2) + \right.$$
$$\left. + \sum \frac{{}^3a_p^{(m,n)}}{(\pi l/2)^p} \cos(\pi l/2) \sin(\pi l/2) \right) \tag{C. 1}$$

which can be further transformed into $(\cos(\pi l) = (-1)^l)$

$$c_1 = \pi(\operatorname{sign} m)^m \left(\sum_{p=P_1(2)}^{P_2} \frac{a_p^{(m,n)}}{(\pi l)^p} \cos(\pi l) + \sum_{p=P_3(2)}^{P_4} \frac{b_p^{(m,n)}}{(\pi l)^p} + \sum_{p=P_5(2)}^{P_6} \frac{d_p^{(m,n)}}{(\pi l)^p} \sin(\pi l) \right) \tag{C. 2}$$

The coefficients a, b and d can be easily calculated numerically, it is also easy to check that the following Property I takes place

PROPERTY I

a) $b_p^{(0,n)} b_p^{(l,n)} = 0$

what means, that there is not the second component in brackets in (C.2) for $m = 0$ or $m = 1$,

b) in (C.2) the summation after p is **step 2** and takes place in the following limits (m and n have the same parity)

$P_1 = 2$ for m even or 1 for m odd,

$P_2 = n$,

$P_3 = 2$ for n even or 1 for n odd,

$P_4 = |m|$,

$P_5 = 1$ for m even or 2 for m odd,

$P_6 = n + 1$,

c) in (C.2) the number of components of $(+1)^l/l^p$ kind is $|m/2|$ (integer part of the product for m odd).

The polynomial (24) can be written as a combination of Tchebyshev polynomials of the lower orders as follows [16]

$$T_n^{(m)} = T_n - \sum_{k(2)}^{|m|-2} t_k^{(m,n)} T_k \tag{C. 3}$$

where t_k are easy to find and where summation after k starts from 0 for m even or 1 for m odd, step 2, to $|m| - 2$.

The following Property II takes place for every m and $n \geq |m|$

PROPERTY II

$$b_p^{(m,n)} - \sum_{k}^{|m|-2} t_k^{(m,n)} b_p^{(m,n)} = 0 \tag{C. 4}$$

The formal proof of (C.4) is expected very tedious, but it is very easy to check it numerically. All numbers appearing in (C.4) are integers so that the numerical check of (C.4) may be considered exact and sufficient for our purpose in the paper.

Now consider charge distribution in the form of (24). On the strength of (C.4) we obtain the representation (26) for potential under the disk, where components like $(+1)^l/l^p$ does not appear and

Table 1. Coefficients $\alpha_p^{(m,n)}$ and $\gamma_1^{(m,n)}$ for some m and $n \geq m$ in following rows, in subsequent columns α_p are arranged with growing p except the cases of even m, where in the first column γ_1 is presented.

		γ_1 even)	α_2 (m even)	α_4	...	
m	n	a_1 (m odd)	α_3 (m odd)	α_5	...	
0	2	1	2			
	4	1	8	-72		
	6	1	18	-912	7200	
	8	1	32	-5280	192000	-1411200
1	1	-1				
	3	-1	12			
	5	-1	84	-720		
	7	-1	312	-13200	100800	
	9	-1	840	-104880	3528000	-25401600
2	2	-2	-6			
	4	0	-8	120		
	6	-2	-22	1200	-10080,	
	8	0	-32	6240	-241920	1814400
3	3	4	-60			
	5	-4	-100	1680		
	7	8	-472	21840	-181440	
	9	-8	-936	146160	-5382720	39916800
4	4	8	80	840		
	6	-16	-128	-1680	30240	
	8	32	320	-11424	483840	-3991680
5	5	-16	1680	-15120		
	7	48	-3696	-35280	665280	
	9	-112	11184	-315504	12640320	-103783680
6	6	-32	-672	40230	-332640	
	8	128	2560	-112896	-887040	17297280

$$\alpha_0^{(m,n)} = (\operatorname{sign} m)^m \left(a_p^{(m,n)} - \sum_k t_k^{(m,n)} a_p^{(m,k)} \right) \tag{C.5}$$

Table I presents values of α for some indices m, n, and p. The calculation were performed in double precision (18 decimal digits). Note that the values presented in Table I are integer numbers so that their values can be considered as exact ones.

Appendix D

Consider an expression $1/(n^2 - \varepsilon^2)$ for $\varepsilon < 1$ firstly. It can be expanded into a Taylor series as follows

$$\frac{1}{n^2 - \varepsilon^2} = \frac{1}{n^2} + \frac{\varepsilon^2}{n^4} + \ldots + \frac{\varepsilon^{2N}}{n^{2N}} \left(\frac{1}{n^2} + \frac{\varepsilon^2}{n^4} + \ldots \right) \tag{D. 1}$$

The Lagrange interpolation formula applied to (D.1) for $n = 1, 2, \ldots, N$ yields (below, there is strict equality for n in the above limits, a_n is given in rel. 3.1.1 of [17], for instance)

$$\frac{1}{n^2 - \varepsilon^2} = \frac{a_1}{n^2} + \frac{a_2}{n^4} + \ldots + \frac{a_{2N}}{n^{2N}}; \quad n = 1, 2, \ldots, N \tag{D. 2}$$

By comparison of (D.1) and (D.2) we see that applying $a_1 = 1$, $a_2 = \varepsilon^2, \ldots, a_N = \varepsilon^{2(N-1)}$ we admit an error to (D.2) of an order of $\varepsilon^{2N}/(1 - \varepsilon^2)$ thus vanishing for $N \to \infty$. It means that $a_1 \to 1$ for $N \to \infty$, similarly a_2 becomes constant dependent on ε etc. This reflects fact that $(n^2 - \varepsilon^2)^{-1}$ is close to n^{-2} for $n > N \to \infty$.

The above is difficult to prove for $\varepsilon > 1$ so we show it numerically in Table II below for N between 4 and 10 and for some ε (only a_1 is shown in the Table)

Table 2. First coefficient a_1 of Lagrange interpolation (D.2)

$\varepsilon^2 \backslash N$	4	5	6	7	8	9	10
.25	.99999	1.	1.	1.	1.	1.	1.
.9	.98270	1.0006	.99998	1.	1.	1.	1.
2.5	1.1978	.97802	1.0016	.99991	1.	1.	1.
3.9	19.927	-1.389	1.2903	.97490	1.0016	.99992	1.
9.5	54.608	-31.86	12.779	-1.833	1.4938	.93439	1.0069

Most important conclusion is that at least the leading term of Lagrange interpolation (D.2), that is the term a_1/n^2, became $1/n^2$ for large N. So applying (D.2) beyond its validity area, that is for all $n = 1, 2, \ldots, N, \ldots\infty$, we admit error of an order of $0(1/N^2)$.

References

[1] J.J. BOWMAN, T.B.A. SENIOR, P.L.E. USLENGHL, *Electromagnetic and acoustic scattering by simple shapes*, Nord-Holland, Amsterdam 1969.

[2] W.H. EGGLMAN, *Higher-order evaluation of electromagnetic diffraction by circular disks*, IRE Trans., **MIT–9**, 5, 408–419 (1961), **81**, 6, 1677–1682 (1987).

[3] F.J. SABINA, *General formulas for low-frequency acoustic scattering by soft body or disk*, JASA, **81**, 6, 1677–1682 (1987).

[4] B.A. AULD, *Acoustic fields and waves in solids*, A. Wiley Interscience Publ., NY.1973.

[5] K.A. INGEBRIGSTEN, *Surface waves in piezoelectrics*, J. Appl. Phys., **40**, 7, 2681–2686 (1969).

[6] R.F. MILSOM, N.H.C. REILLY, M. REDWOOD, *Analysis of generation and detection of surface and bulk acoustic waves by interdigital transducers*, IEEE Trans., **SU-24**, 3, 147–166 (1977).

[7] E. DANICKI, *Propagation of transverse surface acoustic waves in rotated Y-cut quartz substrates under heavy periodic metal electrodes*, IEEE Trans. **SU-30**, 5, 304–314 (1983).

[8] E. DANICKI, *Influence of bulk wave generation on SAW filter performance*, J. Tech. Phys., **21**, 3, 405–420 (1980).

[9] A.P. PRUDNIKOV, J.A. MARICHEV, *Integrals and series*, (in Russian), Nauka, Moscow 1986, v. 2.

[10] F. OBERHETTINGER, W. MAGNUS, *Adwendung der Elliptischen Functionen in Physik und Technik*, Springer Verlag, Berlin 1949.

[11] E. DANICKI, *Green's function for anisotropic dielectric halfspace,* IEEE Trans. **UFFC-35**, 5, 643 (1988).

[12] J.B. FELSEN, N. MARCUVITZ, *Radiation and scattering of waves*, Prentice Hall Englewood Cliff 1973.

[13] E. DIEULESAINT, D. ROYER, *Ondes elastiques dans les solides*, Masson, Paris 1974.

[14] A.A. MARDUDIN, *Surface acoustic waves on real surfaces,* ISSWAS'66 Proc., v.3, 22–62, Novosibirsk 1986.

[15] E. DANICKI, *Theory of Williamson's SAW probe* (in Polish) OSA'88 Proc. Warszawa 1988, 251–254.

[16] H. BATEMAN, A. ERDELY, *Higher transcendential functions*, McGraw-Hill 1953 v.2.

[17] W.H. PRESS, B.P. FLANNERY, S.A. TEUKOLSKY, N.T. VETTERLING, *Numerical recipes*, Cambridge Univ. Press 1986.

[18] J. BOERSMA, E. DANICKI, *On the solution of an integral equation arising in potential problem for circular and elliptic disk*, submitted for publication in SIAM J. Appl. Math., (1992).

Received February 5, 1991

ARCHIVES OF ACOUSTICS
17, 3, 413–423 (1992)

ACOUSTIC PRESSURE OF A FREELY VIBRATING CIRCULAR PLATE WITHOUT BAFFLE

L. LENIOWSKA and W. RDZANEK

Department of Physics, Department of Technics
Pedagogical University
(35-310 Rzeszów, ul Rejtana 16a)

Formula for an acoustic pressure of a circular plate under free vibrations without baffle board is derived with the use of oblate spheroidal coordinate system. The result is obtained in terms of a single series of spheroidal function products. The number of terms ensuring a required accuracy can be determined numerically. The field radiated by a plate without baffle is analysed for the first three vibration modes on the basis of their directional characteristics and accounting for various values of an interference parameter $h = 2\pi a/\lambda$.

1. Introduction

The knowledge of basic quantities that characterize an acoustic field is necessary to employ plates and shells vibrating systems used acoustic diagnostic applicances as well as receivers and transmitters of acoustic waves. It was not earlier than in the eighties that detailed analytical investigations on the acoustic field radiated by a circular plate begun Analysis comprised free vibrations [10, 11] and forced vibrations [12]. Damping effects and modifications of wave emission by its specific field were also accounted for [8, 13]. Relevant phenomena were assumed to be linear and vary in time in a sinusoidal manner. Relatively simple mathematical tools were used since a plate was considered to vibrate in an infinite plane baffle. No such baffle board exist in real situations and the obtained results were valid for sufficiently high frequencies only.

Acoustic fields around sources without baffles or supplied with finite rigid baffles were analysed in [1–5]. Directional characteristics and impedances for pulsating and oscillating piston with uniform wave velocity distribution were found by solving a wave equation with the use of separation of variables in the spheroidal frame of reference.

To date, investigations have been taking on acoustic fields radiated by a circular plate without any baffle or with a finite baffle. This subject is dealt with in this paper, which is an extension of [7] and also refers to [1–5].

Properties of the oblate spheroidal coordinate system are used to derive a formula for acoustic pressure of a circular plate freely vibrating without a baffle. The plate is as-

sumed to be thin, homogeneous and clamped at the circumference; surrounding medium is lossless. Employing the known solution for free vibration of such a plate, wave velocity distribution is found and transformed to the oblate spheroidal frame of reference. Such a degeneration of the frame leads to a formula for an acoustic pressure in terms of series of spheroidal function products. Since no standard numerical procedures have been worked out to calculate values of spheroidal functions, an attempt is made to prepare suitable algorithms. To determine eigenvalues of the wave equation and the expansion coefficients d_r^{mn}, Hodge's method [6] is used. Angular and radical spheroidal functions and the necessary derivatives of radial functions are calculated with the help of recurrence relationships given by FLAMMER [15], to within an accuracy of 6–7 significant figure after decimal point.

Directional characteristics are given for the first three modes of freely vibrating circular plate without baffle and – for the source of comparison – with finite baffle as well as for a piston with uniform vibration velocity distribution are also presented. For wave lengths shorter than the dimensions of considered sources the obtained results fully agree with the characteristics calculated for a freely vibrating plate with an infinite baffle by using Huygens–Rayleigh integral [10].

2. Vibration equation for a plate

Free vibrations of a thin homogeneous plate of density ρ and thickness H, small compared with its diameter $2a$, is described by an equation [16]

$$\frac{\partial^2 w}{\partial t^2} + \frac{B}{M}\nabla^4 w = 0, \tag{2. 1}$$

where M is a plate mass per unit area, B denotes its flexural stiffness and w is a deflection function. For a circular plate the equation (2. 1) is solved in polar coordinates and the deflections are [16]

$$w(r, t) = w(r)e^{-i\omega t} = [A_0 J_0(kr) + B_0 I_0(kr)]e^{-i\omega t} \tag{2. 2}$$

where

$$k^2 = \omega\sqrt{M/B}, \tag{2. 2a}$$

ω – frequency, $A_0 B_0$ – constants, J_0 – Bessel's zero-degree function of the first kind, I_0 – modified Bessel's zero-degree function of the first kind.

The vibration process is harmonic hence the equation (2.2) supplies the following expression for vibration velocity

$$v(r, t) = v(r)e^{-i\omega t} \tag{2.3}$$

$$v(r) = AJ_0(kr) + BI_0(kr) \tag{2. 4}$$

where

$$A = -i\omega A_0, \quad B = -i\omega B_0 \tag{2. 4a}$$

The velocity satisfies the boundary conditions for a clamped plate :

$$v(r)\big|_{r=a} = 0 \tag{2.5}$$

$$\frac{dv(r)}{dr}\bigg|_{r=a} = 0 \tag{2.6}$$

Their use in (2.4) leads to the so-called frequency equation

$$J_0(ka)I_1(ka) + J_1(ka)I_0(ka) = 0, \tag{2.7}$$

whose solution is a series $k = k_l$ for $l = 1, 2, 3$.

On account of the formula (2.2a) the free vibration frequency for the $(0, l)$ mode is

$$f_l = k_l^2\sqrt{M/B}/2\pi \tag{2.8}$$

Formula (2.4) becomes

$$\frac{v_l(r)}{A} = J_0(k_l r) - \frac{J_0(k_l a)}{I_0(k_l a)} I_0(k_l r) \tag{2.9}$$

3. Transformation of velocity distribution for the OSCS

The equation (2.9) will now be expressed in the oblate spheroidal coordinate system OSCS with the use of the following transformation

$$\begin{aligned} x &= b[(1-\eta^2)(\xi_0^2+1)]^{1/2}\cos\varphi \\ y &= b[(1-\eta^2)(\xi_0^2+1)]^{1/2}\sin\varphi \\ z &= b\,\xi\eta \end{aligned} \tag{3.1}$$

where

$$\varphi \in <0, 2\pi>,\ \eta \in <-1, 1>,\ \xi \in <0, \infty> \tag{3.1a}$$

Due to the symmetry with respect to the z–axis, Fig. 1, the problem can be considered in the xz–plane by assuming $\varphi = 0$ in the formulae (3.1). Since $r^2 = x^2 + y^2$ on account of (3.1) we get

$$r = b[(1-\eta^2)(\xi_0^2+1)]^{1/2} \tag{3.2}$$

Denoting the surface of a spheroid on which the source is transformed by ξ_0 and substituting (3.2) into (2.9), the following formula for the vibration velocity is reached in the OSCS

$$\frac{v_l(\eta, \xi_0)}{A} = \left[J_0(k_l b\sqrt{(1-\eta^2)(\xi_0^2+1)}) - \frac{J_0(k_l a)}{I_0(k_l a)} I_0(k_l b\sqrt{(1-\eta^2)(\xi_0^2+1)}) \right] \tag{3.3}$$

where $2b$ is a distance between focal points.

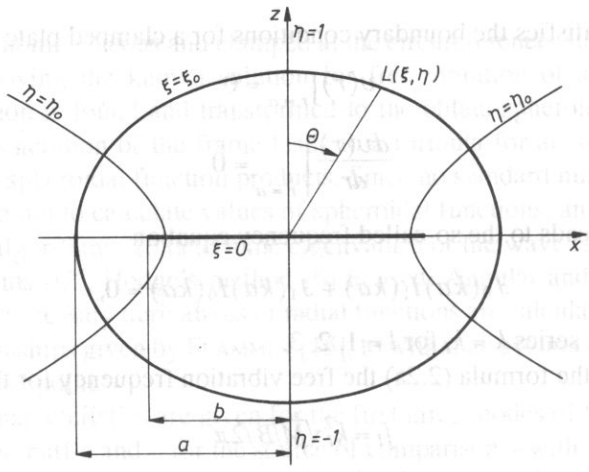

FIG. 1. Circular plate in the oblate spheroidal coordinate system.

4. Solution of Helmholtz equation in the OSCS

Let $\Phi(\xi, \eta, \varphi, t)$ denote a potential of a velocity field radiated by a plate. For harmonic processes can be expressed as $\Phi(\xi, \eta, \varphi, t)$

$$\Phi(\xi, \eta, \varphi, t) = \Psi(\xi, \eta, \varphi)\, e^{-i\omega t} \tag{4.1}$$

In order to determine a distribution of the acoustic field around a considered source, Neuman's boundary value problem for the Helmholtz equation should be solved in the OSCS

$$\left[\frac{\partial}{\partial n}(1-\eta^2)\frac{\partial}{\partial \eta} + \frac{\partial}{\partial \xi}(\xi^2+1)\frac{\partial}{\partial \xi} + \frac{\xi^2+\eta^2}{(\xi^2+1)(1-\eta^2)}\frac{\partial^2}{\partial \varphi^2} + h(\xi^2+\eta^2)\right]\Psi(\eta, \xi, \varphi) = 0 \tag{4.2}$$

where $h = k_0 b$ – dimensionless wave number ($k_0 = 2\pi/\lambda$). Boundary condition on the surface of a chosen spheroid $\xi = \xi_0$ has the form

$$\left.\frac{\partial \Psi}{\partial n} = \frac{1}{h_\xi}\frac{\partial \Psi}{\partial \xi}\right|_{\xi=\xi_0} = \begin{cases} -v(\eta, \xi_0), & 0 \le \eta \le 1 \\ 0 & -1 \le \eta < 0 \end{cases} \tag{4.3}$$

where $v(\eta, \xi_0)$ – according to the formula (3. 3)

$$h_\xi\big|_{\xi=\xi_0} = h_{\xi_0} = b\left(\frac{\xi_0^2+\eta^2}{\xi_0^2+1}\right)^{1/2} \cdot \text{ – the so-called scaling factor [15]} \tag{4.4}$$

In the OSCS the equation (4.2) can be separated into two differential equations, each being satisfied by its eigenfunction that depends on only one spatial variable – ξ or η.

Due to the symmetry of radiated waves with respect to the z–axis ($\varphi = 0$), the solution for outgoing waves is assumed to be a superposition of eigenfunctions, namely

$$\Psi(\eta, \xi) = \sum_{n}^{\infty} A_n S_{on}^{(1)}(-ih, \eta) R_{on}^{(3)}(-ih, i\xi) \tag{4.5}$$

where A_n constant coefficients to be obtained from boundary conditions, $S_{on}^{(1)}(-ih, \eta)$ – angular spheroidal function of the first kind, $R_{on}^{(3)}(-ih, i\xi)$ – radial spheroidal function of the third kind depending on the distance of a wave from its source. Asymptotic properties of radial functions [15],

$$R_{on}^{(3)}(-ih, i\xi) \xrightarrow{\xi \to \infty} (-i)^{n+1} \frac{e^{ih\xi_\infty}}{h\xi_\infty} \tag{4.6}$$

are such that the assumed solution (4.5) does also satisfy Somerfield's conditions.

5. Determination of coefficients A_n

To find A_n that appear in (4.5), the known function $v(\eta, \xi_0)$ describing vibration velocity of a source on the surface of a selected spheroid $\xi = \xi_0$, is expanded into a series with respect to the angular spheroidal functions [17]

$$v(\eta, \xi_0) = \frac{1}{h_{\xi_0}} \sum_{n}^{\infty} V_n S_{on}(-ih, \eta) \tag{5.1}$$

In turn, to determine the expansion coefficients V_n, the series (5.1) is multiplied by an orthogonal spheroidal function $S_{on'}(-ih, \eta)$ and integrated on the surface of spheroid. The following expression for V_n is arrived at:

$$V_n = \frac{1}{N_{on}(-ih)} \int_0^1 h_{\xi_0} v(\eta, \xi_0) S_{on}(-ih, \eta) d\eta \tag{5.2}$$

in which the $N_{on}(-ih)$ has the form

$$N_{on}(-ih)\,\delta_{nn'} = \int_{-1}^{1} S_{on}(-ih, \eta) S_{on'}(-ih, \eta) d\eta \tag{5.3}$$

On account of the condition (4.3), we get

$$v(\eta, \xi_0) = -\frac{1}{h_{\xi_0}} \sum_{n}^{\infty} A_n S_{on}(-ih, \eta) \frac{\partial R_{on}^{(3)}(-ih, \xi_0)}{\partial \xi} \tag{5.4}$$

Equating the corresponding terms in the series (5.1) and (5.4), we finally obtain

$$A_n = \frac{1}{N_{on}(-ih) R_{on}^{(3)'}(-ih, \xi_0)} \int_0^1 h_{\xi_0} v(\eta, \xi_0) S_{on}(-ih, \eta) d\eta \tag{5.5}$$

where

$$R_{on}^{(3)'}(-ih, \xi_0) = \frac{\partial R_{on}^{(3)}(-ih, \xi_0)}{\partial \xi} \tag{5.6}$$

6. Acoustic field of a circular plate

To describe an acoustic field radiated by a plane circular plate with no baffle the following acoustic pressure is applied

$$p = \rho \frac{\partial}{\partial t} \Phi(\xi, \eta, \varphi, t) = -i\rho c h \Psi(\xi, \eta) \tag{6.1}$$

where ρ – density of medium, c – sound velocity. The formula (6.1) together with (4.5) to describe $\Psi(\xi, \eta)$ refers to a source on a spheroid ξ_0. To make this solution valid for the considered plate, the coordinate system must be degenerated by assuming $\xi_0 = 0$. We get

$$p(\xi, \eta) = -i\rho h \sum_n A_n S_{on}(-ih, \eta) R_{on}^{(3)}(-ih, i\xi) \tag{6.2}$$

where

$$A_n = \frac{1}{N_{on}(-ih)} \frac{1}{R_{on}^{(3)'}(-ih, 0)} \int_0^1 v_l(\eta) S_{on}(-ih, \eta) \eta d\eta \tag{6.3}$$

and

$$v_l(\eta) = A \left[J_0(k_l a \sqrt{1-\eta^2}) - \frac{J_0(k_l a)}{I_0(k_l a)} I_0(k_l a \sqrt{1-\eta^2}) \right] \tag{6.4}$$

7. Diagrams and conclusions

When analysis an acoustic field radiated by a circular plate without a baffle, two cases can be examined each depending on a manner in which the waves are emitted by a system with the plate as a source of vibrations.

Model 1. A field radiated by the upper surface of the plate. The source should be assumed on the upper surface of spheroid and the field is to be calculated according to (6.2).

Model 2. A field radiated by both upper and lower surfaces of the plate. In the absence of baffle this results in two axially located sources on the upper and lower surfaces and vibrating in the counterphase manner. The coefficients A_n (6.3) should now be calculated from

$$A_n^* = \frac{-b}{N_{on}(-ih) R_{on}^{(3)'}(-ih, 0)} \left[\int_0^1 v_L(\eta) S_{on}(-ih, \eta) \eta d\eta + \int_{-1}^0 v_L(\eta) S_{on}(-ih, \eta) \eta d\eta \right] \tag{7.1}$$

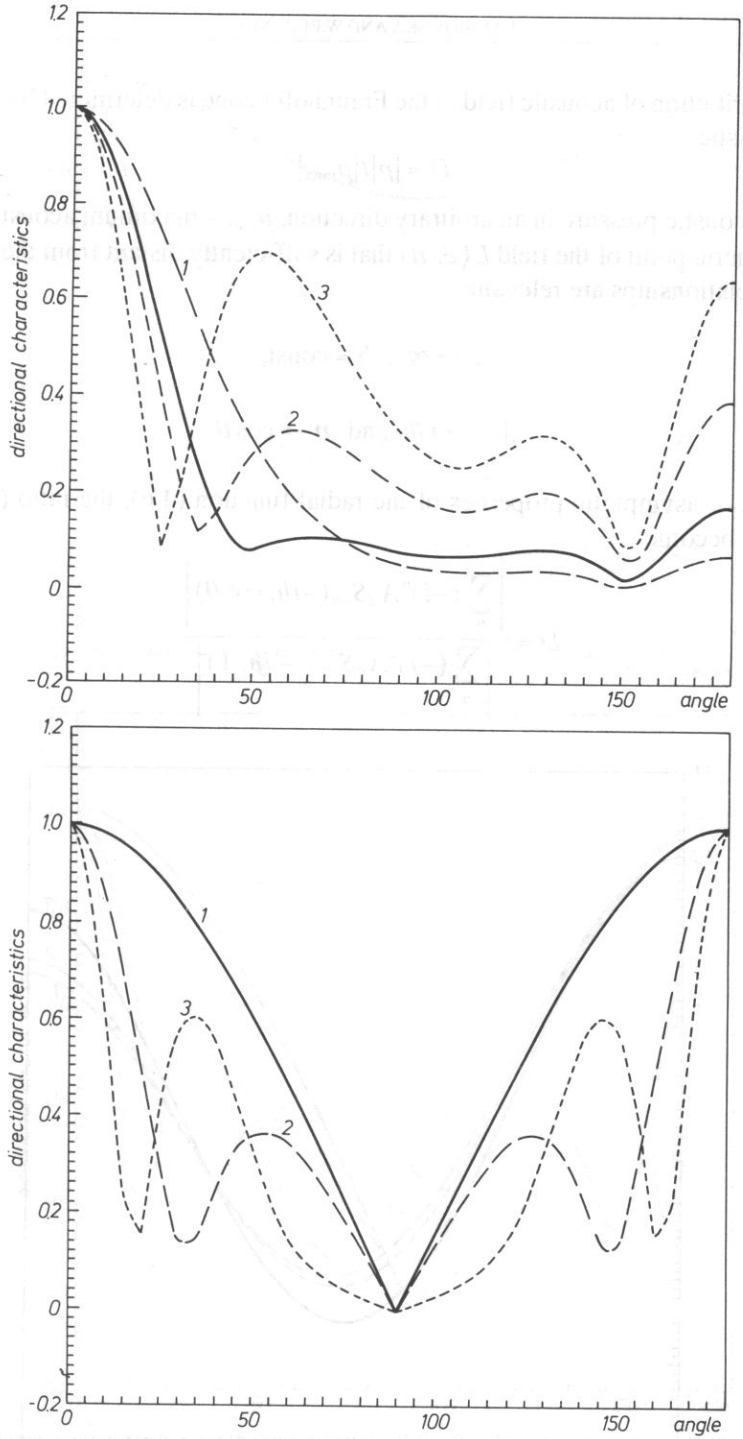

FIG. 2. Directional characteristics of the first three modes of freely vibrating circular plate without a baffle for $h = 5$; a – model 1, b – model 2. Curves are numbered according to the 1st, 2nd and 3rd mode.

The distribution of acoustic field in the Fraunhofer zone is determined by a directional characteristic

$$D = |p|/|p_{\max}| \tag{7.2}$$

where p – acoustic pressure in an arbitrary direction, $p_{\max}$ – maximum acoustic pressure.

At a generic point of the field $L(\xi, \eta)$ that is sufficiently distant from the source, the following relationships are relevant:

if

$$\xi \to \infty \ , \ b = \text{const}, \tag{7.3}$$

then

$$\xi|_{\xi_\infty} \to r/b \ \text{ and } \ \eta \to \cos\theta \tag{7.4}$$

On account of asymptotic properties of the radial function (4.6), the ratio (7.2) can be rewritten to become

$$D = \frac{\left|\sum_n (-i)^n A_n S_{on}(-ih, \cos\theta)\right|}{\left|\sum_n (-i)^n A_n S_{on}(-ih, 1)\right|} \tag{7.5}$$

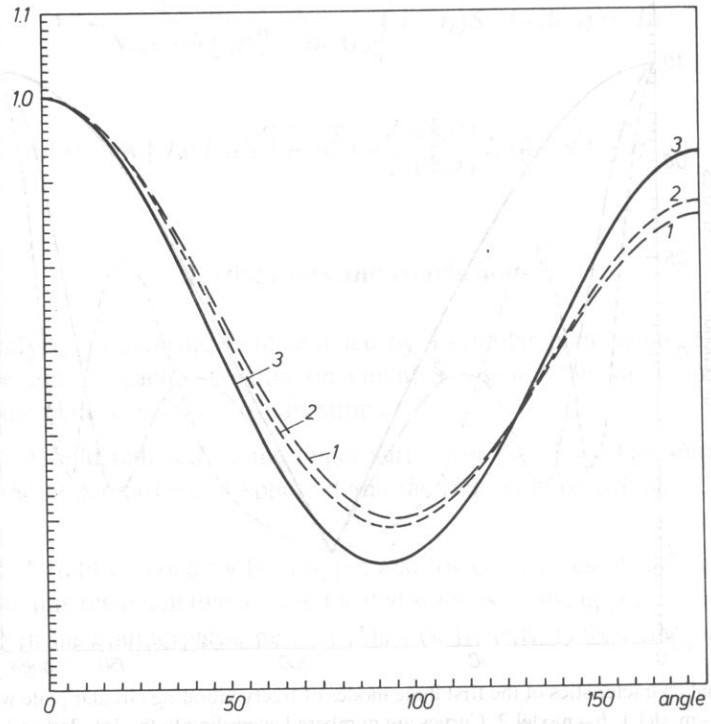

FIG. 3. Directional characteristics of the first three modes of freely vibrating circular plate without a baffle for $h = 1$, model 1. Curves are numbered according to the 1st, 2nd and 3rd mode.

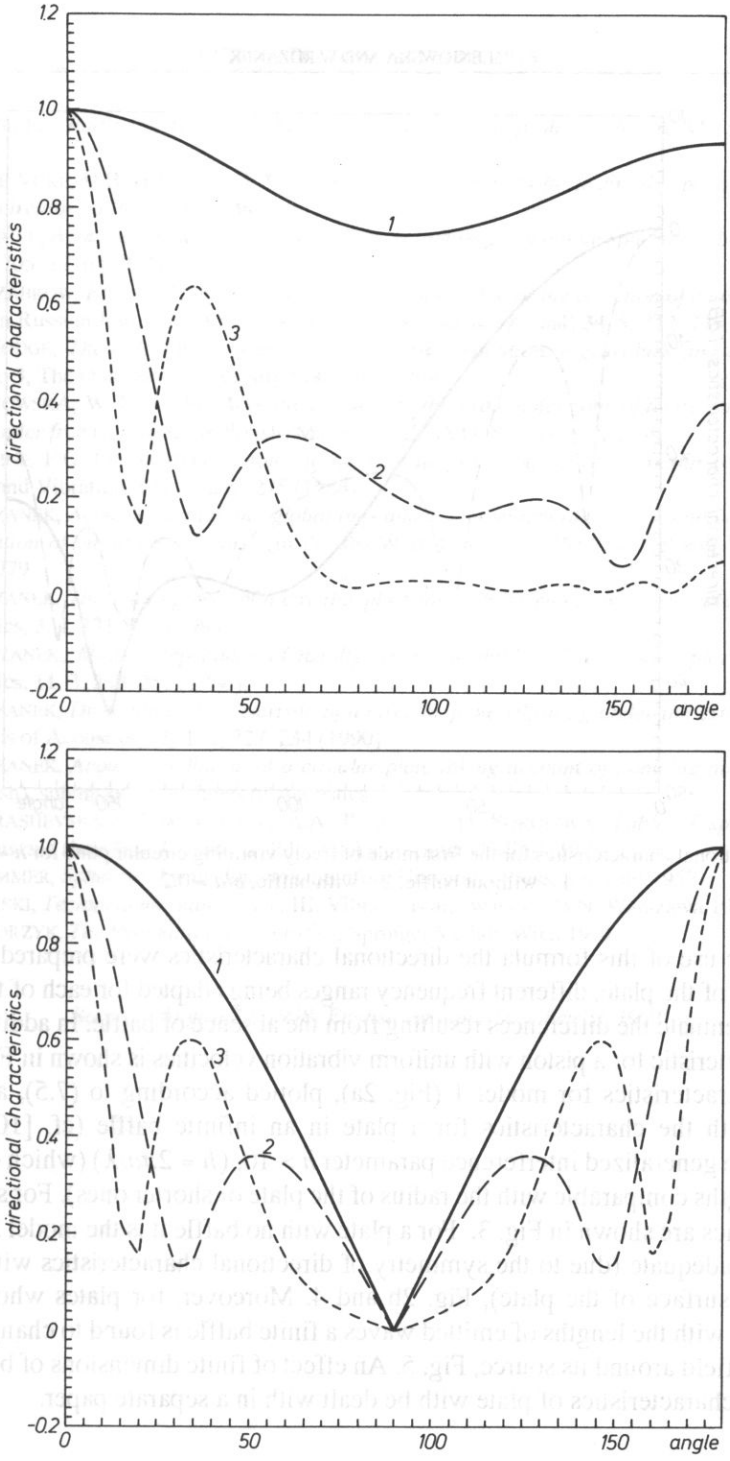

FIG. 4. Directional characteristics for the second mode of freely vibrating circular plate without a baffle for various values of h; a – model 1, b – model 2, 1: $h = 1$, 2: $h = 5$, 3: $h = 10$.

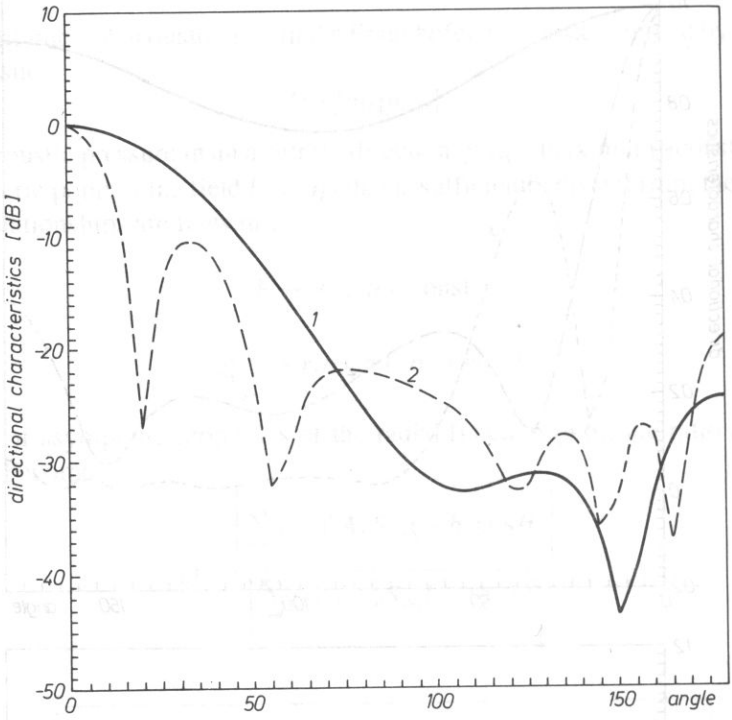

FIG. 5. Directional characteristics for the first mode of freely vibrating circular plate for $h = 5$, model 1. 1 – without baffle, 2 – with baffle, $b/a = 0.2$.

With the use of this formula the directional characteristics were prepared for the first three modes of the plate, different frequency ranges being adapted for each of the modes in order to accentuate the differences resulting from the absence of baffle. In addition, a directional characteristic for a piston with uniform vibration velocities is shown in Fig. 2.

The characteristics for model 1 (Fig. 2a), plotted according to (7.5), are found to coincide with the characteristics for a plate in an infinite baffle (cf. [10, Fig. 15]), provided the generalized interference parameter $h > 10$, ($h = 2\pi a/\lambda$) (which corresponds to wavelengths comparable with the radius of the plate or shorter ones). For smaller h the characteristics are shown in Fig. 3. For a plate with no baffle it is the model 2 that seems to be more adequate (due to the symmetry of directional characteristics with respect to the middle surface of the plate), Fig. 2b and 4. Moreover, for plates whose radius is comparable with the lengths of emitted waves a finite baffle is found to change the shape of acoustic field around its source, Fig. 5. An effect of finite dimensions of baffles on the directional characteristics of plate with be dealt with in a separate paper.

References

[1] T. NIMURA, Y. WATANABE, *Effect of a finite circular baffle board on acoustic radiation*, J.A.S.A **25**, 1, 76–80 (1953).

[2] A. SILBIGER, *Radiation from circular pistons of elliptical profile*, J.A.S.A **33**, 11, 1515–1522 (1961).
[3] R.V. DE VORE, D.B. HODGE, R.G. KOUYOUMJIAN, *Radiation by finite circular pistons imbedded in a rigid circular baffle*, J.A.S.A. **48**, 5, 1128–1134 (1970).
[4] R.V. BAIER, *Acoustic radiation impedance of caps and rings on oblate spheroidal baffles*, J.A.S.A. **51**, 5, 1705–1716 (1972).
[5] A.A. SZABROW, *Effects of the thickness of a finite rigid baffle or the direction of coaxially radiating piston* in Russian Journal of Acoustics (Russian Akusticeskij Żurnał) **34**, 5, 772–775 (1978).
[6] D.B. HODGE, *The calculation of the spheroidal wave equation, eigenvalues and eigenfunctions*, Rep. No 3, The Ohio State University Columbus 1969.
[7] L. LENIOWSKA, W. RDZANEK, *Acoustic pressure in the Fraunhofer zone of a circular plate without baffle under free vibrations* (in Polish) Materiały XXXVI OSA, Szczyrk 1989.
[8] H. LEVINE, F.G. LEPPINGTON, *A note on the acoustic power output of a circular plate*, Journal of Sound and Vibration, **121**, 2, 269–275 (1988).
[9] W. RDZANEK, *Acoustic mutual and global impedance of a system of sources with variable surface distribution of vibration velocities* (in Polish) Wyd. Uczelniane WSP w Zielonej Górze, Zielona Góra 1979.
[10] W. RDZANEK, *The sound power of a circular plate for high-frequency wave radiation*, Archives of Acoustics, **3**, 4, 331–340 (1983).
[11] W. RDZANEK, *Mutual impedance of axially-symmetric modes of a circular plate*, Archives of Acoustics, **11**, 3, 239–251 (1986).
[12] W. RDZANEK, *Directional characteristic of a circular plate vibrating under the external pressure*, Archives of Acoustics, **15**, 1–2, 227–234 (1990).
[13] W. RDZANEK, *Acoustic radiation of a circular plate taking account of damping and environment* (in Polish), submitted to Archives of Acoustics.
[14] S.P. ERASHEVSKAJA, E.A. IVANOV, A.A. PALCEV, N.D. SOKOLOVA, *Table of spheroidal wave functions and their first derivatives*. Ed. "Nauka i technika" Mińsk 1973.
[15] C. FLAMMER, *Spheroidal wave function*, Stanford University Press, Stanford 1957.
[16] S. KALISKI, *Technical mechanics*, vol. III, Vibrations and waves, PWN, Warszawa 1986.
[17] E. SKUDRZYK, *The foundations of acoustics*, Springer Verlag, Wien 1971.

Received August 20, 1990; English version November 20, 1991

ARCHIVES OF ACOUSTICS
17, 3, 425–431 (1992)

MUTUAL ACOUSTIC IMPEDANCE OF CIRCULAR SOURCES WITH PARABOLIC VIBRATION VELOCITY DISTRIBUTION FOR HIGH FREQUENCIES

L. LENIOWSKA, W. RDZANEK and P. WITKOWSKI

Department of Physics, Department of Technics,
Pedagogical University
(35-310 Rzeszów, ul. Rejtana 16a)

In the paper the mutual impedance of circular planar sources with parabolic vibration velocity distribution occurring harmoniously in time is analyzed. It is assumed that the sources set in planar rigid baffle radiate into a lossless and homogeneous gas medium. The acoustic impedance is calculated using the method based on the Fourier representation of acoustic pressure, thanks to which the mutual impedance is expressed in the Hankel representation. The real integrals in the formula are replaced by complex ones and integrates is performed round a closed and smooth integration contour. Using approximation methods, the expression for mutual impedance at high frequencies is obtained.

1. Introduction

The use of circular planar sources as a vibratory system for the reception or propagation of acoustic waves requires a knowledge of the frequency characteristics of many basic acoustic values with mutual acoustic impedance among them.

The paper [4] includes detailed mathematical considerations of the acoustic impedance problem, as well as a review of calculation methods referring to the system of planar sources at a given forced vibration velocity distribution.

The paper gives integrated formulae for the acoustic impedance of two circular sources with parabolic velocity distribution. During the calculation of the acoustic impedance, the integrand functions are developed into Lommel series and next, the Sonine and Schlafly integrals for the imaginary part are applied. In this way the final formula for the mutual impedance is presented as a double series in which the Hankel spherical function of the second kind is used. On the basis of this formula the mutual impedance for low interference parameters is calculated, with the assumption that the distance between the sources is many times longer than their radii. By applying integrated formulae, however, acoustic impedance is calculated and it is proved that in a special case, for normal

velocity distribution, the derived formulae develop into the well-known Rayleigh expression. Formulae for the acoustic impedance for low interference parameters are given as well.

This paper refers to the paper [4] and presents the expression for the mutual impedance for high interference parameters. By replacing the real variable by the complex one, the contour integral is introduced instead of the real one and further integration is done round the close contour [1]. The method of *stationary phase* and the asymptotic expansion of cylindrical functions are applied as well. The derived expressions have a simple mathematical form, what makes it possible to carry out detailed numerical calculations.

2. Mutual acoustic impedance

The system of M circular planar sources of the radius α is set in a planar rigid baffle surrounded on both sides by a gas medium with the rest density ρ. The vibration of each source is harmonic in time and its amplitude is defined by the following surface distribution

$$v_n(r) = v_{on}\left(1 - q\frac{r^2}{a^2}\right) \tag{1}$$

where n denotes a given source, v_{on} amplitude of the midpoint, r – radial variable in a chosen reference system, q – constant whose value depends on the way the source is mounted to the baffle, $0 \le q \le 1$. For such a vibratory system the mechanical impedance of the source with regard to influences from other sources can be expressed as

$$Z_s = \sum_{n=1}^{M} \frac{v_{on}}{v_{os}} Z_{sn}, \tag{2}$$

where Z_{ns} is the mutual impedance defined by the formula [4]

$$Z_{ns} = \frac{1}{v_{on} v_{os}^*} \int_{\sigma_s} \rho_{sn}(r) v_s^*(r) d\sigma_s, \tag{3}$$

in which $\rho_{sn}(r)$ denotes the amplitude of the acoustic pressure from the n–source, exerted on the s–source. Without neglecting further calculations are aimed at deriving the formula for the mutual impedance Z_s of any two sources. The above definition takes a simpler form for axially-symmetrical problem

$$Z_{sn} = 2\pi\rho c k^2 \int_0^{\pi/2 + i\infty} W_s(\vartheta) W_n(\vartheta) J_0(kl\sin\vartheta)\sin\vartheta d\vartheta, \tag{4}$$

where

$$W_n(\vartheta) = \int_0^a f_n(r) J_0(kr\sin\vartheta) r dr \tag{5}$$

is the characteristic function of the source [2], $f_n(r) = v_n(r)/v_{on}$ is the function of the vibration velocity distribution, $\vartheta = \theta + i\psi$, l is the distance between the midpoints of the sources, c – propagation velocity of sound in the medium having the density ρ, k – wave number. This formula can be obtained through the Fourier transform of acoustic pressure expressed by the Huygens–Rayleigh integral. Assuming the same vibration velocity distribution (1) on the surface of the s and n source and applying the formulae (4) and (5), the mutual impedance can be expressed as follows:

$$Z_{sn} = 2\rho c a^2 \left[(1-q)^2 I_{11} + \frac{4q(1-q)}{ka} I_{12} + \frac{4q^2}{(ka)^2} I_{22} \right], \tag{6}$$

where

$$I_{11} = \int_0^{\pi/2 + i\infty} \frac{J_1^2(ka\sin\vartheta)}{\sin\vartheta} J_0(kl\sin\vartheta)\, d\vartheta \tag{6a}$$

$$I_{12} = \int_0^{\pi/2 + i\infty} \frac{J_1(ka\sin\vartheta) J_2(ka\sin\vartheta)}{\sin^2\vartheta} J_0(kl\sin\vartheta)\, d\vartheta \tag{6b}$$

$$I_{22} = \int_0^{\pi/2 + i\infty} \frac{J_2^2(ka\sin\vartheta)}{\sin^3\vartheta} J_0(kl\sin\vartheta)\, d\vartheta \tag{6c}$$

The integrals included in Eq. (6a, b, c) have no exact analytical solutions. Thus there is a need to find a method to solve them, which would be proper for a given range of the interference parameter ka. The method presented below is based on the use of the asymptotic expansion of cylindrical functions as well as on integration using the method of constant phase. The obtained results are valid for sufficiently high frequencies. Each integral (6a, b, c) is a complex function of a complex variable. Separation of variables is done by replacing $\gamma = \theta + i\psi$ what results in

$$\sin(\vartheta) = \sin(\theta + i\psi) = \sin\theta\cos i\psi + \cos\theta\sin i\psi \tag{7}$$

Taking into consideration the chosen integral contour $0 \le \theta \le \pi/2$, $\psi = 0$, $0 \le \psi < \infty$, $\theta = \pi/2$, the first integral (6a) has the following real and imaginary part:

$$\mathrm{Re}(I_{11}) = \int_0^{\pi/2} \frac{J_1^2(ka\sin\theta)}{\sin\theta} J_0(kl\sin\theta)\, d\theta \tag{8}$$

$$\mathrm{Im}(I_{11}) = \int_0^{\infty} \frac{J_1^2(ka\cosh\psi)}{\cosh\psi} J_0(kl\cosh\psi)\, d\psi \tag{9}$$

In order to obtain the solution of the above integrals, let us apply the replacement $x = \sin\theta$ for Eq. (8) and $x = \cosh\psi$ for Eq. (9)

$$\mathrm{Re}(I_{11}) = \int_0^1 \frac{J_1^2(kax)}{x\sqrt{1-x^2}} J_0(klx)\,dx \tag{10}$$

$$\mathrm{Im}(I_{11}) = \int_0^\infty \frac{J_1^2(kax)}{x\sqrt{x^2-1}} J_0(klx)\,dx \tag{11}$$

Let us now consider the real part of the first integral (6a). The remaining ones are transformed analogically in regard to the similarity of their integrands. The integral (6a) is replaced for a complex one by introducing the auxiliary complex function

$$F(z) = J_1^2(kaz) H_0^{(1)}(klz) \tag{12}$$

We choose the smooth, closed integral contour along the positive part of the x axis, omitting the branch cut. Then we follow along the quadrant with an infinite radius, which joins the positive semi-axes x and y. The value of this integral, according to the Cauchy theorem, equals zero. The integration itself is done by adding the integrals around the consecutive parts of the contour.

Let us now consider the real part of the applied contour integral. Since both the real part of the integral along the axis y and the part around the circle with an infinite radius equal zero, we obtain the following equation

$$\mathrm{Re}\left\{\int_c \frac{F(z)}{z\sqrt{1-z^2}}\right\} = \int_0^1 \frac{J_1^2(kax)}{x\sqrt{1-x^2}} J_0(klx)\,dx - \int_1^\infty \frac{J_1^2(kax)}{x\sqrt{x^2-1}} N_0(klx)\,dx = 0 \tag{13}$$

Let us now compare the integrals included in the above equation. The first is Eq. (8) calculated before

$$\int_0^1 \frac{J_1^2(kax)}{x\sqrt{1-x^2}} J_0(klx)\,dx = \int_1^\infty \frac{J_1^2(kax)}{x\sqrt{x^2-1}} N_0(klx)\,dx \tag{14}$$

Applying the asymptotic expansion of the cylindrical functions

$$J_1(kax) = \left[\frac{2}{\pi kax}\right]^{\frac{1}{2}} \cos(kax - 3/4\pi) \tag{15}$$

$$N_0(klx) = \left[\frac{2}{\pi klx}\right]^{\frac{1}{2}} \sin(klx - \pi/4) \tag{16}$$

and integrating using the method of stationary phase, we obtain

$$\mathrm{Re}(I_{11}) = \frac{\sqrt{2/\pi kl}}{\pi ka} \int_1^\infty \frac{[1-\sin(2kax)]\sin(klx - \pi/4)}{x^{5/2}\sqrt{x^2-1}}\,dx =$$

$$= \frac{1}{2\pi ka}\left(\frac{2\sin(kl)}{kl} - \frac{\cos k(l-2a)}{k\sqrt{l(l-2a)}} + \frac{\cos k(l+2a)}{k\sqrt{l(l+2a)}}\right). \tag{17}$$

As opposed to the real parts, the imaginary parts of the integrals (6a, b, c) do not require transformations connected with the change of integration limits. This enables a direct application of approximation methods. The above explained calculations result in:

$$Z_{sn} = R_\infty \frac{6}{q^2 - 3q + 3}\left[(1-q)^2 I_{11} + \frac{4q(1-q)}{ka} I_{12} + \frac{4q^2}{(ka)^2} I_{22}\right], \tag{18}$$

$$I_{11} = \frac{1}{2\pi ka}\left[\frac{2\exp[-i(kl - \pi/2)]}{kl} - \frac{\exp[-ik(l-2a)]}{k\sqrt{l(l-2a)}} + \frac{\exp[-ik(l+2a)]}{k\sqrt{l(l+2a)}}\right], \tag{18a}$$

$$I_{12} = \frac{1}{2\pi ka}\left[\frac{\exp(-i[k(l+2a) - \pi/2])}{k\sqrt{l(l+2a)}} + \frac{\exp(-i[k(l-2a) - \pi/2])}{k\sqrt{l(l-2a)}}\right], \tag{18b}$$

$$I_{22} = \frac{1}{2\pi ka}\left[\frac{2\exp[-i(kl - \pi/2)]}{kl} + \frac{\exp[-ik(l-2a)]}{k\sqrt{l(l-2a)}} - \frac{\exp[-ik(l+2a)]}{k\sqrt{l(l+2a)}}\right], \tag{18c}$$

where $R_\infty = 1/3\pi\rho c a^2(q^2 - 3q + 3)$ is a normalized factor described as the acoustic resistance when $k \to \infty$ [4].

3. Figures and conclusions

After comparing the mutual impedance frequency characteristics obtained by using integral formulae and their approximate expression (Fig. 1), it is concluded that there is a good agreement of both characteristics above the value of the parameter $kl = 10$ and

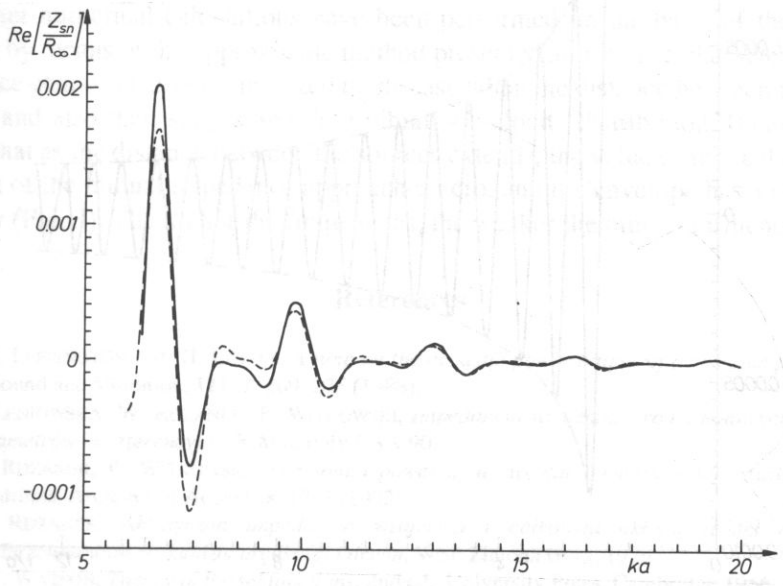

FIG. 1. Normalized mutual resistance depending on the parameter *ka*. The solid line denotes a curve which has been obtained by numerical integration of formulae (6a, b, c); the dashed line denotes a curve which has been calculated using approximation expressions (7a, b, c).

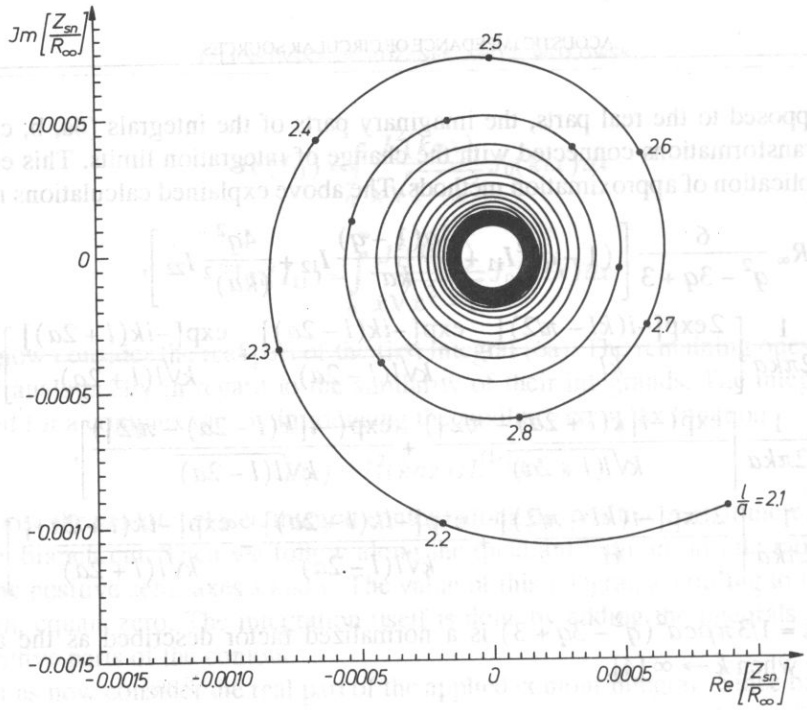

FIG. 2. The normalized mutual impedance as a function of l/a for $ka = 10$, $q = 1$.

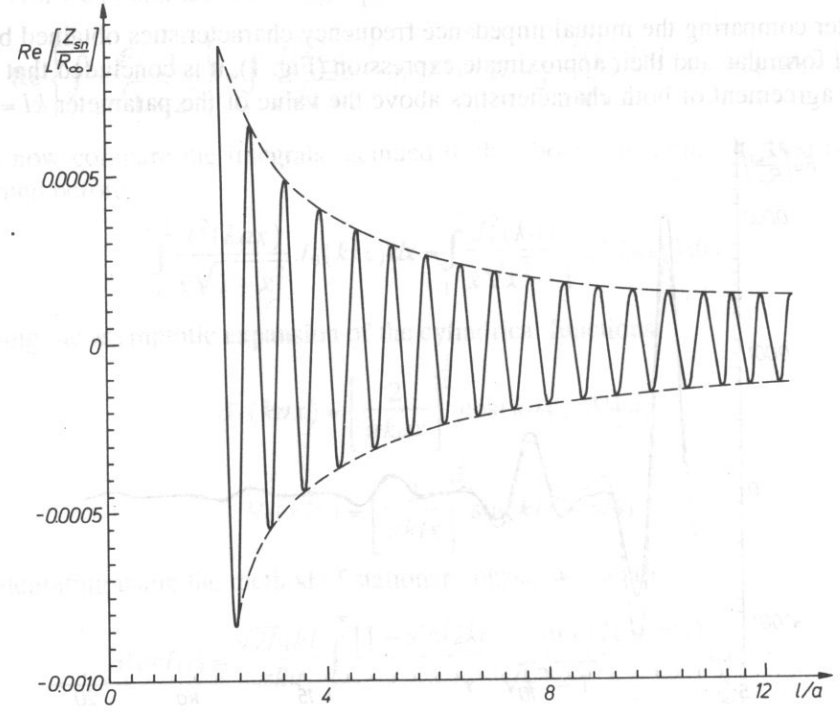

FIG. 3. The normalized mutual resistance as a function of l/a for $ka = 10$ and $q = 1$. The dashed curve denotes the envelope of extreme values of resistance.

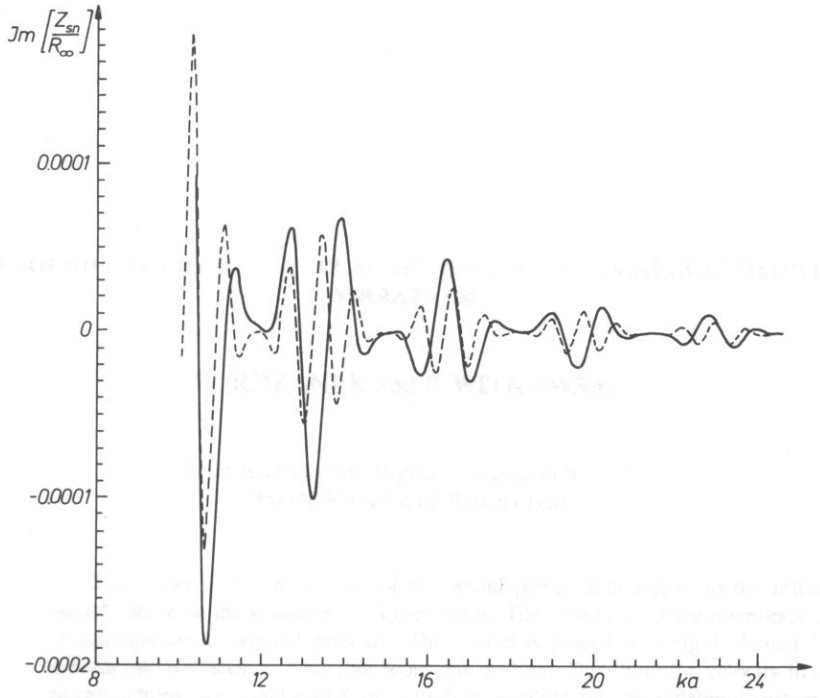

FIG. 4. Normalized mutual reactance as a function ka, $q = 1$. – – – $l/\alpha = 5$, —— $l/\alpha = 8$.

that the relative error does not exceed 1%.

Further numerical calculations have been performed on the basis of the formulae obtained by means of the approximate method presented above. The character of mutual impedance changes has been analyzed in the case when the distance between the sources changes and also their shapes and their vibration velocity distribution. It can be easily noticed that as the distance between the sources extends, the value of the real and imaginary part of the mutual impedance approaches zero, and the envelope has a exponential character (Fig. 3). The higher the frequencies, the weaker the mutual influences.

References

[1] F.G. LEPPINGTON AND H. LEVINE, *A note on the acoustic power output of a circular plate*, Journal of Sound and Vibration, **121**, 2, 269–275 (1988).

[2] L. LENIOWSKA, W. RDZANEK, P. WITKOWSKI, *Impedancja wzajemna źródeł kołowych dla dużych parametrów interferencyjnych*, Materiały OSA'90.

[3] W. RDZANEK, P. WITKOWSKI, *The sound power of a circular membrane for axially-symmetric vibrations*, Archives of Acoustics, **17**, 3 (1992).

[4] W. RDZANEK, *Akustyczna impedancja wzajemna i całkowita układu źródeł o zmiennym powierzchniowym rozkładzie prędkości i drgań*, WSP Zielona Góra, 1979.

[5] G.N. WATSON, *Theory of Bessel functions*, 2nd ed., University Press, Cambridge 1966.

Received March, 7, 1991

ARCHIVES OF ACOUSTICS
17, 3, 433–438 (1992)

THE SOUND POWER OF A CIRCULAR MEMBRANE FOR AXIALLY-SYMMETRIC VIBRATIONS

W. RDZANEK and P. WITKOWSKI

Institute of Physics, Higher Pedagogical School
(35-310 Rzeszów, ul. Rejtana 16a)

This paper gives an analysis of the sound power with regard to the influence of a radiated wave on the vibrations of a membrane. The vibrations of the membrane are forces by time-harmonic external pressure. The source is placed in a rigid plannar baffle and radiates into a lossless and homogeneous gas medium. Distributing a velocity in a series of eigenfunctions, we could transform a motion equation into an algebraic system of linear equations. As the final result of the analysis, a relative real power of self and free vibrations for high frequency was derived using an approximate method. The expressions derived here are very useful and convenient for numerical calculations.

1. Introduction

The problem of radiation of surface sources, specified as classical, still exists and is very often considered. It results from the necessity of solving newer and newer theoretical and practical problems as well as from the upgrading of computational methods.

Lately there have been published solutions concerned with the interaction of plates, membranes for axially-symmetric vibrations and also the interaction of two modes of the same source.

Recent studies [1, 4–8] are devoted to sources fixed in a coplanar rigid baffle and radiated into a lossless gas medium. The paper [1] presents an analysis of forced vibrations of a plate with regard to the damping effects caused by an internal friction and the influence of radiated waves through a plate on its vibration. The second part of the paper [1] also shows an approximate method of calculating real power by integration in a complex space using an asymptotic expansion of cylindrical functions. The same results were obtained in the paper [4] applying another approximate method.

With reference to the papers [1, 4], the present one is concerned with the calculation of the acoustic power of a circular membrane set in a planar rigid baffle. The forced vibrations are considered with regard to the influence of a radiated wave on the vibrations of the membrane. The losses inside membrane caused by internal friction were

disregarded due to the slender thickness of the membrane. The expressions obtained have a simple mathematical form and can be the basis for further detailed numerical calculations.

2. Damped vibrations of membrane

A circular membrane of a radius a and surface density η, placed in a rigid planar baffle, is surrounded by a gaseous medium with a rest density ρ_0. The membrane is excited to vibrations by an external force $f(r, t) = f_0(r)\exp(-i\omega t)$ for $0 \le r \le a$. The vibrations are modified as a consequence of the interaction of the medium with acoustical pressure p on the membrane surface.

The equation of axially-symmetric vibrations of the circular membrane is as follows:

$$(T\nabla^2 - \eta\frac{\partial^2}{\partial t^2})\,\xi(r, t) = f(r, t) - 2p(r, t), \tag{1}$$

where ξ is the distribution of the transverse vibrations, T, the force stretching the membrane, related to a unit length. Using known formulations for harmonic phenomena between the displacement $\xi_0(r)$ and normal velocity $\xi_0(r) = iv(r)/\omega$ and the acoustical pressure $p_0(r)$ and velocity potential $p_0(r) = \rho_0 i\omega\phi(r)$, Eq. (1) could be presented in a changed form:

$$(k_p^{-2}\nabla^2 + 1)\,v(r) + 2\varepsilon_1 k\phi(r) = -\frac{i}{\eta\omega}f_0(r), \tag{2}$$

where k_p is the wave number defined as $k_p^2 = \eta\omega^2/T$, $\varepsilon_1 = \rho_0/\eta k$, $k = 2\pi/\lambda$.
Let us present the normal velocity in the form of an infinite series of eigenfunctions

$$v(r) = \sum_n c_n\, v_n(r) \tag{3}$$

in which

$$v_n(r) = v_{on}J_0(k_n r),\ 0 \le r \le a \tag{3a}$$

and use the orthonormality property

$$\int_0^a v_n(r)\, v_m(r) r\,dr = \delta_{mn} \tag{4}$$

for normalized velocity $v_{on} = \sqrt{2}/aJ_1(k_n a)$ equation; the previous equations (2) turns into an algebraic system of linear equations

$$c_n\left(\frac{k_n^2}{k_p^2} - 1\right) + 2\varepsilon_1 i\sum_m c_m g_{mn} = f_n \tag{5}$$

The quantity f_n expressed as

$$f_n = \frac{1}{\eta\omega}\int_0^a f_0(r)\, v_n(r) r\,dr \tag{6}$$

is the coefficient of expansion of the external force into a orthogonal series, whereas g_{mn} is a normalized mutual impedance of axially-symmetric modes for free vibrations [7]:

$$g_{mn} = 2(k_m a)(k_n a)\int_0^{ka-i\infty} \frac{J_0^2(x)x\,dx}{\gamma[x^2-(k_m a)^2][x^2-(k_n a)^2]} \tag{7}$$

where $x = ka\sin\theta$, $\gamma = \sqrt{1-(x/ka)^2}$ for $0 \le x < ka$ or $\gamma = i\sqrt{(x/ka)^2-1}$ for $ka < x < \infty$. The real part of $g_{nn}(m=n)$ can also be interpreted as a relative real power of free vibrations.

In order to calculate the acoustical power of a circular membrane let us use the definition [4]:

$$N = \frac{1}{2}\int_\sigma p(r)\,v(r)\,d\sigma \tag{8}$$

which, in the case of axially-symetric velocity (3), leads to

$$N = \pi\rho_0 c_0 k^2 \sum_m \sum_n c_m c_n^* \int_0^{\pi/2-i\infty} W_m(\vartheta) W_n^*(\vartheta)\sin\vartheta\,d\vartheta. \tag{9}$$

When we regard the value of the characteristic function $W_m(\vartheta)$ [4] and the relation (7), the acoustical power has the following form [6]:

$$N = \pi\rho_0 c_0 \sum_m \sum_n c_m c_n^* g_{mn}. \tag{10}$$

It is possible to reach another form of the formula describing acoustical power. Let us multiply Eq. (5) by c_n^* and the sum by n, then employ Eq. (10). The formula for the acoustical power of forced vibration takes the form of single series:

$$N = \frac{i\rho_0 c_0 \pi}{2\varepsilon_1}\sum_n \left[c_n^2\left(\frac{k_n^2}{k_p^2}-1\right) - c_n^* f_n \right], \tag{11}$$

where ε_1 determines the influence of the wave radiated by a membrane on its vibration.

If we assume that the density of the gaseous medium is much smaller than that of the membrane, ε_1 approaches zero and then we get

$$c_n = f_n\left(\frac{k_n^2}{k_p^2}-1\right)^{-1}. \tag{12}$$

3. The real power for high frequency wave radiation

Considering the linear phenomena sinusoidally dependent on time, the axially-symmetric vibration of a circular membrane can be described by Eq. (3a). For that distribution of velocity, the characteristic function [4] $W_n(\vartheta)$ for the $(0, n)$ modal is as follows:

$$W_n(\vartheta) = v_{on} k_n a J_1(k_n a) \frac{J_0(ka\sin\vartheta)}{k_n^2 - k^2\sin^2\vartheta}. \tag{13}$$

Basing on the relation (13) and expression [4]

$$N_n = \rho_0 c_0 \pi k^2 \int_0^{\pi/2} W_n^2(\vartheta)\sin\vartheta d\vartheta, \tag{14}$$

the real power is expressed by the integral formula

$$N_n = \pi\rho_0 c_0 k^2 v_{on}^2 a^4 (k_n a)^2 J_1^2(k_n a) \int_0^{\pi/2} \frac{J_0^2(ka\sin\vartheta)\sin\vartheta d\vartheta}{[(k_n a)^2 - (ka\sin\vartheta)^2]^2} \tag{15}$$

Now, adopting the notations $\zeta = \sin\vartheta$, $ka = \beta$, $\delta_n = k_n a/ka$, the new version of the expression (15) becomes

$$\sigma_n = \frac{N_n}{N_0} = 2\delta_n^2 \int_0^1 \frac{J_0^2(\beta\zeta)\zeta d\zeta}{\sqrt{1-\zeta^2}(\zeta^2 - \delta_n^2)^2}. \tag{16}$$

The factor

$$N_0 = 1/2\pi\rho_0 c_0 v_{on}^2 a^2 J_1^2(k_n a) \tag{17}$$

specifies the radiated power for the n-th axi-symmetric modal velocity profile at vanishing small wavelengths, viz. $k \to \infty$ [4]. The coefficient δ_n means a relative real power. Let us introduce the function of a complex variable

$$F(z) = J_0(\beta z) H_0^{(1)}(\beta z), \tag{18}$$

selected such that

$$\mathrm{Re}\, F(\zeta) = J_0^2(\beta\zeta), \tag{19}$$

and consider the complex integral

$$\int_C \frac{F(z)z dz}{\sqrt{1-z^2}(z^2 - \delta_n^2)^2} \tag{20}$$

instead of Eq. (16).

The contour C (Fig. 1) bypasses the singular point of second order at $z = \delta_n$, the branch point at $z = 0$ and branch cut, between $z = 1$ and $z = \infty$. The integral (20) is equal to zero. This is the consequence of its single-valued and regular integrans within C. The contour C consists of several parts; this can be written symbolically as

$$\int_0^1 + \frac{1}{2}\int_{r_z} + \int_1^\infty + \int_{R_\infty} + \int_\infty^0 = 0 \tag{21}$$

The contribution of two integrals vanishes: from the large circular R_∞ when the radius grows indefinitely and also the real part of the integral along an imaginary axis, what results from the relation $\mathrm{Re}\, F(i\tau) = 0$, τ is real.

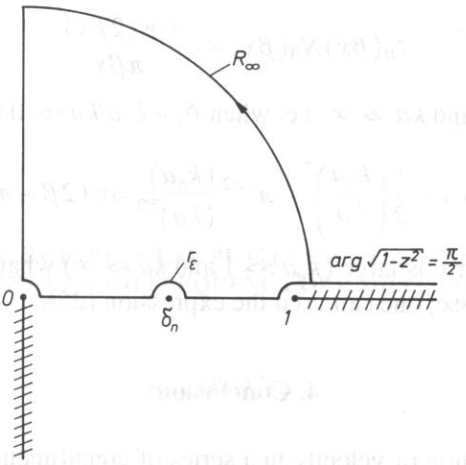

FIG. 1. The integration contour C for pattern (20).

Then there only remains

$$\int_0^1 \frac{F(x)xdx}{\sqrt{1-x^2}\,(x^2-\delta_n^2)^2} - \pi i F'(\delta_n) + \int_1^\infty \frac{F(x)xdx}{-i\sqrt{x^2-1}\,(x^2-\delta_n^2)^2} + \int_\infty^0 \frac{F(i\tau)i\tau i d\tau}{\sqrt{1+\tau^2}\,(\tau^2+\delta_n^2)^2} = 0, \tag{22}$$

where

$$F(z) = \frac{F(z)z}{\sqrt{1-z^2}\,(z+\delta_n)^2}. \tag{23}$$

Taking the real part of the expression (22), we get a value of the integral (16):

$$\int_0^1 \frac{J_0^2(\beta x)xdx}{\sqrt{1-x^2}\,(x^2-\delta_n^2)^2} = \mathrm{Re}[\,\pi i F'(\delta_n)\,] + \int_1^\infty \frac{J_0(\beta x)N_0(\beta x)xdx}{\sqrt{x^2-1}\,(x^2-\delta_n^2)^2}, \tag{24}$$

because

$$\mathrm{Re}\int_0^1 \frac{F(x)xdx}{\sqrt{1-x^2}\,(x^2-\delta_n^2)^2} = \int_0^1 \frac{J_0^2(\beta x)xdx}{\sqrt{1-x^2}\,(x^2-\delta_n^2)^2} \tag{24a}$$

Finally, the normalized real power radiated by the membrane is given as

$$\sigma_n = \frac{1}{(1-\delta_n^2)^{1/2}} - \frac{\delta_n^2}{(1-\delta_n^2)^2}\frac{1}{\pi^{1/2}\beta^{3/2}}\cos(2\beta+\pi/4). \tag{25}$$

In order to determine the last integral in Eq. (24), the method of a constant phase was used. Besides, the cylindrical functions were presented in an asymptotic form, right in the high frequency ($ka \Rightarrow \infty$) [3]:

$$J_0(\beta x)N_0(\beta x) \cong -\frac{\cos(2\beta x)}{\pi\beta x} \tag{26}$$

For the case of fixed n and $ka \Rightarrow \infty$, i.e. when $\delta_n = k_n a/ka \Rightarrow 0$ the result is

$$\sigma_n = 1 + \frac{1}{2}\left(\frac{k_n a}{ka}\right)^2 - \pi^{-1/2}\frac{(k_n a)^2}{(ka)^{7/2}}\cos(2\beta + \pi/4). \tag{27}$$

When the mode number n is large ($k_n a >> 1$ and $ka \Rightarrow \infty$) what means that δ_n is of the order of unity; in this case, one can used the expression (25).

4. Conclusions

By using a distribution of velocity in a series of eigenfunctions, the acoustic power radiated by an excited membrane with regard to the influence of a radiated wave on the vibrations of this membrane has been derived. The solutions obtained have the form of series (10), (11). Because of the high rate of convergence of series, the first solution (10) is especially useful for numerical calculations. It results from the character of changes of mutual impedance, the values of which are strong decreasing together with an increase of the mode numbers m and n. The second shape of the solution (11), expressed by a single series, is simpler but slowly convergent. It is the consequence of the small difference between the values of the $c_n^2(k_n^2/k_p^2 - 1)$ and $c_n^* f_n$ dependent on summation.

The real part of normalized self impedance obtained for high frequency consists of a polynomial and oscillatory term. This solution is generalized of the pattern received in [8].

References

[1] F.G. LEPPINGTON AND H.LEVINE, *A note on the acoustic power output of a circular plate*. Journal of Sound and Vibration, **121**, 2, 269–275 (1988).

[2] I. MALECKI, *Theory of waves and acoustical systems*, (in Polish) PWN, Warszawa 1964.

[3] N. MCLACHLAN, *Bessel functions for engineers*, PWN, Warszawa 1964.

[4] W. RDZANEK, *The sound power of a circular plate for high-frequency wave radiation*, Archives of Acoustics, **3**, 4, 331–340 (1983).

[5] W. RDZANEK, *Mutual impedance of axially-symmetric modes of a circular plate*. Archives of Acoustics, **11**, 3, 239–252 (1986).

[6] W. RDZANEK, *Acoustical radiation of circular plate with regard to damping effect and influence of environment*, will be published in Archives of Acoustics.

[7] W. RDZANEK, *Mutual and total acoustic impedance of a system of sources with a variable superficial vibration velocity distribution*. Academic Publ. of the Higher Pedagogic School in Zielona Góra 1979 (in Polish).

[8] W. RDZANEK, *Acoustic resistance of a circular membrane for frequencies much higher than resonance ones*, (in Polish), Proc. XXVIII Open Seminar on Acoustics, Gliwice 1981.

Received January 21, 1990; English version November 11, 1991

ARCHIVES OF ACOUSTICS
17, 3, 439–448 (1992)

MUTUAL IMPEDANCE OF CIRCULAR PLATE FOR AXIALLY SYMMETRIC FREE VIBRATIONS AT HIGH FREQUENCY OF RADIATING WAVES*

W. RDZANEK

Department of Physics
Pedagogical University
(35-310 Rzeszów, ul. Rejtana 16a)

Mutual normalized impedance of radiation of single axially symmetric normal modes is analysed for a circular clamped plate with a plane rigid baffle. Damping in the plate is ignored and the acoustic waves are assumed to radiate in a homogeneous lossless fluid medium. Selecting an integral representation of the considered acoustic impedance and using the Cauchy theorem of residues, an expression is obtained in an elementary form valid for high frequencies.

1. Introduction

Acoustic power output of a circular plate under forced vibrations was analysed by LEVIN and LEPPINGTON [1] and the present author [5]. Losses in the material and coupled vibrations of surrounding air were both taken into account. The applied mathematical method led to the expressions for a load forcing vibrations, displacements and vibration velocities in the form of known series expansions with respect to the complete set of eigen functions. As a result, the acoustic power of the plate with internal losses and influenced by its surroundings was obtained in the form of double series with rapid convergence. Application of the series to numerical calculations depends on the knowledge of a general term in the series that comprises the normalized specific and mutual impedance of circular plates for the case of axially symmetric free vibrations. For high frequencies of acoustic waves elementary expressions were obtained for free resistance of one mode [1, 3] and mutual resistance of two different modes for the same plate [4].

Elementary formulae for the radiation reactance have up to now been lacking, both for a single mode and for two mutually interacting modes.

Paper prepared within the grant CPBPO2.03

On account of results arrived at in [4] and with the use of LEVIN and LEPPINGTON'S method [1], based on the Cauchy theorem on residues, an elementary formula is derived for a normalized mutual resistance, account being taken of its oscillatory character as dependent on the frequency. A formula for mutual reactance of radiation of two different modes of the same plate is obtained by means of a direct integration of the expression from the papers [1, 5]. Asymptotic formulae for the Bessel functions are used in the presence of sufficiently large values of the interference parameter. It is also shown that the expression for a reactance of a single mode follows from an expression for mutual reactance.

The frequency characteristics of the considered normalized impedance of radiation are also shown diagrammatically.

2. Assumptions

A thin circular plate is thickness h, small with respect to its diameter $2a$, made of homogeneous material of density ρ is immersed in a lossless fluid medium. The plate is clamped at the circumference. For sinusoidal time dependence a normal velocity of the axially symmetric free vibration can be expressed in the form [6]

$$v_n(r)/v_{0n} = J_0(\gamma_n r/a) - \frac{J_0(\gamma_n)}{I_0(\gamma_n)} I_0(\gamma_n r/a), \tag{1}$$

where r – radial coordinate of a point, J_m – Bessel function, I_m – modified Bessel's function (both of order m), γ_n – the n-th root of the frequency equation [2]

$$I_0(\gamma_n) J_1(\gamma_n) = -I_1(\gamma_n) J_0(\gamma_n), \tag{2}$$

that describes the frequency of free vibrations for the n–th mode,

$$f_n = \frac{1}{2\pi a^2} \gamma_n^2 \left(\frac{B}{\rho h}\right)^{1/2} \tag{3}$$

where, in turn, B denotes flexural stiffness of the plate. The constant v_{0n} can be expressed with the use of an amplitude of vibrations for the centre of the plate v_{0n}' in the following manner

$$v_{0n}'/v_{0n} = 1 - J_0(\gamma_n)/I_0(\gamma_n). \tag{4}$$

Mechanical mutual impedance between $(0, n)$ and $(0, s)$ axially symmetric vibration modes of a circular plate with a plane rigid baffle is calculated from the formula, cf. [5]

$$Z_{ns} = \frac{1}{2\sqrt{\langle |v_n|^2 \rangle \langle |v_s|^2 \rangle}} \int_\delta p_{ns} v_s \, d\delta, \tag{5}$$

where p_{ns} is an acoustic pressure generated by the $(0, n)$ mode of the plate and exerted on the same plate through the $(0, s)$ vibration mode. Mean square of the velocity of $(0, n)$ mode is expressed by

$$\langle |v|^2 \rangle = \frac{1}{2\delta} \int_\delta v_n^2(r) \, d\delta, \tag{6}$$

where $\delta = \pi a^2$.

Referring the mechanical mutual impedance to the specific resistance of fluid medium $\rho_0 c$ and to the area δ of the plate, the normalized mutual impedance between $(0, n)$ and $(0, s)$ modes is obtained [1, 4, 5]:

$$\zeta_{ns} = 4\delta_n^2\delta_s^2 \int_0^\infty \frac{x}{\gamma}\left[\frac{a_n\delta_n J_0(\alpha x) - xJ_1(\alpha x)}{x^4 - \delta_n^4}\right] \times$$

$$\times\left[\frac{a_s\delta_s J_0(\alpha x) - xJ_1(\alpha x)}{x^4 - \delta_s^4}\right] dx. \tag{7}$$

where $\gamma = (1 - x^2)^{1/2}$ for $0 \le x \le 1$, $\gamma = i(x^2 - 1)^{1/2}$ for $1 \le x < \infty$, $\alpha = k_0 a$, $\delta_n = \gamma_n/\alpha$, $a_n = J_1(\gamma_n)/J_0(\gamma_n)$

Moreover,

$$\zeta_{ns} = \theta_{ns} - i\chi_{ns} \tag{8}$$

where θ_{ns} is a normalized mutual resistance and χ_{ns} is a normalized mutual reactance.

When $k_0 a/\gamma_n >> 1$ and $k_0 a/\gamma_s >> 1$, the normalized mutual resistance between the $(0, n)$ and $(0, s)$ modes of free vibrating circular plate can be shown in the form

$$\theta_{ns} = h_{ns}\alpha^{-2}, \tag{9}$$

where

$$h_{ns} = 2(\gamma_n\gamma_s)^2 \frac{a_n\gamma_n - a_s\gamma_s}{\gamma_n^4 - \gamma_s^4} \tag{9'}$$

for $n \neq s$. Although the value of h_{ns} for $n = s$ does exist, the formula (9') is not valid for the case. Suitable formulae were given in [1].

3. Normalized mutual resistance

To obtain more accurate formula for the normalized mutual resistance than (9), the derivation will be based on the real part of its integral representation (7).

Following LEVIN and LEPPINGTON [1], the following function of complex variable is introduced

$$F(z) = a_n\delta_n a_s\delta_s J_0(\alpha z)H_0^{(1)}(\alpha z) - (a_n\delta_n + a_s\delta_s)zJ_0(\alpha z)H_1^{(1)}(\alpha z) +$$

$$+ z^2 J_1(\alpha z)H_1^{(1)}(\alpha z) \tag{10}$$

such that

$$\mathrm{Re}F(x) = a_n\delta_n a_s\delta_s J_0^2(\alpha x) - (a_n\delta_n + a_s\delta_s)xJ_0(\alpha x)J_1(\alpha x) + x^2 J_1^2(\alpha x), \tag{11}$$

where x is a real variable.

Further, a contour integral is used,

$$\int_c \frac{zF(z)dz}{\sqrt{1 - z^2}\,(z^4 - \delta_n^4)(z^4 - \delta_s^4)} = 0 \tag{12}$$

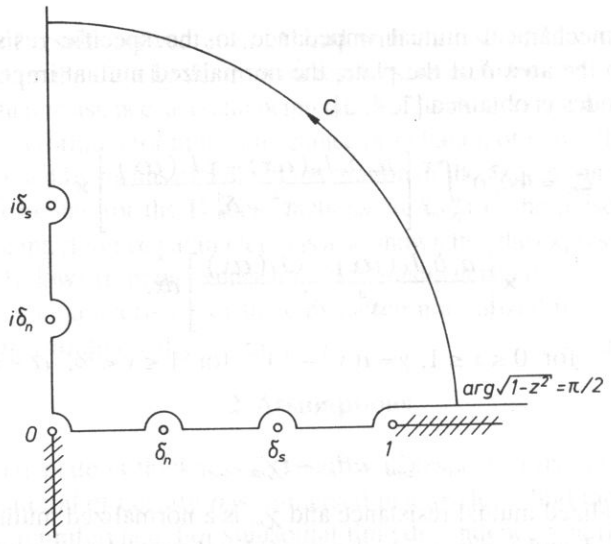

FIG. 1. Integration path for the expression (12), cf. [1].

calculated along the path C, Fig. 1. Assuming δ_n, $\delta_s < 1$, the integrand stays unique and regular inside C. As a consequence, the frequency range is limited because $\delta_n = \gamma_n/\alpha$, $\delta_s = \gamma_s/\alpha$, $\alpha = k_0 a$ and the formula (3) is valid. Employing the Cauchy theorem on residues, the integral (12) can be shown symbolically as

$$\int_0^1 + \int_1^\infty + \int_{C_R} + \int_\infty^0 = \pi i \sum_{j-1}^{4} \operatorname{Rez}(z_j), \tag{13}$$

where for $z_j = \delta_n, i\delta_n, \delta_s, i\delta_s$ singular points exist with first order poles and the integrals $\int_0^1$ $\int_\infty^0$ are interpreted in the eigenvalue tense. The latter vanish on integration along a large circle when its radius tends to infinity. They also vanish on integration along small circles around the bifurcation points ($z = 0$, $z = 1$) when their radii shrink to zero. The following auxiliary functions are introduced to determine residua at singular points as first order poles:

$$F_1(z) = \frac{zF(z)}{\sqrt{1-z^2}(z+\delta_n)(z^2+\delta_n^2)(z^4-\delta_s^4)}, \quad z = \delta_n,$$

$$F_2(z) = \frac{zF(z)}{\sqrt{1-z^2}(z+i\delta_n)(z^2-\delta_n^2)(z^4-\delta_s^4)}, \quad z = i\delta_n,$$

$$F_3(z) = \frac{zF(z)}{\sqrt{1-z^2}(z+\delta_s)(z^2+\delta_s^2)(z^4-\delta_n^4)}, \quad z = \delta_s,$$

$$F_4(z) = \frac{zF(z)}{\sqrt{1-z^2}(z+i\delta_s)(z^2-\delta_s^2)(z^4-\delta_n^4)}, \quad z = i\delta_s. \tag{14}$$

Accounting for $\mathrm{Re}\,F(iy) = 0$ for real values of y, the expression (13) yields

$$\mathrm{Re}\int_0^1 \frac{xF(x)dx}{\sqrt{1-x^2}\,(x^4-\delta_n^4)(x^4-\delta_s^4)} = \int_1^\infty \frac{x\,\mathrm{Im}F(x)dx}{\sqrt{x^2-1}\,(x^4-\delta_n^4)(x^4-\delta_s^4)} + \\ + \mathrm{Re}(\pi i\,[F_1(\delta_n) + F_2(i\delta_n) + F_3(\delta_s) + F_4(i\delta_s)]). \qquad (15)$$

It immediately finishes $\mathrm{Im}F(\delta_n) = \mathrm{Im}F(i\delta_n) = \frac{2}{\pi\alpha}\alpha_s\delta_s$, $\mathrm{Im}F(\delta_s) = \mathrm{Im}F(i\delta_s) = \frac{2}{\pi\alpha}\alpha_n\delta_n$.

The second integral in (15) can be calculated with the use of known asymptotic relationships:

$$J_1(\alpha x)N_1(\alpha x) \sim -J_0(\alpha x)N_0(\alpha x) \sim (\pi\alpha x)^{-1}\cos 2\alpha x, \\ J_0(\alpha x)N_1(\alpha x) \sim -(\pi\alpha x)^{-1}(1+\sin 2\alpha x), \qquad (16)$$

for $\alpha \to \infty$ $x > 1$. Since the "non-oscillating" part of the integral is equal to

$$\frac{4}{\alpha}\int_1^\infty \frac{x\,dx}{\sqrt{1-x^2}\,(x^4-\delta_n^4)(x^4-\delta_s^4)} = \frac{1}{\delta_n^4-\delta_s^4}\left[\frac{1}{\delta_n^2}\left(\frac{1}{\sqrt{1-\delta_n^2}} - \frac{1}{\sqrt{1+\delta_n^2}}\right) + \right. \\ \left. - \frac{1}{\delta_s^2}\left(\frac{1}{\sqrt{1-\delta_s^2}} - \frac{1}{\sqrt{1+\delta_s^2}}\right)\right], \qquad (17)$$

the "oscillating" part can be dealt with by means of asymptotic method

$$2\sqrt{\alpha/\pi}\,(1-\delta_n^4)(1-\delta_s^4)\int_1^\infty [\,(x^2 - a_n\delta_n a_s\delta_s)\cos 2\alpha x + \\ + (a_n\delta_n + a_s\delta_s)x\sin 2\alpha x\,]\frac{dx}{\sqrt{x^2-1}\,(x^4-\delta_n^4)(x^4-\delta_s^4)} = \qquad (18) \\ = (1 - a_n\delta_n a_s\delta_s)\cos(2\alpha + \pi/4) + (a_n\delta_n + a_s\delta_s)\sin(2\alpha + \pi/4)$$

Accounting for

$$\mathrm{Re}\left(\pi i\left[F_1(\delta_n) + F_2(i\delta_n) + F_3(\delta_s) + F_4(i\delta_s)\right]\right) = \\ = \frac{1}{2\alpha}\frac{1}{\delta_n^4-\delta_s^4}\left[\frac{a_n\delta_n}{\delta_s^2}\left(\frac{1}{\sqrt{1-\delta_s^2}} - \frac{1}{\sqrt{1+\delta_s^2}}\right) + \right. \\ \left. - \frac{a_s\delta_s}{\delta_n^2}\left(\frac{1}{\sqrt{1-\delta_n^2}} - \frac{1}{\sqrt{1+\delta_n^2}}\right)\right], \qquad (19)$$

the following formula for the normalized mutual resistance is finally arrived at:

$$\theta_{ns} = \alpha^{-1}\frac{a_n\delta_n - a_s\delta_s}{\delta_n^4 - \delta_s^4}\left[\delta_n^2\left(\frac{1}{\sqrt{1-\delta_s^2}} - \frac{1}{\sqrt{1+\delta_s^2}}\right) + \right.$$

$$+ \delta_s^2\left(\frac{1}{\sqrt{1-\delta_n^2}} - \frac{1}{\sqrt{1+\delta_n^2}}\right) + 2\pi^{-1/2}\alpha^{-3/2}\frac{\delta_n^2\delta_s^2}{(1-\delta_n^4)(1-\delta_s^4)}\left[\left(1 - \right.\right.$$

$$\left.\left. + \quad a_n\delta_n\alpha_s\delta_s\right)\cos(2\alpha + \pi/4) + (\alpha_n\delta_n + \alpha_s\delta_s)\sin(2\alpha + \pi/4)\right] \tag{20}$$

within an accuracy of $o(\delta_n^2\delta_s^2\alpha^{-3/2})$.

When δ_n^2, $\delta_s^2 << 1$, an approximate formula $(1 \pm t^2)^{-1/2} \approx 1 \mp \frac{1}{2}t^2$ for $t << 1$ is used leading to the expression (20) in the form

$$\theta_{ns} = 2(\gamma_n\gamma_s)^2\alpha^{-2}\frac{\alpha_n\gamma_n - \alpha_s\gamma_s}{\gamma_n^4 - \gamma_s^4} + 2\pi^{-1/2}(\gamma_n\gamma_s)^2\alpha^{-11/2}\cos(2\alpha + \pi/4). \tag{20'}$$

Its first term is identical to (9) which comes from the paper [4].

It should be emphasized that:

– the formulae (20) and (20') are valid for $n \neq s$ only and the limiting case $n = s$ is not possible,

– the formula for the resistance of a single mode can be found in [1] where the same mathematical procedure was used,

– for $n = s$ the terms of (20) and (20') containing trigonometric functions (characterizing oscillatory character of variations in radiation resistance) are of the same form as those relevant for free resistance equations (20) and (21) in [1].

4. Normalized mutual reactance

The starting point to calculate the mutual reactance of a circular plate radiating acoustic waves with the help of two axially symmetric modes $(0, n)$ and $(0, s)$ is an imaginary part of the integral formula (7)

$$\chi_{ns} = 4\delta_n^2\delta_s^2\int_1^\infty\left[\frac{\alpha_n\delta_n J_0(\alpha x) - xJ_1(\alpha x)}{x^4 - \delta_n^4}\right]\times$$

$$\times\left[\frac{\alpha_s\delta_s J_0(\alpha x) - xJ_1(\alpha x)}{x^4 - \delta_s^4}\right]\frac{x\,dx}{\sqrt{x^2-1}}. \tag{21}$$

Integration of (21) will be made for sufficiently large interference parameter $\alpha = k_0 a >> 1$ i.e. for $\alpha \to \infty$. The asymptotic formulae

$$J_0(\alpha x)J_1(\alpha x) \sim -(\pi\alpha x)^{-1}\cos(2\alpha x),$$

$$J_0^2(\alpha x) \sim (\pi\alpha x)^{-1}(1 + \sin 2\alpha x),$$

$$J_1^2(\alpha x) \sim (\pi\alpha x)^{-1}(1 - \sin 2\alpha x), \tag{22}$$

are used for $\alpha \to \infty$ ($x > 1$) to be put into the integrand of (21). "Non-oscillating" part of the integral is calculated with the use of the formulae

$$\int_1^\infty \frac{dx}{\sqrt{x^2-1}\,(x^2-t^2)} = \frac{\arcsin t}{t\sqrt{1-t^2}},$$

$$\int_1^\infty \frac{dx}{\sqrt{x^2-1}\,(x^2+t^2)} = \frac{\operatorname{Arsh} t}{t\sqrt{1+t^2}}, \tag{23}$$

whereas the "oscillating" part is arrived at with the use of asymptotic method. The result is

$$\chi_{ns} = \frac{2}{\pi\alpha(\delta_n^4 - \delta_s^4)}\left[\alpha_n\alpha_s\left(\delta_s^3\left(\frac{\arcsin\delta_n}{\sqrt{1-\delta_n^2}} - \frac{\operatorname{Arsh}\delta_n}{\sqrt{1+\delta_n^2}}\right) - \right.\right.$$

$$-\delta_n^3\left(\frac{\arcsin\delta_s}{\sqrt{1-\delta_s^2}} - \frac{\operatorname{Arsh}\delta_s}{\sqrt{1+\delta_s^2}}\right)\Big) + \delta_n\delta_s^2\left(\frac{\arcsin\delta_n}{\sqrt{1-\delta_n^2}} + \right.$$

$$\left. + \frac{\operatorname{Arsh}\delta_n}{\sqrt{1+\delta_n^2}}\right) - \delta_s\delta_n^2\left(\frac{\arcsin\delta_s}{\sqrt{1-\delta_s^2}} + \frac{\operatorname{Arsh}\delta_s}{\sqrt{1+\delta_s^2}}\right)\Big] +$$

$$+ \frac{2\delta_n^2\delta_s^2}{\pi^{1/2}\alpha^{3/2}(1-\delta_n^4)(1-\delta_s^4)}\Big[\left(\alpha_n\delta_n\alpha_s\delta_s - 1\right)\sin(2\alpha + \pi/4) +$$

$$+ (\alpha_n\delta_n + \alpha_s\delta_s)\cos(2\alpha + \pi/4)\Big] \tag{24}$$

with the accuracy of $o(\delta_n^2\delta_s^2\alpha^{-3/2})$.

For δ_n^2, $\delta_0^2 << 1$ the expression (24) takes the form

$$\chi_{ns} = \frac{32}{15\pi}(\gamma_n\gamma_s)^2\alpha^{-5} - 2\pi^{-1/2}(\gamma_n\gamma_s)^2\alpha^{-11/2}\sin(2\alpha + \pi/4). \tag{24'}$$

The expression (24) was simplified to become (24') after taking account of the first three terms of expansions with respect to $x = \delta_n\delta_s$ for the root function and for arc sin x, Arsh x.

In the limiting case $n = s$ the formula (24) yields a normalized reactance of circular plate radiating with the help of the axially symmetric vibration mode $(0, n)$

$$\chi_{nn} = (\pi\alpha)^{-1}\Big[(a_n^2(-3 + 4\delta_n^2) - 1 + 2\delta_n^2)\frac{\arcsin\delta_n}{2\delta_n(1-\delta_n^2)^{3/2}} +$$

$$+ \left(\alpha_n^2(3 + 4\delta_n^2) - 1 - 2\delta_n^2\right)\frac{\operatorname{Arsh}\delta_n}{2\delta_n(1+\delta_n^2)^{3/2}} + \frac{1 + a_n^2\delta_n^2}{1-\delta_n^4}\Big] +$$

$$+ 2\delta_n^4\pi^{-1/2}\alpha^{-3/2}(1-\delta_n^4)^{-2}\left[(\alpha_n^2\delta_n^2 - 1)\sin(2\alpha + \pi/4) + \right.$$

$$\left. + 2\alpha_n\delta_n\cos(2\alpha + \pi/4)\right] \tag{25}$$

with the accuracy of $o(\delta_n^4\alpha^{-3/2})$.

5. Final remarks

The theoretical analysis of the radiations of a thin circular plate fournished elementary formulae for normalized impedance of axially symmetric modes of free vibrations. They can be applied only for sufficiently short acoustic wave length as compared with the diameter of the plate.

Suitable terms, characterizing the "oscillatory" character of variations in both the real part (20), (20') and in the imaginary part (24) of the normalized mutual impedance of circular plate, were determined, Fig. 2.

When the interference parameter $k_0 a$ tends to infinity, the expression (20') takes the form (9), given in [4].

The normalized mutual reactance (24) of two vibration modes $(0, n)$ and $(0, s)$ in the limit $n = s$ assumes the form (25) which corresponds to the normalized specific case is possible in the case of the real part of the mutual impedance.

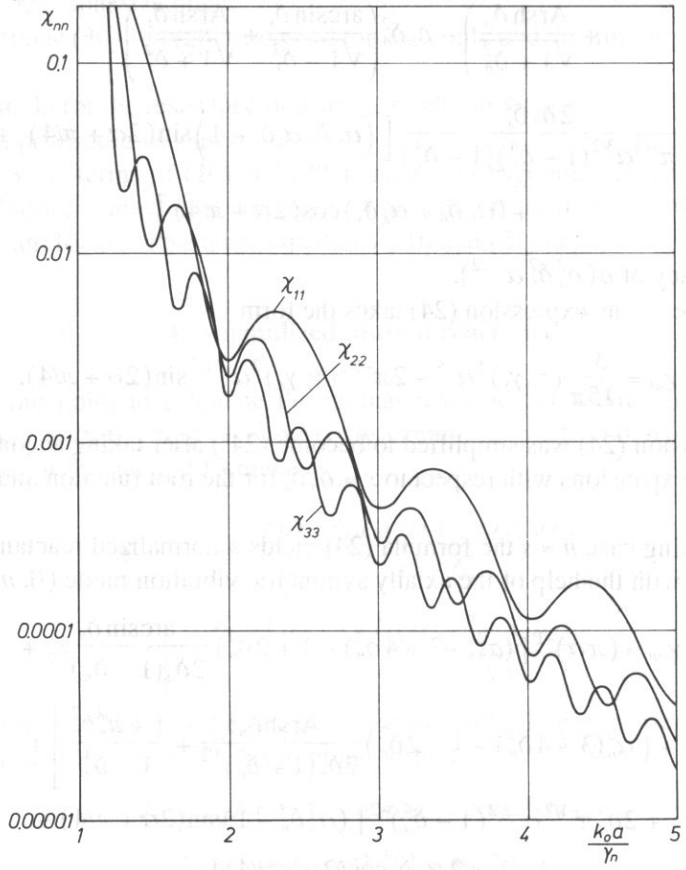

FIG. 2. Normalized reactance of a circular plate (25) vs. parameter $k_0 a/\gamma_n$ for the first three axially symmetric vibration modes.

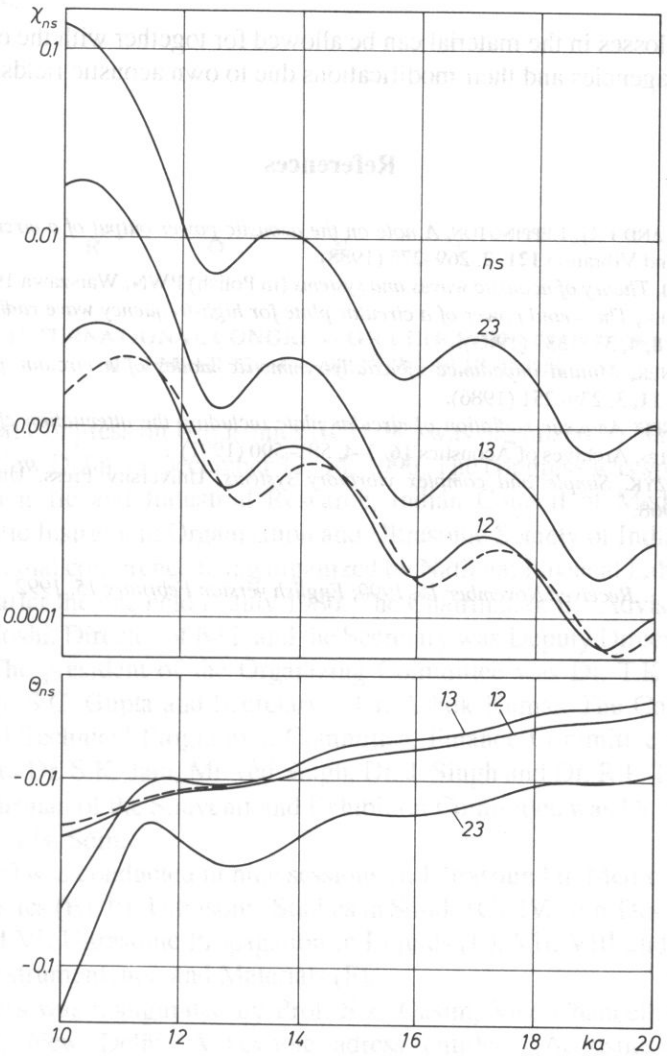

FIG. 3. Normalized mutual impedance of a circular plate (20), (24), vs. parameter $k_0 a$ for axially symmetric vibration modes. Curves obtained from the formula (7) are dashed.

Exceptionally simple form of the approximate formula (25) for the normalized reactance can be onset for computations under less rigorous constraints than $k_0 a >> \gamma_n$. For instance, at $k_0 a > 3\gamma_n$, the normalized reactance (25) of the circular plate is, for a number of initial vibration modes, determined to within an accuracy of several per cent, Fig. 3.

When $k_0 a << \gamma_1 \gamma_s$ or when great accuracy of results is required, computer-sided numerical integration of the formula (7) can be used.

The obtained simple expressions for the normalized mutual impedance of axially symmetric vibration modes for a circular plate can be employed to analyse more complex

situations, e.g. losses in the material can be allowed for together with the effects of vibration enforcing agencies and their modifications due to own acoustic fields, cf. [1, 5].

References

[1] H. LEVINE AND F.G. LEPPINGTON, *A note on the acoustic power output of a circular plate*, Journal of Sound and Vibration **121**, 2, 269–275 (1988).

[2] I. MALECKI, *Theory of acoustic waves and systems* (in Polish) PWN, Warszawa 1964.

[3] W. RDZANEK, *The sound power of a circular plate for high-frequency wave radiation*, Archives of Acoustics, **8**, 4, 331–339 (1983).

[4] W. RDZANEK, *Mutual impedance of axially-symmetric modes of a circular plate*, Archives of Acoustics, **11**, 3, 239–251 (1986).

[5] W. RDZANEK, *Acoustic radiation of circular plate including the attenuation effect and influence surroundings*, Archives of Acoustics **16**, 3–4, 581–590 (1991).

[6] E. SKUDRZYK, *Simple and complex vibratory systems*, University Press, University Park and London 1968.

Received November 15, 1990; English version February 15, 1992

ARCHIVES OF ACOUSTICS
17, 3, 449–450 (1992)

C H R O N I C L E

INTERNATIONAL CONGRESS ON ULTRASONICS (ICU–90)
DECEMBER 12–14, 1990, NEW DELHI, INDIA

International Congress on Ultrasonics (ICU–90) was organized by National Physical Laboratory at New Delhi on December 12–14, 1990. The congress was sponsored by the Council of Scientific and Industrial Research, Indian Council of Medical Research, Central Scientific Instrument Organisation and Ultrasonic Society of India. This was the second international conference being organized by National Physical Laboratory (NPL) in ultrasonics, after the one held in July 1980. The Chairman of the Advisory Board was Prof. Dr. S.K. Joshi, Director of NPL and the Secretary was Deputy Director of NPL, Dr. V.N. Bindal. The president of the Organizing Committee was Dr. T.K. Saksena, Co-Chairman – Mr. S.C. Gupta and Secretary – Dr. Ashok Kumar. The Convenors of the Publication and Technical Programme Committee, Finance Committee and Reception Committee were Dr. S.K. Jain, Mr Ved Singh, Dr. J. Singh and Dr. R.P. Tandon, respectively. The Chairman of the Souvenir and Exhibition Committee was Dr. S.P. Signal and Convenor – Dr. J.N. Som.

The ICU–90 was conducted in nine sessions (I. Ultrasound in Medicine (A), II. Underwater Acoustics (B), III. Ultrasonic Studies in Solids (C), IV. Non-Destructive Evolution (D), V and VI. Ultrasonic Propagation in Liquids (E), VII, VIII and IX Ultrasonic Transducers, Instrumentation and Materials (F).

The congress was inaugurated by Prof. S.Z. Qasim, Vice-Chancellor of the Jamia Millia Islamia, New Delhi. A keynote adress entitled „Acoustics-Infrasonics to Ultrasonics" was delivered by Dr. V.K. Aatres, Director of the Naval Physical and Oceanographic Laboratory, Cochin, during the Inaugural Session. The scientific programme included 9 invited contributions (3 of them were published as abstracts and 1 as invited paper) and 56 research papers. The invited talks were presented by: Prof. V.R. Minicha (Lithotripsy – Issues and Perspective), Prof. Dubrovskii (Delphine acoustics), Prof. Z. Kaczkowski (Ultrasonic studies in metallic glasses), Prof. P.K. Raju (Non-destructive evaluation of the composites using acousto-ultrasonics), Prof. L.M. Lyamshev (Radiation acoustics), Prof. V.P. Bhatnagar (Modern trends in acousto-optics diffraction), Dr. S. Khandpur (Challenges in ultrasound hyperthermia). The list of participants contained 171 names from India and abroad.

An exhibition had been organized by the Ultrasonic Society of India, which also brough out the Souvenir containing the programme, abstracts of the accepted papers and

lists of participants and exhibitors. The Proceedings of the ICU–90, edited by the Publication Committee with Dr. T.K. Saksena as the Chairman, were given to the 102 participants during registration. The proceedings contained 49 papers (1 invited and 48 contributed) from India (39), Egipt (3), Spain (1), Italy (1), Soviet Union (1), Great Britain (1) and Poland (3). On Ultrasound in Medicine were published 7 papers (35 pages), on Underwater Acoustics – 3 papers (26 pages), on Ultrasonic studies in Solids – 7 papers (6 contributed and 1 invited, 45 pages), on Non-Destructive Evaluation – 5 papers (29 pp.) on Ultrasonic Propagation in Liquids – 14 papers (86 pp.) and on Ultrasonic Transducers Instrumentation and Materials – 13 papers (79 pp.). The index of the proceedings contained 115 author names. On the list of exhibitors were Accutrol Systems Pvt. Ltd. New Delhi, Blue Star Ltd, New Delhi, Electronics Corporation India Ltd, Hyderabad, L and T – Gould Ltd., Mysore, Mekaster Electronic Service Centre Pvt. Ltd. and Systronics (Agency Division) Ahmedabad. As the co-chairman of the Round Table Session were invited Dr. V.N. Bindal, Dr. T.K. Saksena, Professors: Dubrovski, Raju and Kaczkowski. As the introduction to the discussion Prof. Dubrovskii has talked on ultrasonic research in Acoustical Institute of the Academy of Sciences of the USSR, prof. Raju spoke on the non-destructive investigation at the Auburn University (USA) and prof. Kaczkowski spoke on the current research status and opportunities in ultrasound in Poland. In the discussion the delegates presented their institutions, organizations and factories.

The Proceedings of the Congress ICU–90 were dedicated to Dr. W.N. BINDAL.

Dr. V.N. BINDAL, Member of the Editorial Committee of the Archives of Acoustics, was born on December 25, 1930 in India. He received his M.Sc degree from Agra University and Ph.D. degree from Delhi University. He is Deputy Director and Scientist Fellow of the National Physical Laboratory at New Delhi. He is also Head of the Materials Division of the NPL. He has played a key role in giving a momentum of the Research and Development efforts towards applied ultrasonic technology in India. He is currently engaged in the works on underwater acoustics, ultrasonic standards and ceramical transducer materials.

Dr V.N. BINDAL is the author or co-author of more than 300 papers and 15 patents. He is Founder President of the Ultrasonic Society of India and Chairman of the Delhi Headquarter of the NDT Society of India.

He is member of Editorial Board of Journal od Pure and Applied Ultrasonics (India), Acoustics Letters (UK), Archives of Acoustics and Ultrasonics (UK). He is also chairman and member of various ISI committees and Advisor from Asia to WHO for Environmental Health Criteria on Ultrasound.

Dr. V.N. BINDAL received 6 National Awards in the area of ultrasonics.

Zbigniew Kaczkowski